Fall 10-26-2017

Asymptotic Neutronic Solutions for Fast Burst Reactor Design

Edward L. Hobbs
University of New Mexico

Edward Lee Hobbs
Candidate

Nuclear Engineering
Department

This dissertation is approved, and it is acceptable in quality and form for publication:

Approved by the Dissertation Committee:

Cassiano R. Endres de Oliveira , Chairperson

Adam Hecht

Barry D. Ganapol

Patrick J. McDaniel

HyeongKae Park

ASYMPTOTIC NEUTRONIC SOLUTIONS
FOR
FAST BURST REACTOR DESIGN

by

EDWARD LEE HOBBS

B.S., Physics, East Central University, 1995
M.S., Nuclear Science, Air Force Institute of Technology, 2006

DISSERTATION

Submitted in Partial Fulfillment of the
Requirements for the Degree of

Doctor of Philosophy
Engineering

The University of New Mexico
Albuquerque, New Mexico

December, 2017

DEDICATION

I dedicate this dissertation to all the courageous savants who contend that there is more to learn from the *Dragon* than there is to fear.

ACKNOWLEDGMENTS

I am extremely grateful to my advisor, and committee chair Dr. Cassiano de Oliveira for his years of dedication to my progress during a very trying time in his life's journey. I will never forget all that he has done for me.

Dr. Pat McDaniel provided me with knowledge of the practical application of my work. He has expanded my understanding of reactors beyond the neutronics. Additionally, his wisdom as a teacher and mentor was a significant force in bringing this work to completion.

Dr. Hyeonkae "Ryosuke" Park went well beyond my expectations in his efforts to teach me the skills needed to utilize modern coding techniques in the application of my methods. Dr. Park's work with non-linear solution methods to solve eigenvalue problems was my inspiration to apply the similar methods to transient problems.

Very special thanks to Dr. Barry Ganapol for showing interest in my work. I am very grateful that he was willing to serve as the honest broker on my committee. His insight was invaluable. He has made this academic work much more useful, comprehensive, and credible. I am grateful for the sacrifices he made in order to participate in this effort.

Dr. Adam Hecht was a lifesaver to this research effort. I truly appreciate his great flexibility and willingness to provide his credentials, and expertise to the team. Without his efforts, this work would have not reached completion. His compassion for students and their success at the University of New Mexico is unsurpassed in my experience.

I would also like to thank the late Professor Emeritus Charles J. Bridgeman, who passed in the fall of 2015, for his written works, lectures, and inspiration to me, and countless other students in pursuit of mastery in the nuclear sciences. The readers of this dissertation should attribute anything presented that is valuable to him. His dedication to the nuclear field and to students is the origin of my academic interests in the subject.

ASYMPTOTIC NEUTRONIC SOLUTIONS
FOR
FAST BURST REACTOR DESIGN

by

Edward Lee Hobbs

B.S., Physics, East Central University, 1995
M.S., Nuclear Science, Air Force Institute of Technology, 2006
Ph.D., Nuclear Engineering, University of New Mexico, 2017

ABSTRACT

Deterministic numerical methodologies for solving time-eigenvalue problems are valuable in characterizing the inherent rapid transient neutron behavior of a Fast Burst Reactor (FBR). New nonlinear solution techniques used to solve eigenvalue problems show great promise in modeling the neutronics of reactors. This research utilizes nonlinear solution techniques to solve for the dominant time-eigenvalue associated with the asymptotic (exponential) solution to the neutron diffusion and even-parity form of the neutron transport equation, and lays the foundation for coupling with other physics phenomena associated with FBRs.

High security costs and proliferation risks associated with Highly Enriched Uranium (HEU) fueled FBRs are the motivation for this research. Use of Low Enriched Uranium (LEU) as fuel reduces these risks to acceptable levels. However, the use of LEU fuel introduces complexities such as, increased volume, and longer neutron lifetimes. Numerical techniques are sought to explore these complexities and determine the limitations and potential of a LEU fueled FBR.

A combination of deterministic and stochastic computational modeling techniques are tools used to investigate the effects these complexities have on reactor design and performance. Monte Carlo N-Particle (MCNP) code is useful to determine criticality and calculate reactor kinetics parameters of current and proposed designs. New deterministic methods are developed to directly calculate the fundamental time-eigenvalue in a way that will support multi-physics coupling. The methods incorporate Jacobian Free Newton Krylov solution techniques to address the nonlinear nature of the neutronics equations.

These new deterministic models produce data to determine LEU designs that may meet the performance requirements of proven HEU FBRs in terms of neutron burst yield and burst duration (pulse width) based on the Nordheim-Fuchs model. This computational data and measured performance characteristics of historical LEU FBRs show that LEU designs can generate pulses that are beneficial for meeting Research and Development (R&D) requirements. These modern computational neutronic results indicate that a LEU fueled FBR is a plausible alternative to current HEU fueled reactors.

TABLE OF CONTENTS

LIST OF FIGURES ..... **XI**

LIST OF TABLES ..... **XIV**

CHAPTER 1 INTRODUCTION **1**

Practical Motivation 2

Objectives of the Research 3

Literature Review 4

Fast Burst Reactors 4

Computational Methods 9

Methodology 12

CHAPTER 2 FBR THEORY **17**

Basic Design and Operation 17

The alpha parameter 19

The alpha and *k* Relationship 22

The Nordheim-Fuchs Model 27

CHAPTER 3 THE NEUTRON DIFFUSION EQUATION **30**

Analytical Solution of the Time-Eigenvalue Diffusion Equation 32

Numerical Solution of the Time-Eigenvalue Diffusion Equation 36

Derivation and Spatial Discretization 36

Solution by Power Iteration 39

CHAPTER 4 THE EVEN-PARITY TRANSPORT EQUATION 42

CHAPTER 5 NON-LINEAR SOLUTION METHOD 46

Initialization Methods 46

Newton's Method 47

Block Gaussian Elimination 50

Generalized Minimum Residual 54

CHAPTER 6 RESULTS AND ANALYSES 57

One-Dimensional Diffusion Case 57

Nuclear Data 57

Numerical Performance Analysis 58

Validation of the One-Dimensional Case 63

Two-Dimensional Transport Case 68

CHAPTER 7 CONCLUSIONS 74

Conclusions from the Numerical Analyses of Performance 74

Conclusions from the Test Cases 74

Continued Related Work & Improvements 75

Summary 77

APPENDIX A ACRONYMS AND ABBREVIATIONS 79

APPENDIX B DELAYED NEUTRONS 83

APPENDIX C CHARACTERISTIC EQUATION 86

APPENDIX D DIFFUSION EQUATION 88

APPENDIX E EVEN PARITY TRANSPORT EQUATION 98

APPENDIX F FINITE DIFFERENCE APPROXIMATION 103

APPENDIX G GLOSSARY 106

APPENDIX H PDE CLASSIFICATION & CHARACTERISTICS 116

APPENDIX I SYMBOLS AND NOTATION 119

APPENDIX J NORDHEIM-FUCHS 124

APPENDIX K LEAKAGE MINIMIZATION 127

APPENDIX L LINEARITY 130

REFERENCES 139

LIST OF FIGURES

Figure 1.1 View of Lady Godiva Components 5

Figure 1.2 View of MollyG Components 7

Figure 1.3 View of Super Kukla Components 8

Figure 2.1 Comparison of a Tailed and Tailless Burst 19

Figure 2.2 The Asymptotic Behavior of Scalar flux 22

Figure 2.3 Asymptotic and Generational Neutronic Solution Comparison 24

Figure 2.4 Compounding Effect of the Neutron Population 27

Figure 2.5 Burst Derived from Max Flux and FWHM 29

Figure 3.1 Spherical Coordinates 31

Figure 3.2 First Five Eigen-pairs of a Notional Spherical FBR 35

Figure 3.3 Early and Late Time Flux Comparison 36

Figure 3.4 One-Dimensional Spherical Spatial Discretization 37

Figure 3.5 Discretized Spherical Reactor 38

Figure 3.6 Alpha PI Algorithm Flowchart 41

Figure 4.1 Cylindrical Coordinates 43

Figure 4.2 Surface to Volume Ratio for a Cylinder 45

Figure 5.1 JFNK Flux and Fixed Point alpha Algorithm Flowchart 53

Figure 5.2 JFNK Flux & alpha With Fixed Point alpha in Coefficients Algorithm Flowchart 53

Figure 5.3 Full Nonlinear Elimination JFNK Flux & alpha Solution Algorithm Flowchart 54

Figure 5.4 JFNK Algorithm Flowchart..... 56

Figure 6.1 First Five Eigen-pairs of the Numerical Test Case 59

Figure 6.2 Calculated Burst Characteristics of a HEU and LEU Spherical FBR 67

Figure 6.3 Analytical & Numerical Scalar Flux Comparison..... 68

Figure 6.4 Calculated Burst Characteristics of HEU and LEU Cylindrical FBRs 71

Figure 6.5 JAKES Calculated Burst Characteristics of HEU and LEU Cylindrical FBRs 73

Figure D.1 Reference Plot of Sine and Cosine 91

Figure D.2 Spatial Solution of the Flux 92

Figure D.3 Residual Function Plot of the Analytical Alpha Solution Using Dk..... 95

Figure D.4 Residual Function Plot of the Analytical Alpha Solution 97

Figure H.1 Plots of the descriptive polynomial of PDE classifications..... 117

Figure H.2 Parabola: A geometric representation..... 118

Figure I.1 Discrete Notation for the Transport Equation:..... 123

Figure K.1 Bessel Function, J_0 127

Figure L.1 Homogeneity and Superposition Properties of Linear Systems 136

Figure L.2 Example of an Initially Relaxed System..... 138

LIST OF TABLES

Table 2.1 Relation of α and *k* to Criticality 23

Table 6.1 One-D, One-Group, Microscopic Cross-section Data 57

Table 6.2 One-D, Enrichment, Density and Neutron Energy Data 58

Table 6.3 Comparisons of Numerical Performance 60

Table 6.4 Complete List of Eigenvalues for the Numerical Test Matrix 61

Table 6.5 Summary of Numerical Performance Metrics 63

Table 6.6 One-Dimensional Test Case Results 65

Table 6.7 Historical FBR Reference Data 68

Table 6.8 Two-D, Material Enrichment and Density 69

Table 6.9 Two-Dimensional EVENT Test Case Results 70

Table 6.10 Two-Dimensional JAKES-EVENT Test Case Results 72

Table B.1 Delayed Neutron Data for Uranium Fuel, Fast Spectrum 84

Table H.1 PDE Classification 116

Chapter 1

Introduction

A Fast Burst Reactor (FBR) is a nuclear reactor that obtains fission primarily from fast (fission spectrum) neutrons [1]. The reactor operates by the rapid insertion of excess reactivity that places the system into a super prompt critical state and produces a short (~25-700 micro-seconds) burst (or pulse[1]) of neutrons (10^{16}-10^{18}) [1, 2]. Negative temperature-reactivity feedback, or thermal expansion, quenches the reactor and returns it to a sub-critical state [1, 2]. In addition to thermal quenching, many designs utilize a shock-induced disassembly of the core that aides in the return to sub-criticality [2]. FBRs support a variety of radiation effects experiments as well general research in to fast-reactor-dynamics [2, 3].

This work seeks to provide modern computational neutronic solutions to support research in the practicality of a Low Enriched Uranium (LEU) fueled FBR. Specifically, this research seeks to solve for the time-eigenvalue associated with the time dependent solution and behavior of the neutron economy in HEU and LEU fueled FBRs and determine the resulting burst duration.

---

[1] The FBR is a Pulsed Aperiodic Reactor that operates on Fast Neutrons. This is a subset of Pulsed Reactors [1]. For this reason, literature often uses the terms burst and pulse interchangeably.

Practical Motivation

Scientists require a short burst duration for specific radiation effects research. Material properties of LEU fuel tend to produce a longer burst than HEU. This research expects to inform users on whether LEU FBRs have potential to achieve an adequate burst duration that will meet Research, Development, Testing, and Experimental (RDT&E) needs.

Increased security requirements for a Highly Enriched Uranium (HEU) fueled Fast Burst Reactor (FBR) are making continued operation of these reactors cost prohibitive. Of the three FBRs used in defense radiation effects testing at the turn of the century, only the Molybdenum Godiva (MollyG), located at the White Sands Missile Range (WSMR) remains in operation. To reduce costs, stakeholders in the field are searching for alternatives to the HEU fueled MollyG to conduct required tests and experiments on materials requiring neutron exposure for relatively short durations [3].

In addition to increased security costs, the availability of HEU is in deliberate jeopardy. Many programs of the U.S. National Nuclear Security Administration (NNSA) are seeking to reduce drastically the demand for HEU worldwide. The Material Management and Minimization (M^3) program seeks to eliminate the civilian use of HEU, and down blend the fuel to 19.75 percent LEU for use in research reactors [4]. The Global Threat Reduction Initiative (GTRI) Convert Fuel Development program, formerly the Reduced Enrichment for Research and Test Reactors (RERTR), is also determined to eliminate the demand for HEU. This program has led both the Idaho National Laboratory (INL), and Oak Ridge National Laboratory (ORNL) to develop processes to down blend

HEU and produce 19.75 percent LEU alloyed with 10 percent molybdenum (moly) for use in research and test reactors [5, 6].

This combination of decreased availability, and increased security cost support research into developing alternatives to the HEU fueled FBRs. To support this research, it is valuable to capitalize on the many recent advances in nonlinear solution techniques in steady-state neutronic problems [7, 8]. These techniques have great potential for application in the heavily time-dependent transient neutronic problems of FBRs. Additionally, non-linear solution techniques provide a convenient interface for coupling neutronic solution with other important physics associated with a FBR [9].

Objectives of the Research

The overall objective of the research is to provide the fundamental mode of time-eigenvalue calculations to help determine the practicality of an LEU fueled FBR that meets the burst duration requirements for research currently conducted using MollyG. The supporting objectives required to meet the overall objective satisfactorily are:

1. Consolidate applicable historical research efforts in the use of LEU fuel for FBRs.
2. Implement modern nonlinear solution methods to solve for the fundamental mode of the time-eigenvalue neutron diffusion and even-parity transport equations.

3. Develop an efficient and intuitive desktop tool that maintains the flexibility for use in parallel computing systems, and is ready to couple with other physics required to support FBR research.

By meeting these objectives this research will inform decisions affecting the future methods of producing required neutron environments for research and testing.

Literature Review

Fast Burst Reactors

Scientist at Los Alamos designed the earliest FBR in 1945, the Dragon Machine, using measured cross-sections, and analytical methods, which were not especially predictive. Scientist built early designs incrementally based on measurements during assembly. The Dragon experiments were successful, and did support the theory of fast fission reactions at the time. However, follow on experiments that relied heavily on real-time measurements during assembly resulted in at least two deaths [10, 11].

Following these early experiments, Los Alamos scientists designed another critical assembly using a HEU metallic spherical design called Lady Godiva (see figure 1.1). Scientists designed Godiva with more caution than the previous reactors, and certainly used lessons learned from the early Dragon experiments, but still lacked adequate predictive design analyses. The original simple spherical design failed to reach criticality due in part to a lacking in both design and manufacturing capability. Godiva required the addition of a cylindrical disk of HEU to the design to achieve criticality. Godiva went into delayed

critical operation in 1951, but did not achieve burst operation until 1953 [12, 2].

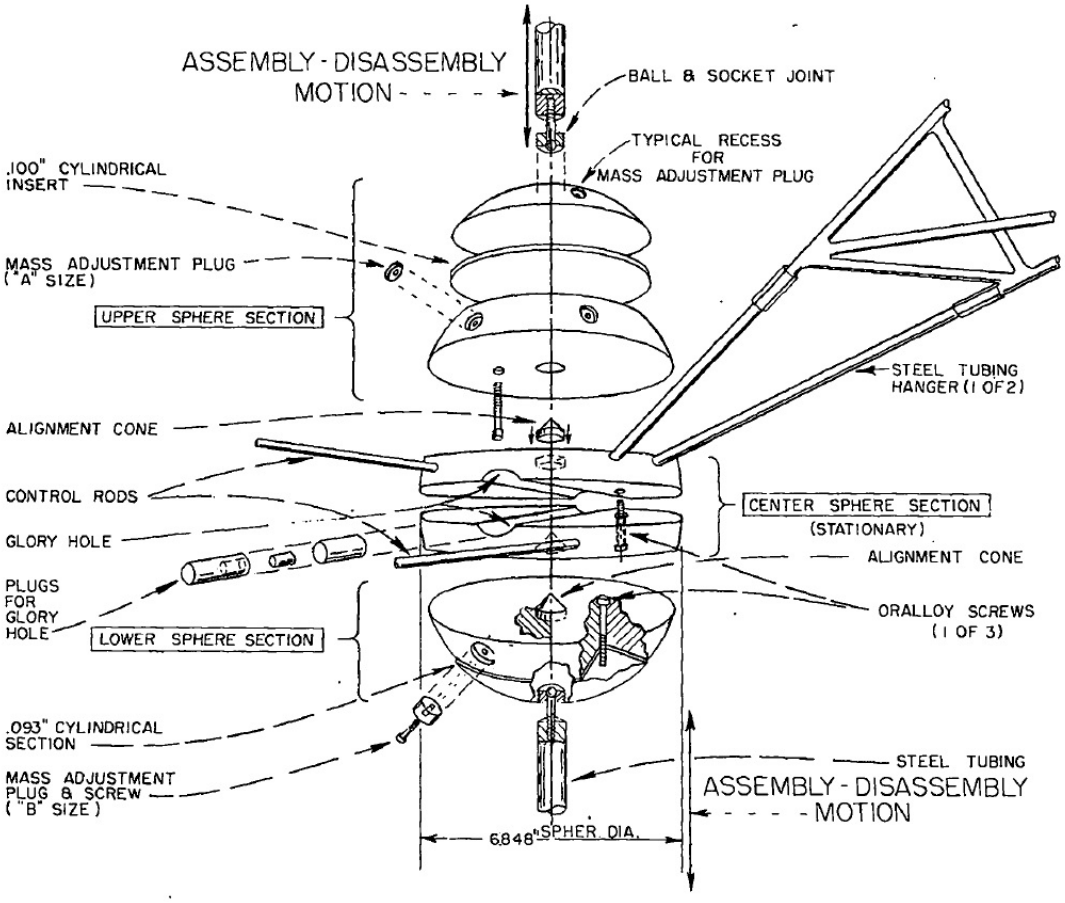

Figure 1.1 View of Lady Godiva Components[1]

Godiva experiments provided much information that supported the design of other FBRs. One element of interest was the measurement of the time constant associated with

[1] Most parts shown are of HEU material. Exceptions are the steel tubing structure and the ball portions of the flexible couplings. The radius of the reactor is 8.697 cm [12].

prompt fission chain reactions, “alpha”, that is essential in predicting the neutron economy in FBRs. LANL scientist used the Rossi and betatron methods to conduct measurements of alpha on the Godiva assembly [12, 13]. Both methods of measurement are challenging, time consuming and face difficulties making measurements during peak reactivity, but academic work continues to improve these experimental measurement techniques [14]. The time constant, “alpha”, is synonymous with the time-eigenvalue, the calculation of which is the focus of this research.

In the years following the burst operation of Godiva, many FBRs were manufactured using lessons learned from the previous designs [2]. In 1964, the cylindrical FBR, MollyG, was placed in operation at WSMR, and is the only remaining FBR of its type in current operation in the United States [3]. Testing of material and system response to intense radiation of short duration is the primary purpose of MollyG [15]. MollyG is a HEU fueled design and produces 35-50 microsecond burst [15, 16]. WSMR is now considering replacing MollyG with a device that meets research requirements but does not carry the overhead of HEU. MollyG serves as the base design for the neutron transport calculations of this research and an adequate LEU replacement is the ultimate material goal.

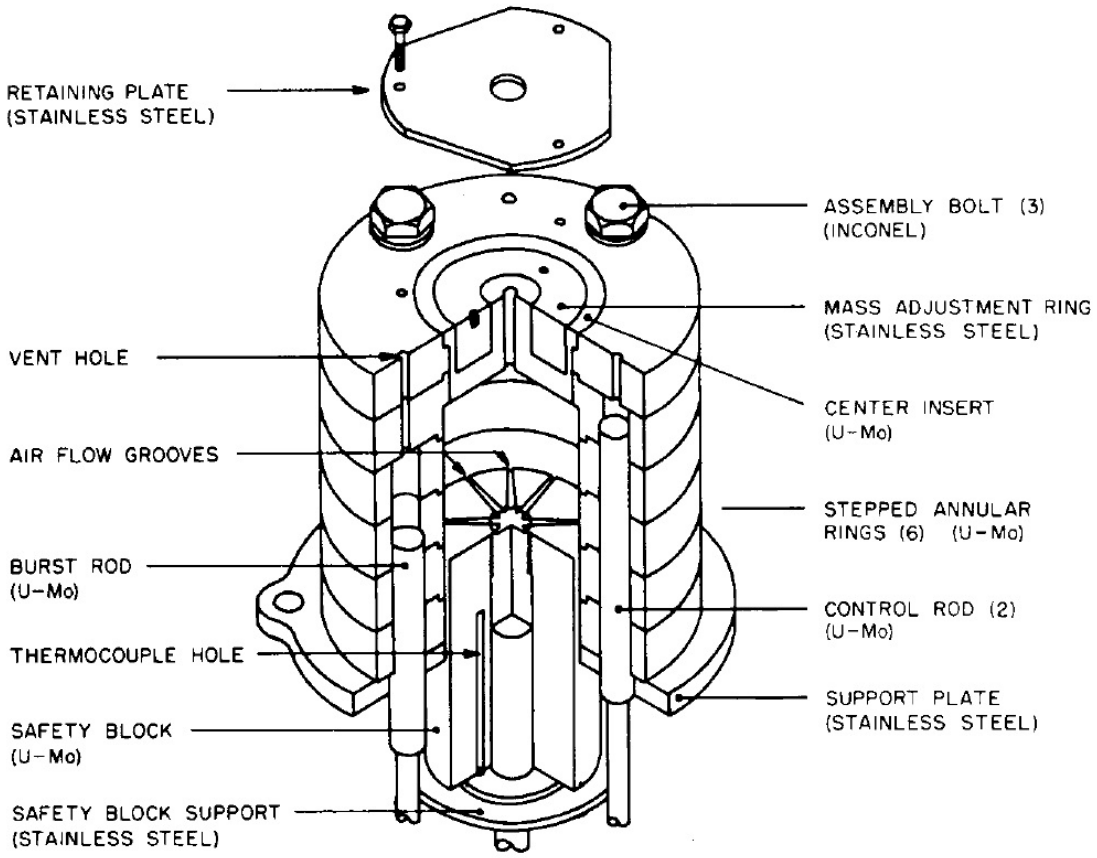

Figure 1.2 View of MollyG Components[1]

Also in 1964, the Lawrence Radiation Laboratory (LRL) designed LEU FBR Super Kukla, went into operation [2]. This LEU design achieved sub millisecond burst, but the annular design contained a significant void in the center of the reactor [17, 18]. The void

[1] The assembly bolts are depicted here as, Inconel X, a special high-strength nickel alloy. U-Mo bolts were also fabricated for use, which made the system more homogeneous [2]. The height of the cylindrical core is 19.3 cm and the radius is 10.3 cm [15].

was desirable for experiments requiring exposure to a high neutron flux, but is likely to have increased the pulse width significantly.

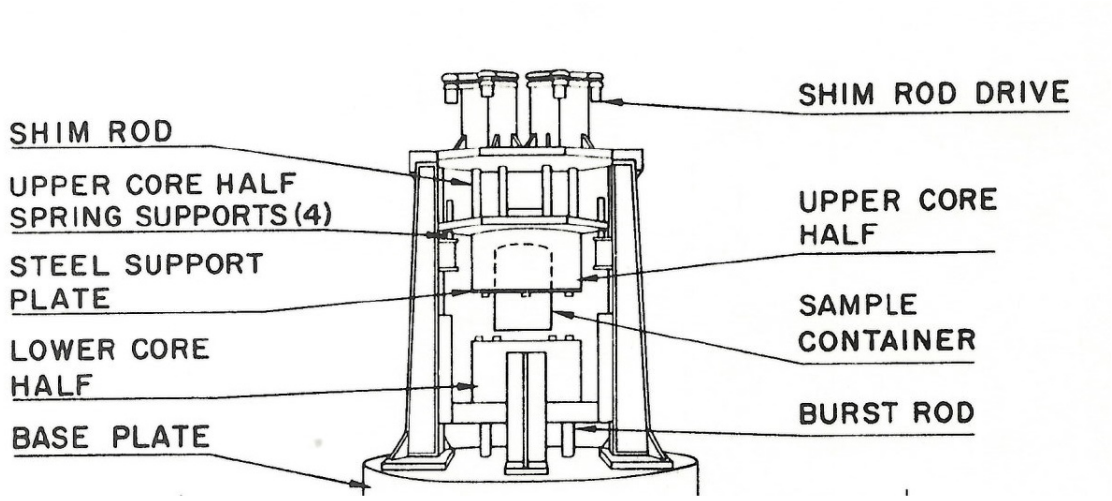

Figure 1.3 View of Super Kukla Components[1]

The HEU fueled Sandia Pulsed Reactor III (SPR III), also an annular design, was of a more modern design, and went into operation in 1975, but was decommissioned in 2006 [19, 3]. SPR III was the latest FBR designed and built in the U.S., which translates to a time lag of over 40 years in the field of development and design of FBRs. Research related to FBRs has continued over this period, but often relies heavily on empirical data obtained from reactor operation [20].

[1] The core element of Super Kukla was 38.1 cm in radius and 93.98 cm in height. This measurement includes the sample container of 22.86 cm in radius and 60.96 cm in height [18].

Computational Methods

The small number of reactors and their highly specialized purpose limit academic work in the field of FBR neutronic calculations. Recent research in predictive modeling tends to focus on physics other than neutronics using only a diffusion approximation and the multiplication factor, *k*, to calculate the neutronic contributions [20, 21]. These trends make the neutronics contribution to FBR modeling the area most needing refinement [21].

Current trends in engineering, fiscal constraints and an appreciation for safety make it unlikely that the incremental development and improvements of multiple FBRs that existed in the 1950s and 60s will be acceptable for developing a new FBR. Extensive computational modeling will certainly be required prior to building a new FBR. Fortunately, computational methods have improved since 1975. Many of these improvements have applicability to FBR design. Computational hardware improvements alone represent a significant improvement in capability over what was commonly available in 1975. In addition to hardware improvements, scholars and scientists have developed many schemes to calculate the time-eigenvalue. The fundamental time-eigenvalue translates to the inverse period of an FBR and is very useful in describing the transient nature of a FBR [22]. Solution of the time-eigenvalue is complicated by the fact that the fundamental mode is not the dominant eigenvalue of the system, but instead the algebraically largest. This characteristic increases the computational effort required to calculate the time-eigenvalue over a more familiar, *k*-eigenvalue calculation. This has often resulted in using *k*-eigenvalue calculations as the recommended technique to solve most neutronic problems [23].

The LANL Monte Carlo N-Particle (MCNP) code does not have a standard feature to calculate the time-eigenvalue [24]. However, Monte Carlo methods, some using MCNP, are available to calculate the time-eigenvalue, but the methods are time consuming and do not readily support coupling with other physics [25, 26]. Deterministic methods often attempt to calculate the time-eigenvalue through modification of solvers designed to determine the multiplication factor, *k*, of a system [27, 28]. These modified *k* solvers require many complete *k* calculations to arrive at a converged time-eigenvalue [29]. Other techniques tend to manipulate algebraically the time-eigenvalue to a form suitable for solution by a traditional power iteration [30]. Other methods use the robust Arnoldi Package (ARPACK) to solve for all modes the time-eigenvalues [31]. Unfortunately, the previous two methods result in a form of the equation that requires the reciprocal of the eigenvalue for solution, which causes complications in near critical systems where the fundamental mode is near or equal to zero. Researches have made few attempts to solve the even-parity transport equation due to the inherent nonlinear nature of these forms of the time-eigenvalue problem [31]. Lathouwers used ARPACK to solve the P_1 even-parity time-eigenvalue problem. His method required calculating both the even and odd fluxes, which diminishes some of the advantage of the even-parity form, and required the reciprocal of the eigenvalue [32]. The LANL code, NIKE, uses the even-parity form of the transport equation and calculates the fundamental mode of the time-eigenvalue problem. The NIKE solution method is a Preconditioned Conjugate Gradient (PCG). The fundamental mode of the time-eigenvalue, α, is approximated by a time step ratio of neutron population,

$$\alpha_t \approx \frac{1}{\Delta t} \ln\left(\frac{n_t}{n_{t-1}}\right). \tag{1-1}$$

In this case, NIKE approximates α dynamically and does not directly solve for α as part of the transport equation[1] [33]. The NIKE code is the most similar to the codes used in this work. Unfortunately, it is not available at this time for comparison calculations [34]. Additionally, the NIKE method for determining the time-eigenvalue is significantly different from the methods presented in this work. In 2013, Fichtl and Warsa of LANL presented results of first order transport time-eigenvalue calculations [29]. These calculations utilized a S_N method that initialized the nonlinear method using indirect methods described above. Specifically, they used a modified *k* solver that at least occasionally resulted in solving for other than the fundamental mode. Although the methods were not the same as the ones used in this work, they serve as a good proof of concept for utilizing nonlinear solvers for time-eigenvalue calculations. At this time, there seems to be no published method of directly solving for the time-eigenvalue of the diffusion equation, or that takes advantage of the efficiencies of the even-parity, second order form of the transport equation.

Nonlinear solution techniques used to efficiently solve for the dominate eigenvalue of a matrix have shown great applicability in solving for the neutron multiplication factor,

[1] NIKE seems to be the most similar code to the one developed in this research. Unfortunately, the NIKE code is not available from RSICC, and as a result, no comparative calculations are available for inclusion in this research [34].

k [35, 7, 8, 36, 37]. These nonlinear solution methods have proven successful in coupling multi-physics problems into a single solution routine [9]. As mentioned previously in this section, the time-eigenvalue is of great importance to the prompt fission chain reaction of FBRs. Although the time-eigenvalue is inherently more computationally intensive than a *k* calculation, these modern non-linear solution techniques when computed on modern equipment show great promise in providing robust time-eigenvalue calculations that will provide the refinement necessary to model predictively, the inherently transient neutron behavior in FBRs. Additionally, these methods are inherently suited to address the non-linear nature of the time-eigenvalue problem of the diffusion equation and even-parity form of the transport equation.

Methodology

This work first solves the one-dimensional, time-dependent neutron diffusion equation in spherical coordinates,

$$\frac{1}{\mathrm{v}}\frac{\partial \phi}{\partial t} = \nu\sigma_f\,\phi - \sigma_a\,\phi + D\left(\frac{\partial^2 \phi}{\partial r^2} + \frac{2}{r}\frac{\partial \phi}{\partial r}\right) \tag{1-2}$$

where,

- v ≡ neutron velocity
- ϕ ≡ scalar flux
- t ≡ time variable
- ν ≡ mean number of neutrons per fission

- $\sigma_f \equiv$ macroscopic fission cross-section
- $\sigma_a \equiv$ macroscopic absorption cross-section
- $D \equiv$ diffusion coefficient $= \frac{1}{3\left(\sigma_{tr}+\frac{\alpha}{v}\right)}$
- $r \equiv$ radial spatial variable,

both analytically and numerically (see appendix D) [38]. The purpose of the analytical solution is to facilitate study of the nature of the associated eigen-functions, and verify the solution techniques of the numerical equation.

For simplicity, the spatial discretization of the numerical equation is finite difference. The numerical equation is solved using a FORTRAN code, the Jacobian Free Newton-Krylov (JFNK) Alpha, and *k* Eigen-value Solver (JAKES) written to support this work. JAKES calculates the fundamental mode of the time-eigenvalue (α), using a three-stage standard power iteration, see Figure 3.6, and by a Newton-Krylov nonlinear method, see Figure 5.3. The power iteration algorithm is original to JAKES, and is straightforward and simple to implement. The primary purpose of the power iteration routine is to provide understanding of the problem during development and to serve as preconditioner to ensure the nonlinear solver converges to the fundamental mode. JAKES also contains *k* eigen-solvers. The nonlinear solvers can also use the *k* solution to initialize the routine and ensure convergence to the fundamental alpha mode. Additionally, the *k* solution, when combined with the alpha solution, provides an estimate to the neutron lifetime, *l*. JAKES obtains its nonlinear solver capability through solution modules that incorporate the Argonne National Laboratory (ANL) code Portable, Extensible Toolkit for Scientific Computation (PETSc).

This solver package is chosen for its FORTRAN interfaces, robust linear and nonlinear solution routines as well as an inherent, but optional parallel computing capability [39, 40, 41].

The primary purpose of the one-dimensional code is to verify the solution techniques. The Lady Godiva design will serve as the basis for the one-dimensional test cases. The one-dimensional case only considers homogeneous uranium fuel. One-dimensional calculations use spherical coordinates to provide immediate utility to FBR calculations at the cost of incrementally developing to a three-dimensional code in Cartesian coordinates.

JAKES then applies the one-dimensional solution techniques to solve the time-eigenvalue, even-parity neutron transport equation,

$$\left(\hat{\mathbf{\Omega}}\cdot\nabla\right)\frac{1}{\left[\frac{\alpha}{\mathrm{v}}+\sigma\right]}\left(\hat{\mathbf{\Omega}}\cdot\nabla\right)\psi^{+}-\sigma\psi^{+}+Q=\frac{\alpha}{\mathrm{v}}\psi^{+} \tag{1-3}$$

- $\alpha \equiv$ time-eigenvalue
- $\sigma \equiv$ total macroscopic cross-section
- $\hat{\mathbf{\Omega}} \equiv$ directional unit vector
- $\psi^{+} \equiv$ the even-parity angular flux (time-independent)
- $Q \equiv$ combined source terms (scattering and prompt fission)

in cylindrical (*r*-*z*) geometry, see appendix E. The time-eigenvalue, even-parity form of the transport equation is clearly nonlinear in α, and requires special techniques to solve [31]. However, the even-parity form has several advantages [23, 42, 43, 44]:

- requires calculation of only half the angular domain
- spatial and angular matrices are suitable for direct solvers
- provides the scalar flux directly.

A commonly perceived disadvantage of the even-parity form is poor performance in voids ($\sigma \cong 0$), due to the $1/\sigma$ term of the equation [43, 44]. However, the FBR design considered here is for a possible LEU replace of MollyG which is a cylindrical design with few relatively small voids in the actual system, making even-parity a suitable form[1].

The neutron transport program EVEn-parity Neutron Transport (EVENT) supports this work by incorporating the solution methods of JAKES developed in the one-dimensional case. By using EVENT, the research gains the benefit of using a previously benchmarked three-dimensional, finite element, spherical harmonics even-parity neutral particle transport code. EVENT is a FORTRAN code capable of handling anisotropic scattering and up scatter. The code is capable of solving for the *k*-eigenvalue, and has a preprocessor for the front-end data processing that can take many different multi-group cross-

[1] The addition of α/v to σ in the even-parity time-eigenvalue equation is expected to also reduce problems associated in voids, especially when modeling FBR transients where alpha is equal to zero only for a short time.

section formats. The two-dimensional cylindrical (*r*-*z*) geometry is resident in the code as well [42, 44, 45]. EVENT gains the capability to solve time-eigenvalues from this research[1].

The research considers two-fuel types of varying uranium enrichments in the two-dimensional case. The first is a uranium fuel alloyed with 10% moly. MollyG uses 10% moly fuel, and Super Kukla used the same when in operation, both with good durability [15, 17]. The second is a 1.5% moly alloy. Godiva IV used a 1.5% moly alloyed HEU fuel, and LANL is currently considering a 1.5% moly alloy for use in a proposed LEU Burst reactor design [46, 47]. The reduction in mass and volume required for a 1.5% moly alloy reduces the burst duration from that obtained using the 10% moly alloy.

This work uses MCNP calculations with the kinetics option to assist in scoping and validating designs, and new computational methods [24]. Data from the operation of Lady Godiva, MollyG, Super Kukla, and other reactors also support validation efforts of the research. The commercial code Mathematica provides assistance in analytical development, data processing and graphing [48]. All numerical calculations are conducted on office type laptops, and desktops using Linux or Unix based operating systems.

[1] EVENT also gains a GMRES linear solver as an option for use in its other routines, and the ability to run parallel processing from the incorporation of PETSc to the code.

Chapter 2

FBR Theory

Basic Design and Operation

This work considers FBRs that generate a burst of neutrons by a large step increase of reactivity into a subcritical system resulting in a short duration of super-critical operation. The FBRs considered are self-limiting by thermal expansion and quickly return to a sub-critical state. The insertion of a burst rod consisting of fuel rapidly increases reactivity. Burst reactors do not typically incorporate *poisons* for control of the reactor. Instead, control systems reduce reactivity by the removal of fuel rather than insertion of a poison. FBRs tend to operate on the 10s of microseconds to millisecond timeframes. These short excursions do not allow the delayed neutrons to contribute to the generation of the burst. However, the delayed neutrons resulting from the super-critical excursion will contribute to post burst heating and a slower decay of the burst when compared to the rise of the burst. The FBRs of interest have a shock induced disassembly mechanism to "clip" the tail of the burst, and avoid continued heating and slow decay due to delayed neutrons [11, 49, 50]. Figure 2.1 depicts a burst from a FBR with a tailed burst (solid line) and a tailless or clipped burst. The solid line depicts the result of a burst terminated only by thermal expansion. The dashed line depicts the burst if the reactor uses a shock-induced disassembly to negate the delayed neutron effects. The tailless burst contains only a prompt neutron contribution (see Appendix B).

The primary effort of this work is to study a potential replacement for MollyG, and thus focuses efforts on solid (without "glory holes") cylindrical and spherical designs with a shock induced disassembly mechanism to produce a tailless burst. Strictly speaking, Godiva (the model for the one-dimensional case) did not have a shock induced disassembly mechanism when in operation. However, since the goal is to replace FBRs that do, only a prompt burst is calculated.[1]

[1] The burst duration of interest is in the range of microseconds. The shortest-lived delayed neutron precursors have a half-life in the range of a tenth of a second [67]. There is no time in normal operation of the reactors of interest for a delayed-neutron contribution.

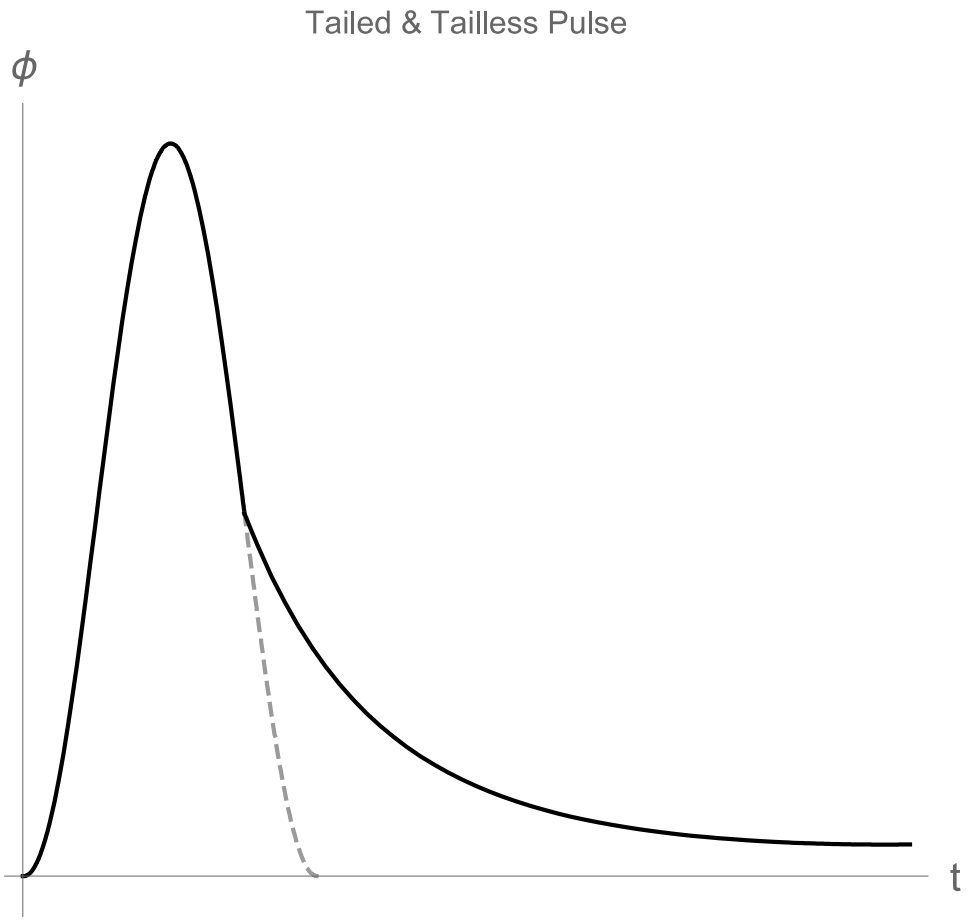

Figure 2.1 Comparison of a Tailed and Tailless Burst

The alpha parameter

FBRs operate in a transient condition for a short time period with a rapidly changing neutron population. To begin study of these types of reactors it is beneficial to consider the neutron density of a system as a function of time, $n(t)$. The time-dependent behavior of the system is described by [51],

$$\frac{d\,n(t)}{dt} \equiv \lim_{\Delta t \to 0} \frac{n(t+\Delta t) - n(t)}{\Delta t}. \qquad (2\text{-}1)$$

For relatively small Δt, equation (2-1) is approximated by,

$$\frac{d\,n(t)}{dt} \cong \frac{n(t+\Delta t) - n(t)}{\Delta t}. \tag{2-2}$$

The prompt neutron lifetimes in an FBR are on the orders of $10^{-6} - 10^{-9}$ seconds, depending on the material makeup and geometry [52, 53, 24, 54].

For a system containing fissile material, assume there is a multiplication factor, *k*, for the entire system that depends on the average prompt neutron lifetime, *l*. That is, for every neutron lost, the system produces *k* neutrons in return. Therefore, for every time-step of *l*, the neutron population changes by a factor of *k*. Substituting the values of *k* and *l* into equation (2-2) gives,

$$\frac{d\,n(t)}{dt} \cong \frac{n(t+l) - n(t)}{l} = \frac{k\,n(t) - n(t)}{l} = n(t)\left[\frac{k-1}{l}\right]. \tag{2-3}$$

Using this approximation provides the differential equation,

$$\frac{d\,n(t)}{dt} = n(t)\left[\frac{k-1}{l}\right]. \tag{2-4}$$

With a solution of [54],

$$n(t) = n(0)e^{\left[\frac{k-1}{l}\right]t}. \tag{2-5}$$

We now define the alpha parameter of the system as [55][1],

$$\alpha \equiv \frac{k-1}{l}. \tag{2-6}$$

The scalar flux, $\phi(r,t)$ is equal to neutron density, $n(r,t)$, multiplied by the neutron speed. Therefore, the time dependence of scalar flux must be,

$$\phi(r,t) = \phi(r,0)e^{\alpha t} \tag{2-7}$$

A similar relation exist between the angular neutron density, $N(r,\hat{\boldsymbol{\Omega}},t)$, and the angular flux, $\psi(r,\hat{\boldsymbol{\Omega}},t)$ [56, 23],

$$\psi\left(r,\hat{\boldsymbol{\Omega}},t\right) = \psi(r,\hat{\boldsymbol{\Omega}},0)e^{\alpha t} \tag{2-8}$$

This work uses solutions to the flux of the forms found in equations (2-7), and (2-8) to derive both the diffusion and even-parity transport time-eigenvalue equations (see Appendix D and Appendix E). Solving for alpha is fundamental to the use of the flux solution and is the primary focus of effort in this research. Alpha is also useful in its own right in describing the burst characteristics of an FBR.

---

[1] Inspection of equation (2-6) gives some indication of why the parameter alpha is often of less interest than *k*. Given a typical thermal power reactor operating near critical, $k \cong 1$, the effective neutron lifetime is ~0.1 seconds making $\alpha \cong 0.0$ [38]. However, in the case of a FBR a prompt super-critical state is required to generate a burst, and the neutron lifetime is on the order of micro to nanoseconds, making alpha a much more significant factor [24, 1].

Equations (2-7) and (2-8) establish the asymptotic, time-dependent, neutronic, solution (see Figure 2.2). When alpha is positive the neutron population increases with time. When equal to zero the population remains the same, and the neutron population will decrease with time when alpha is negative [23].

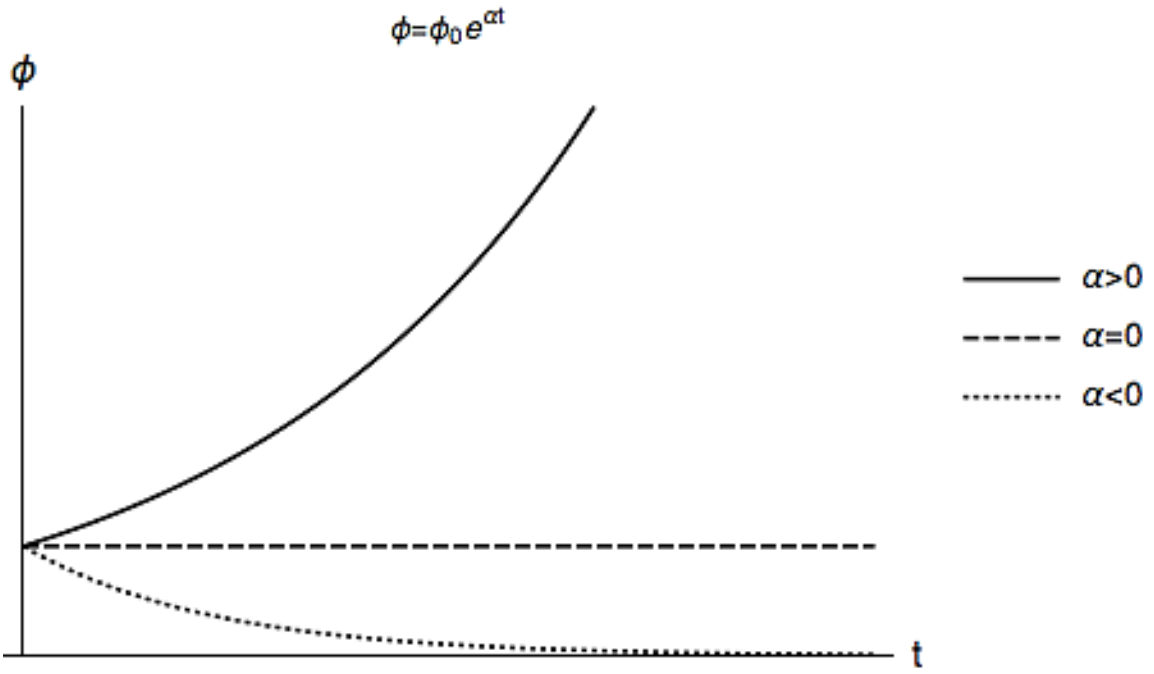

Figure 2.2 The Asymptotic Behavior of Scalar flux

The alpha and *k* Relationship

Equation (2-5) and the definition found in equation (2-6) show that the relationship of alpha to the neutron population with respect to time shown in Figure 2.2 equates to *k* values of greater that one, one and less than one respectively (see Table 2.1). It is also helpful in establishing the solution techniques of Chapter 5 to study another method of describing the time dependent behavior of the neutron population of a system that uses the concepts of *neutron generations* and the multiplication factor *k*.

Table 2.1 Relation of α and *k* to Criticality

	Subcritical	Critical	Supercritical
α	$\alpha < 0$	$\alpha = 0$	$\alpha > 0$
k	$k < 1$	$k = 1$	$k > 1$

The concept of neutron generations can also derive equation (2-5) from a different perspective that is also appropriate for FBRs operating with a *k* value near unity. If the generation zero is defined as,

$$n(0) \equiv \text{neutron population of genertation zero} \tag{2-9}$$

then the population of subsequent generations is given by,

$$k\, n(0) = \text{neutron population of generation one} \tag{2-10}$$

$$k^2 n(0) = \text{neutron population of generation two}$$

$$k^{gen} n(0) = \text{nuetron population of generation } s.$$

Equation (2-11) now describes the time dependent neutron population [57].

$$n(t) = n(0)k^{gen} \tag{2-11}$$

Equation (2-12) determines the scalar flux using the same relationships of the previous section.

$$\phi(r,t) = \phi(r,0)k^{gen} \tag{2-12}$$

Figure 2.3 shows a graphic comparison of the two solution methods. The asymptotic solution allows for neutron production throughout the time step and is used to model

prompt critical and transient systems [54]. The *k* based generation model only allows for neutron production at the end of a time-step. This effectively produces a steady-state solution between time-steps, and steady-state systems that operate with relatively long neutron lifetimes often use this method to model mild transients [58].

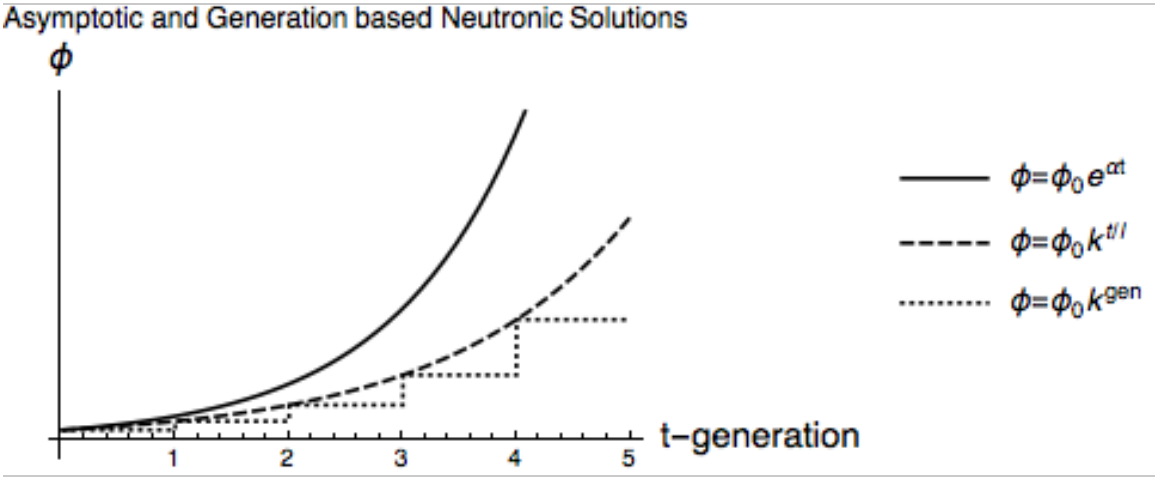

Figure 2.3 Asymptotic and Generational Neutronic Solution Comparison

On average the time when the generation, *gen*, is born is,

$$t = gen \cdot l. \tag{2-13}$$

Solving equation (2-13) for *gen* and substituting in to the last line entry of equation (2-13), the neutron population as a function of time is now,

$$n(t) = n(0)k^{t/l}. \tag{2-14}$$

Logarithmic identities [51] transform equation (2-14) to,

$$n(t) = n(0)\, e^{[\left(\frac{t}{l}\right)\ln(k)]}. \tag{2-15}$$

Expanding ln(*k*) by Taylor series about one [59, 51] provides equation (2-16).

$$\ln(k) = (k-1) + \text{higher order terms.} \tag{2-16}$$

If k is close to one then

$$\ln(k) \cong k - 1. \tag{2-17}$$

Substituting equation (2-17) into equation (2-15) again provides equation (2-5) [57].[1] This relationship between the asymptotic and steady state solutions for near critical systems proves useful in initializing the non-linear solution method described in Chapter 5.

It is important to understand some things about the time dependence on the neutron population:

1. The depiction of neutron population in Figure 2.3 is not spatially dependent. It only represents the magnitude of the flux. The spatial flux profile is largely independent of time and identical for all of the solution schemes presented in this section. Chapter 3 shows this in detail.

2. The solutions are all equivalent for k = 1 and alpha = 0. However, nothing can be determined about the lifetime based on decay or multiplication of the neutron population under this condition.

3. The same generational assumption of time dependence is the root of all the solutions presented. However, the asymptotic is the least restrictive and most accurate for describing transients.

---

[1] *Generations per second* often describes alpha, presumably due to this derivation method.

The asymptotic solution allows for not only the creation of neutrons between time steps, but also allows those neutrons to contribute to multiplication. The concept of compounding is useful in explaining this effect. Let the lifetimes of equations (2-5) and (2-14) be independent of each other and set the equations equal to each other.

$$n(0)e^{\left[\frac{k-1}{l_\alpha}\right]t} = n(0)k^{t/l_k} \tag{2-18}$$

Now solve for the ratio of l_α/l_k

$$l_\alpha/l_k = \frac{(k-1)}{\ln(k)} \tag{2-19}$$

Plotting (2-19) shows that if $l_k$is reduced by this proportion with respect to l_α the solution are identical. This is because equation (2-14) now is able to compound the neutron multiplication at a faster rate. Figure 1.1 shows that this effect becomes more prominent as *k* increases.

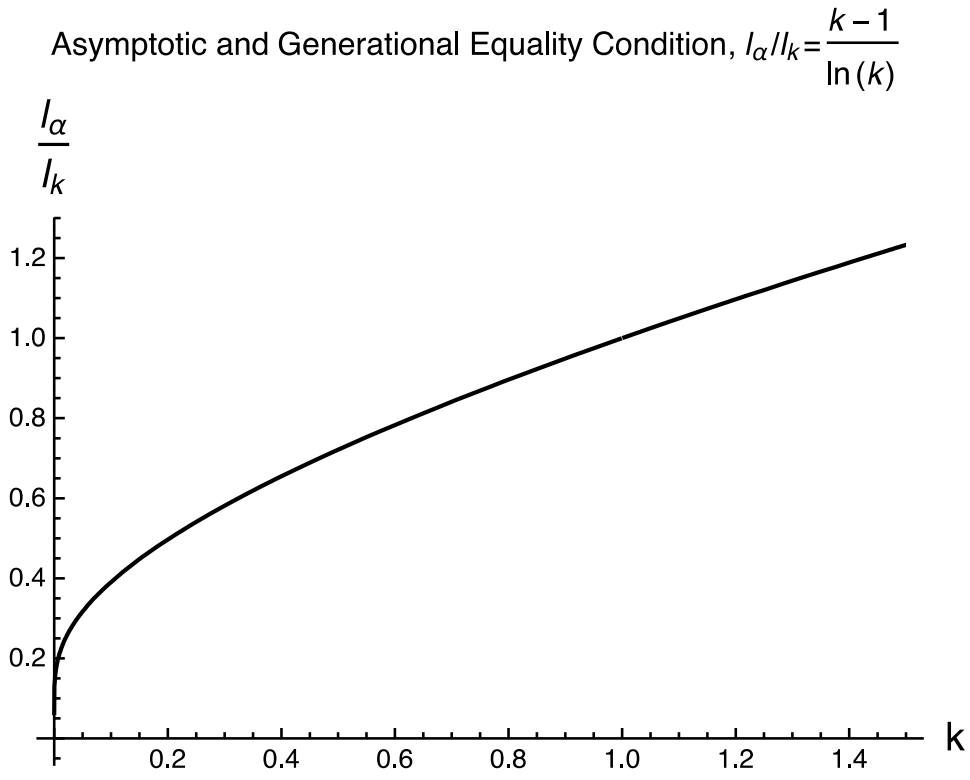

Figure 2.4 Compounding Effect of the Neutron Population

FBRs typically produce 10^{16}-10^{18} fissions in a timeframe of 35 microseconds to a millisecond [2]. These numbers are not obtainable without an exponential rise in neutron population. Therefore, for modeling FBRs, the asymptotic solution is the most appropriate. In order to use the asymptotic solution to the neutron flux calculation of alpha is required and that is the primary computational effort of this research.

The Nordheim-Fuchs Model

The Nordheim-Fuchs model describes self-limiting excursions that take place in a short enough amount of time that all neutron sources except prompt fission neutrons are neglected [22]. This description matches the subject FBRs exactly. The following

equation describes this type of system (which is identical to equation (2-4) in the preceding section),

$$\frac{d\,n}{dt} = n\left[\frac{k-1}{l}\right] = n\,\alpha\,. \tag{2-20}$$

An immediately useful derivation from the Nordheim-Fuchs model is an equation for determining the burst width of an excursion, Full Width at Half Maximum (FWHM) [2, 49, 22, 1].

$$FWHM \equiv \tau = \frac{3.524}{\alpha_0} \tag{2-21}$$

Additionally, peak power is determined by,

$$\phi_{\text{peak}} = \frac{{\alpha_0}^2\, l\, k_0}{2\Theta}\,. \tag{2-22}$$

Where,

- $l \equiv$ the prompt neutron lifetime
- $\Theta \equiv$ energy coefficient of feedback reactivity [22]
- α_0 & k_0 are the peak values

The codes developed in this work will include *k* calculations as well as alpha in order to determine the neutron lifetime using equation (2-6) and ultimately determine the peak of the pulse using equation (2-22). Alpha alone is all that is required to determine the FWHM by equation (2-21).

The results of the alpha and *k* calculations developed in later chapters are used to determine the FWHM and peaks of the neutron pulses of the case study FBRs. This combined with the established behavior of an exponential rise will provide the three points necessary to model bursts associated with the FBRs of interest (see Figure 2.5).

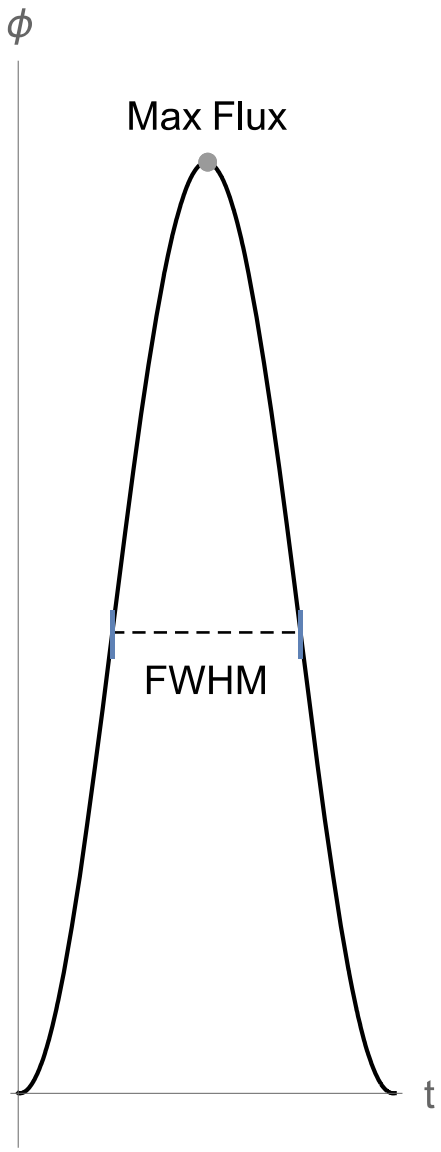

Figure 2.5 Burst Derived from Max Flux and FWHM

Chapter 3

The Neutron Diffusion Equation

A model that includes material and geometrical properties is required to calculate the time-eigenvalue of a FBR and make use of the characterizing equations of the burst provided by the Nordheim-Fuchs model. For simplicity, the neutron diffusion equation is the first method considered.

The time-dependent neutron diffusion equation,

$$\frac{1}{\mathrm{v}}\frac{\partial \phi}{\partial t} = \nu\sigma_f\,\phi - \sigma_a\,\phi + D\,\nabla^2\phi\,, \tag{3-1}$$

simplifies the time-eigenvalue neutronic calculations when compared to the transport equation. This allows for an initial focus on the novel solution methods for the time-eigenvalue required to model the burst of an FBR. The diffusion coefficient, *D*, does, however, replicate the complication of non-linearity of alpha found in the coefficient of the streaming term in the even-parity transport equation, see equations (1-3) and (3-5) and also Appendix D and Appendix E.

The diffusion equation considered consists of a single spatial dimension (one-dimensional). These initial calculations utilize the spherical coordinate system depicted in Figure 3.1 in order to provide practicality to the models, and comparisons to the Godiva FBR. JAKES is capable of solving the system in one-dimensional slab or cylindrical geometries, but these cases include the assumption of at least one infinite spatial dimension.

The spherical coordinate system in one-dimension has no infinity term, and results in a geometry that is possible to build.

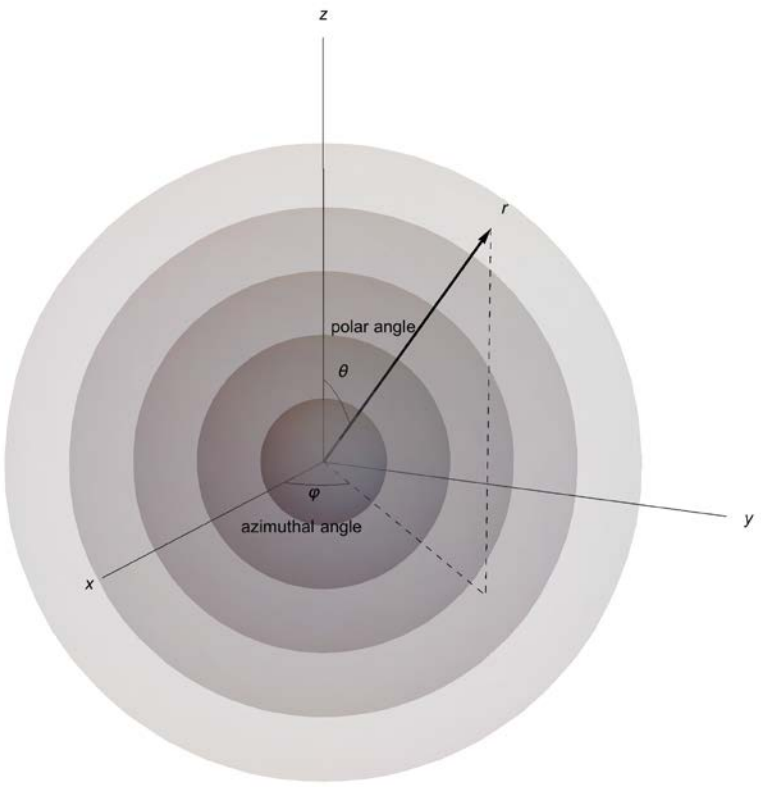

Figure 3.1 Spherical Coordinates[1]

Equation (3-2) gives the *Laplacian* of equation (3-1) in spherical coordinates [59].

$$\nabla^2 = \frac{1}{r^2}\frac{\partial}{\partial r}\left(r^2\frac{\partial \phi}{\partial r}\right) + \frac{1}{r^2\sin\theta}\frac{\partial}{\partial \theta}\left(\sin\theta\frac{\partial \phi}{\partial \theta}\right) + \frac{1}{r^2\sin^2\theta}\frac{\partial^2 \phi}{\partial \varphi^2} \qquad (3\text{-}2)$$

[1] The numerical solution methods of the following section uses the discretized sphere overlaid on the coordinate systems. The analytical solution utilizes a continuous variable in *r*.

For a sphere of homogeneous material, it is reasonable to assume that the flux is only dependent on the radial distance from the center of the sphere, thus reducing equation (3-2) to,

$$\nabla^2 = \frac{1}{r^2}\frac{\partial}{\partial r}\left(r^2\frac{\partial \phi}{\partial r}\right) = \frac{1}{r^2}\left(r^2\frac{\partial^2 \phi}{\partial r^2} + 2r\frac{\partial \phi}{\partial r}\right) = \frac{\partial^2 \phi}{\partial r^2} + \frac{2}{r}\frac{\partial \phi}{\partial r}. \tag{3-3}$$

Substituting equation (3-3) into equation (3-1) gives equations (1-2) and (3-4).

Analytical Solution of the Time-Eigenvalue Diffusion Equation

Solving equation (1-2),

$$\frac{1}{\mathrm{v}}\frac{\partial \phi}{\partial t} = \nu\sigma_f\,\phi - \sigma_a\,\phi + D\left(\frac{\partial^2 \phi}{\partial r^2} + \frac{2}{r}\frac{\partial \phi}{\partial r}\right) \tag{3-4}$$

$$D = \frac{1}{3\left(\sigma_t + \frac{\alpha}{v}\right)} \tag{3-5}$$

by separation of variables provides an infinite set of eigen-pairs of eigenvectors in scalar flux and eigenvalues in alpha.

$$\phi(r,t) = \sum_{n=1}^{\infty} C_n e^{\alpha_n t} \frac{sin\left(\frac{n\pi}{R+2D}r\right)}{r} \quad (3\text{-}6)^1$$

$$\alpha_n = \mathrm{v}D\left[\frac{\sigma_a}{D}\left(\frac{\nu\sigma_f}{\sigma_a} - 1\right) - \left(\frac{n\,\pi}{R+2D}\right)^2\right] \quad (3\text{-}7)$$

Inspection of equation (3-6) reveals that the term dependent on time, $e^{\alpha_n t}$, only acts as a scalar to the shape of the flux, $\frac{sin\left(\frac{n\pi}{R+2D}r\right)}{r}$, determined by geometry and position.

The extrapolated boundary, R + 2D, introduces additional non-linearity to the solution of the diffusion equation. However, since the transport equation does not have this non-linearity, numerical solutions to the diffusion equation in this work do not include the $\frac{\alpha}{v}$ term in the diffusion coefficient used to calculate the extrapolated boundary. Instead, numerical calculations use the extrapolated boundary using the diffusion coefficient for a *k* calculation to improve the validity of solutions and remain consistent with solution methods for even parity transport. This requires adjustments to the analytical solutions used to verify and validate the numerical calculations. In this case, $D_k \equiv \frac{1}{\sigma_{tr}}$, and equation (3-7) becomes,

$$\alpha_n = \mathrm{v}D\left[\frac{\sigma_a}{D}\left(\frac{\nu\sigma_f}{\sigma_a} - 1\right) - \left(\frac{n\,\pi}{R+2D_k}\right)^2\right]. \quad (3\text{-}8)$$

[1] The solution of the scalar flux in equation (3-6) clearly shows the asymptotic dependence in time that was established in Chapter 2, but from a very different approach.

Additionally, the analytical solution used for the flux, or eigenvector is,

$$\phi(r,t) = \sum_{n=1}^{\infty} C_n e^{\alpha_n t} \frac{sin\left(\frac{n\pi}{R+2D_k}r\right)}{r} \tag{3-9}$$

Appendix D provides additional details of the analytical solution as well as motivation for the form used with numerical calculations.

Other than for general interest, this work only considers the fundamental eigen-pair where $n = 1$ for calculation. The fundamental mode is what the Nordheim-Fuchs model requires to model the burst. However, all eigen-pairs contribute the flux shape that the reactor produces. The eigenvalues of typical FBRs are characterized by a single positive eigenvalue (the fundamental mode), and multiple (infinite in the analytical case) negative eigenvalues of increasing magnitude. Figure 3.1 shows the shapes of the first five eigen-pairs of a Godiva like FBR. The constant in equation (3-6) is determined through initial conditions of a physical problem. For illustration purposes, this constant is adjusted to normalize the peak in the center of the sphere.

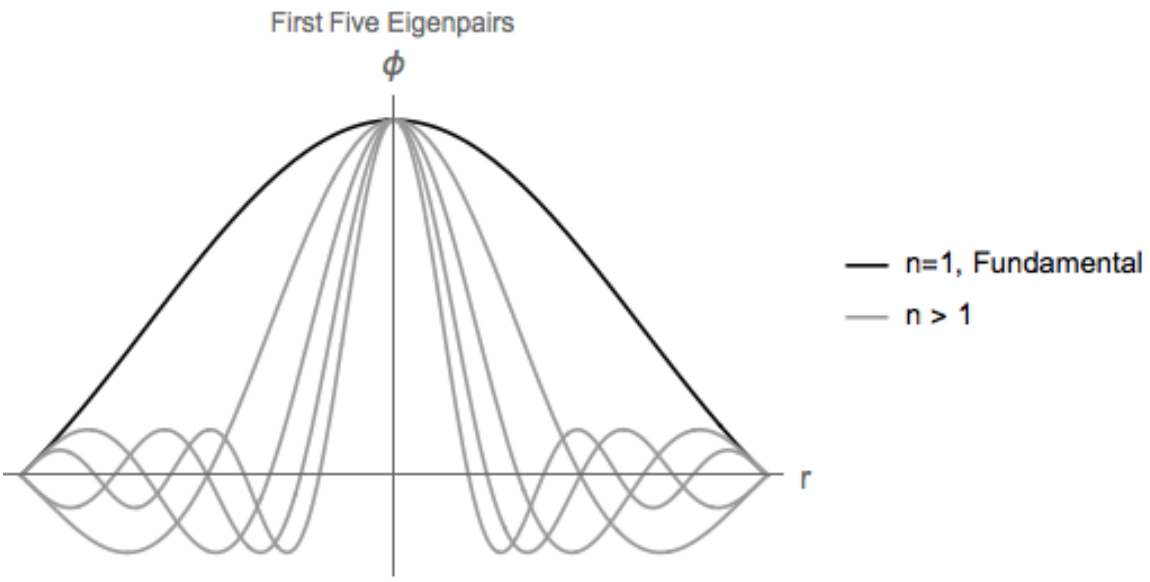

Figure 3.2 First Five Eigen-pairs of a Notional Spherical FBR

Inspection of the exponential in equation (3-6) shows that over time the eigen-pairs associated with negative values of alpha will contribute less and less to the sum that describes the flux. Thus, fundamental node (n = 1) is a good approximation of the neutronics, and this value is best suited for calculations related to the alpha parameter derived in chapter 2. However, FBRs operate on short timescales, and other FBR modeling may require calculation of additional eigen-pairs. Figure 3.2 depicts the flux shape (sum of the first five eigen-pairs) of the same Godiva like FBR used to calculate Figure 3.1, at early and late times of operation.

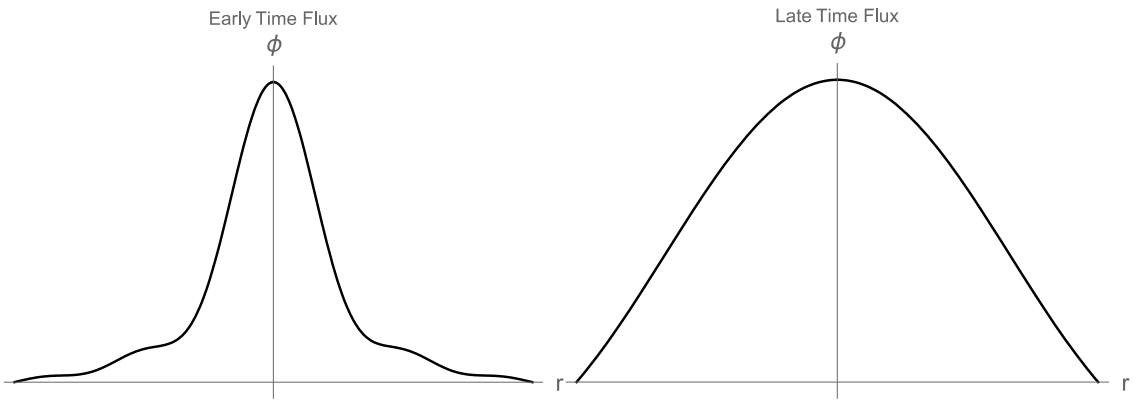

Figure 3.3 Early and Late Time Flux Comparison

The analytical solution to the neutron diffusion equation derived in this section is useful in providing insight into the neutronic behavior of simple FBRs. Additionally, the analytical solution assists in verification of the numerical methods developed in the next section to solve for the time-eigenvalue.

Numerical Solution of the Time-Eigenvalue Diffusion Equation

Derivation and Spatial Discretization

For the numerical case, it is simplest to assume a time-dependent scalar flux solution of the form given by equation (2-7). Substituting equation (2-7), into equation (3-1) provides the time-eigenvalue neutron diffusion equation (see appendix D).

$$D\nabla^2\phi - \sigma_a\,\phi + \nu\,\sigma_f\,\phi = \frac{\alpha}{\mathrm{v}}\phi \tag{3-10}$$

For one-dimensional spherical coordinates equation (3-8)becomes,

$$D\left(\frac{\partial^2\phi}{\partial r^2}+\frac{2}{r}\frac{\partial\phi}{\partial r}\right)\phi-\sigma_a\,\phi+\nu\,\sigma_f\,\phi=\frac{\alpha}{\mathrm{v}}\phi. \tag{3-11}$$

In order to solve the equation the spatial components of the modelled reactor require discretization. Equally dividing the radius that defines the homogenous sphere into equally spaced sections of length Δ accomplishes the task in this simple case. See Figure 3.4.

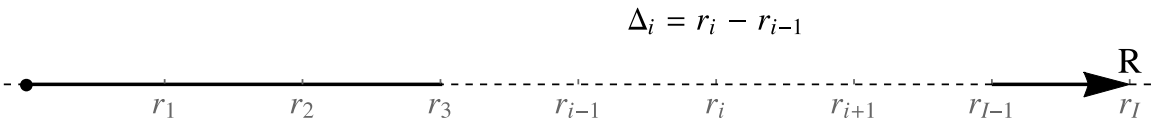

Figure 3.4 One-Dimensional Spherical Spatial Discretization

The resulting discretized geometry is a sphere made up of shells. Figure 3.5 depicts a spherical reactor discretized into five sections[1].

[1] Figure 3.5 is for illustration purposes only. The results in Chapter 6 will show that it is very unlikely that only five spatial cells would produce a numerical result of acceptable accuracy.

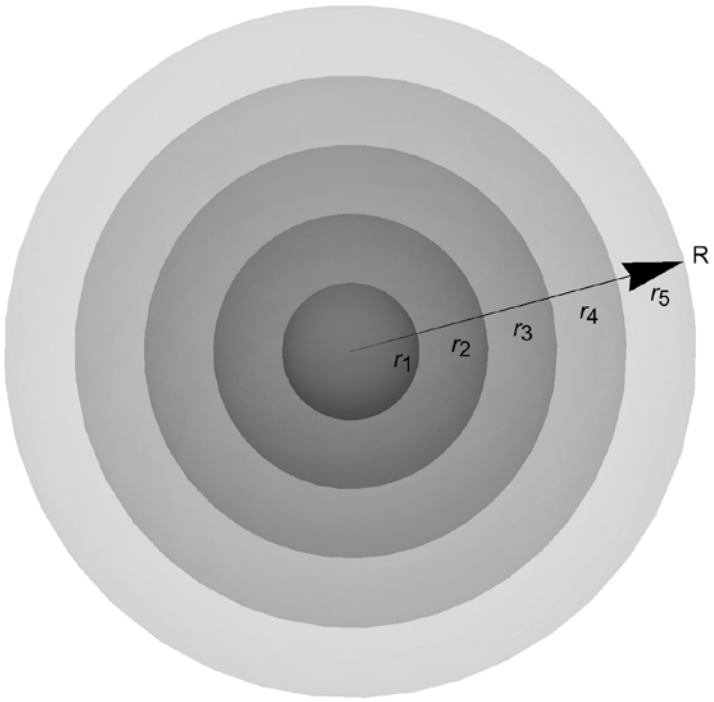

Figure 3.5 Discretized Spherical Reactor

Discretizing spatially using finite difference[1], see Appendix F, transforms equation (3-11) to,

[1] It is not necessary for the entire sphere to be of homogenous material, or that the radius be discretized into equal partitions to accomplish one-dimensional calculations. Changing the material composition for each shell to accommodate modifications such as a reflector, and adjusting the size of shells is easily accomplished by modifying the spatial discretization scheme. However, the physical model for these one-dimensional calculations is Godiva, which was an un-reflected, bare metal, homogeneous, spherical reactor.

$$\frac{\alpha}{\mathrm{v}}\phi_i = \frac{D}{\Delta^2}\left[1-\frac{1}{i}\right]\phi_{i-1} + \left[\bar{\nu}\sigma_f - \sigma_a - \frac{2\,D}{\Delta^2}\right]\phi_i + \frac{D}{\Delta^2}\left[1+\frac{1}{i}\right]\phi_{i+1}. \tag{3-12}$$

Renaming the coefficients in equation (3-12), and moving the velocity term to the left hand side provides a more compact form.

$$\mathrm{v}\left[a_{i,i-1}\,\phi_{i-1} + a_{i,i}\phi_i + a_{i,i+1}\phi_{i+1}\right] = \alpha\,\phi_i \tag{3-13}$$

For boundary conditions of equation (3-13), the physics and symmetry of the system requires the derivative with respect to ϕ equal zero at the origin (reflective), see Figure 3.2 and Figure 3.3.

$$\left.\frac{\mathrm{d}\phi}{\mathrm{d}r}\right|_{r=0} = 0 \Rightarrow a_{1,0} = 0 \tag{3-14}$$

A sphere with a radius of, *R*, with, *I*, cells requires the flux at, *R*, is to be zero (vacuum).

$$\phi_I = 0 \tag{3-15}$$

The numerical system now contains $I - 1$ equations for solution by the techniques to follow [38].

Solution by Power Iteration

Equation (3-13) is now written in matrix form for ease of explaining the power iteration algorithm used for solution.

$$A\,\boldsymbol{\phi} = \alpha\,\boldsymbol{\phi} \tag{3-16}$$

Standard scaled power iteration, using *the method of successive substitution* with the largest resulting value scaled to *one* each iteration solves equation (3-16) for the eigenvector associated with the dominate (largest magnitude) eigenvalue α_{max} [60, 61, 62]. Once the eigenvector has converged to tolerance the dominate eigenvalue is calculated using the Rayleigh Quotient [61].

$$\alpha_{max} = \frac{A\boldsymbol{\phi} \cdot \boldsymbol{\phi}}{\boldsymbol{\phi} \cdot \boldsymbol{\phi}} \tag{3-17}$$

However, unlike a *k* eigenvalue calculation, the dominate eigenvalue does not represent the fundamental mode. For a time-eigenvalue calculation, the algebraically largest eigenvalue is the fundamental mode (see the analytical solution derived Chapter 2, for context). To solve for the fundamental mode, α_{max} , which will certainly be negative, is essentially added to the diagonal of *A*.

$$A - \alpha_{max} I \tag{3-18}$$

This changes the *characteristic equation* of the matrix (see Appendix C) so that all eigenvalues are now such that the dominate eigenvalue λ is related to the fundamental mode of the original problem by,

$$\alpha = \lambda + \alpha_{max}. \tag{3-19}$$

Therefore, the power iteration scheme is repeated again to find λ, and then equation (3-19) is used to find the fundamental mode of the time-eigenvalue problem. Once, this is complete the value for α is substituted into the appropriate coefficients of the matrix *A* in a

fixed-point iteration routine. The entire process is repeated until α has converged to tolerance by fixed-point iteration.

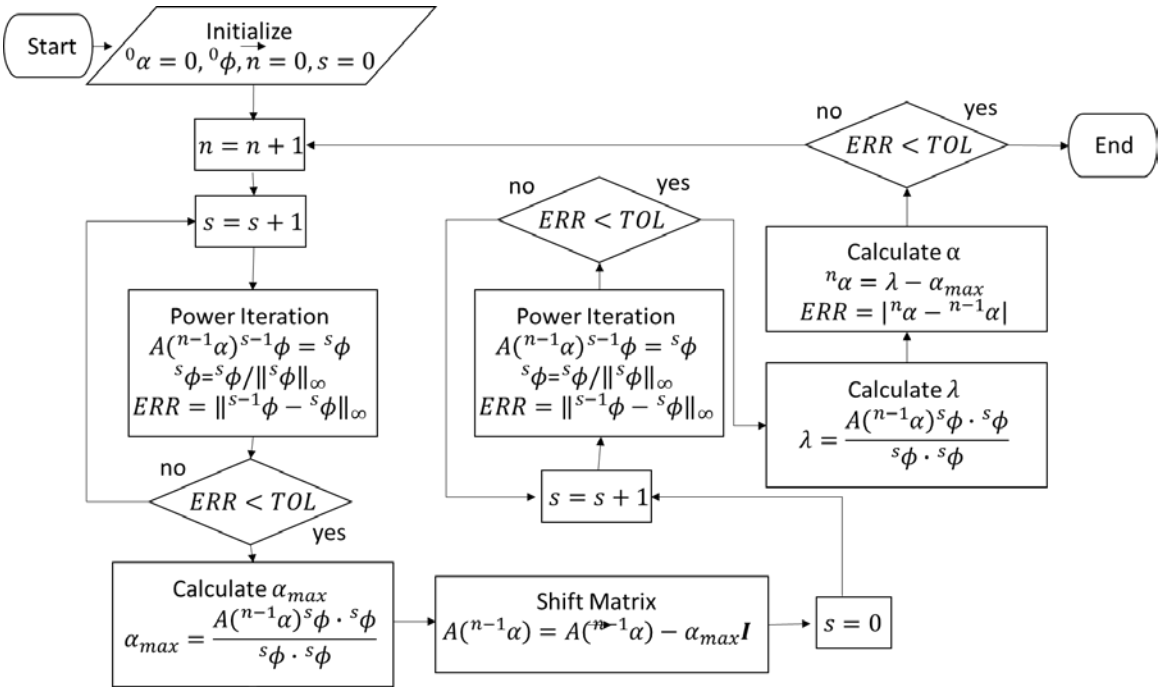

Figure 3.6 Alpha PI Algorithm Flowchart

Chapter 4

The Even-Parity Transport Equation

The even-parity form of the time-eigenvalue transport equation is solved for the two-dimensional case (see Appendix E).

$$\left(\hat{\boldsymbol{\Omega}}\cdot\nabla\right)\frac{1}{\left[\frac{\alpha}{\mathrm{v}}+\sigma\right]}\left(\hat{\boldsymbol{\Omega}}\cdot\nabla\right)\psi^{+}-\sigma\psi^{+}+Q=\frac{\alpha}{\mathrm{v}}\psi^{+} \tag{4-1}$$

The solution of the even-parity transport equation will use two-dimensional cylindrical coordinates (*r*-*z*) depicted in Figure 4.1, for reasons similar to choosing spherical coordinates for the one-dimensional case. This coordinate system will provide practicality to the models, and comparisons to the MolyG FBR. Two-dimensional slab models include the assumption of at least one infinite spatial dimension. The cylindrical coordinate system in two-dimensions has no infinity term, and, as in the one-dimensional case, results in a geometry that is possible to build.

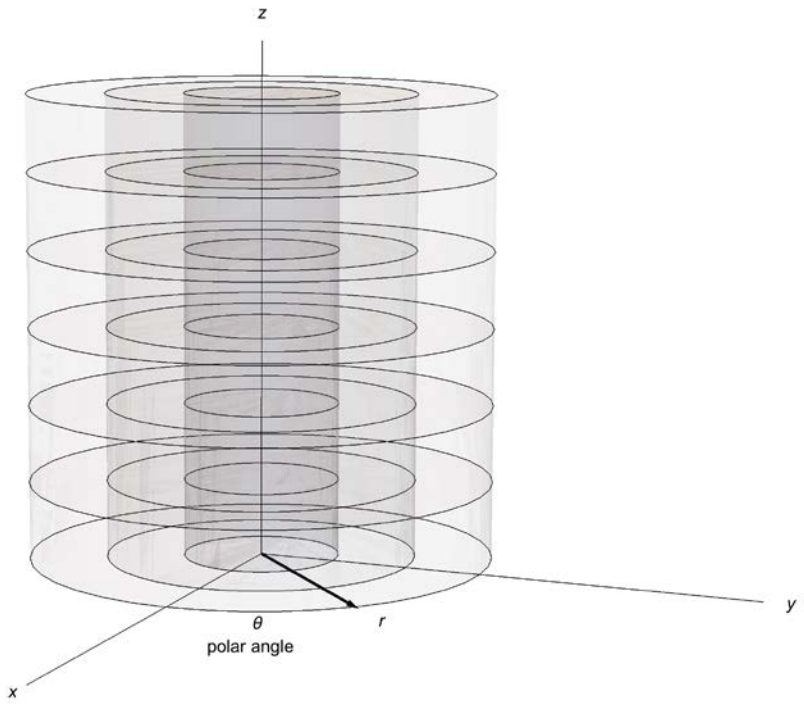

Figure 4.1 Cylindrical Coordinates[1]

Equation (4-2) provides the Laplacian for cylindrical coordinates [59].

$$\nabla^2 = \frac{1}{r}\frac{\partial}{\partial r}\left(r\frac{\partial \phi}{\partial r}\right) + \frac{1}{r^2}\frac{\partial^2 \phi}{\partial \theta^2} + \frac{\partial^2 \phi}{\partial z^2} \tag{4-2}$$

[1] Unfortunately, cylindrical coordinates represent the polar angle similarly to the azimuthal angle of spherical coordinates. This arises from the two-dimensional polar coordinates that serves as the basis for the cylindrical system. The polar coordinate system calculates the polar angle counter-clockwise from the traditional x-axis, or pole.

For the two-dimensional case, the flux has no spatial dependence on the polar angle and the Laplacian reduces to equation

$$\nabla^2 = \frac{1}{r}\frac{\partial}{\partial r}\left(r\frac{\partial \phi}{\partial r}\right) + \frac{\partial^2 \phi}{\partial z^2} = \frac{\partial^2 \phi}{\partial r^2} + \frac{1}{r}\frac{\partial \phi}{\partial r} + \frac{\partial^2 \phi}{\partial z^2}. \quad (4\text{-}3)$$

The neutron transport program EVEn-parity Neutron Transport (EVENT) produces and evaluates the systems of equations that result from the discretization of equation (4-1). EVENT spatially discretizes using finite element techniques. The angle representation is achieved through spherical harmonics. The code contains a capable *k*-eigenvalue, solver that is suitable to initialize the non-linear solver that is presented in Chapter 5. The code has a preprocessor for the front-end data processing that can take many different multi-group cross-section formats. The two-dimensional cylindrical (*r*-*z*) geometry is a longtime capability in EVENT. The details of development and capability of EVENT are subject of many academic and other professional writings, and can be found elsewhere [42, 44, 45]. For this work, the primary use of EVENT is to validate the unique solution methods for time-eigenvalue calculations in a multi-dimensional transport environment.

In setting up the geometry for the EVENT cylindrical calculations, it is useful to do some analysis to ensure the runs are productive. Minimizing the *neutron leakage* is a good nuclear engineering practice. In the spherical case, the radius determines the surface to volume ratio.

$$\frac{sph\ Surf}{sph\ Vol} = \frac{3}{4\,r} \quad (4\text{-}4)$$

However, in the cylindrical case the height and radius determines the ratio.

$$\frac{Cyl\ Surf}{Cyl\ Vol} = \frac{2}{r}\left(1 + \frac{1}{h/r}\right) \quad (4\text{-}5)$$

The plot in Figure 4.2 depicts the surface to volume ratio of a cylinder for a normalized radius. The graph shows that a height to radius ratio of up to ~ one, improves the surface to volume ratio significantly. At about a height to radius ratio of ~ two, the surface to volume ratio continues to improve, but at a diminished rate. The height to radius ratio of Molly G is 1.874 [15]. From diffusion theory, the leakage is minimized by a height of 1.847 times the radius, see Appendix K. This work uses a height to radius ratio of 1.874 for the proposed LEU cylindrical designs. This ratio is expected to maintain a desirable surface to volume ratio as well as reasonable ease of manufacturing and keeps the basic design of MolyG.

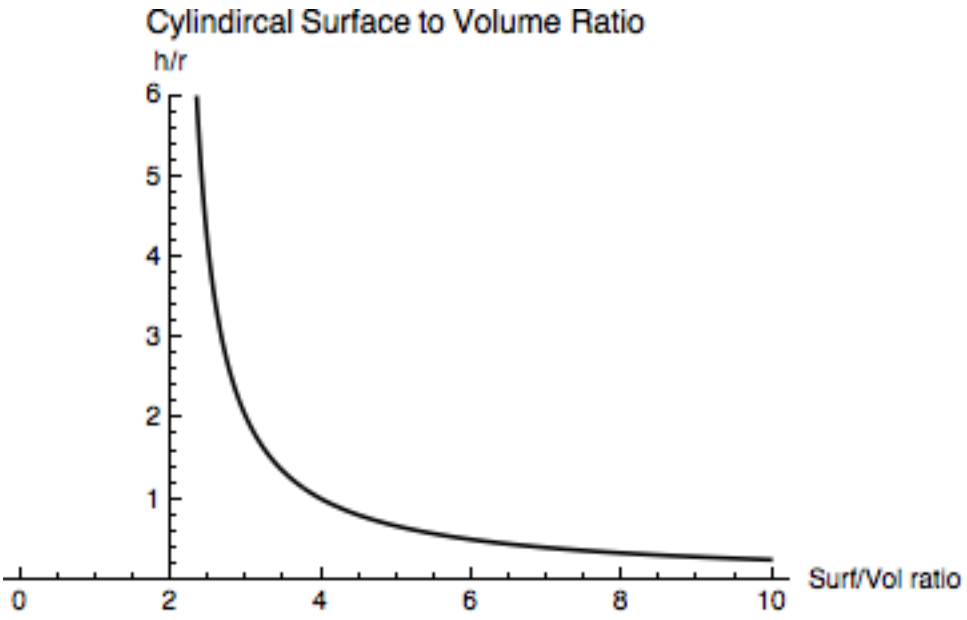

Figure 4.2 Surface to Volume Ratio for a Cylinder

Chapter 5

Non-Linear Solution Method

The power iteration algorithm described in Chapter 3 is over twice the effort of a *k* calculation not counting the required outer fixed-point iterations required to account for the α dependence of the matrix itself. This difficulty alone warrants a search for acceleration methods.

Additionally, as the next chapter will show in detail, the time-eigenvalue problem is *stiff*, ill conditioned, and requires power-iterations on a system with a *dominance ratio* of essentially unity for matrixes of a size required for accuracy. The system is also inherently nonlinear in alpha and the flux (see Appendix J), and warrants a Newton method [63]. These issues make robust nonlinear solution techniques worthy of consideration.

Initialization Methods

The use of nonlinear techniques, specifically Newton's method, does not guarantee convergence to any particular eigen-pair and an adequately accurate starting point is required to arrive at the desired result [7, 29, 64]. This makes the starting point of the routine important to the result. Newton's method is more efficient than most, but efficiency at finding the wrong answer is not desirable. Therefore, the routine uses a coarse power-iteration on alpha, or a *k* calculation to chaperone Newton's methods and guide it to the correct solution set [64].

The full algorithm may use a coarse alpha power iteration, to provide a good start for the nonlinear solver. This is the most intuitive method. However, a *k* calculation is also an option for initialization. The similarity of the time dependent neutron population between the alpha and *k* based solution when $k \sim 1$ and alpha is ~ 0 was presented in Chapter 2. Additionally, the shape of the flux (flux profile) is similar for the steady-state solution as it is for the time-dependent. For an eigenvalue calculation, any scalar of the eigenvector will satisfy the solution [61]. Since the shape is similar and only the magnitude differs between the solution methods over time, a normalized flux from a *k* calculation will serve as excellent initialization solution vector. Combining the calculated *k* eigenvalue with an educated estimate of the neutron lifetime[1], and using equation (2-6) to solve for alpha provides a good initial estimate for alpha.

Newton's Method

The setup of the nonlinear system for solution by Newton's method requires adjustment of equations (3-14) and (3-15) into a set of functions equal to zero[2].

$$F_{\phi}(\boldsymbol{\phi}, \alpha) = A\,\boldsymbol{\phi} - \alpha\,\boldsymbol{\phi} = 0 \tag{5-1}$$

---

[1] 10^{-8} seconds proved an adequate estimate for all calculations used here.

[2] Here the scalar flux is used as a representative solution or eigenvector for simplicity and applicability to the one-dimensional diffusion case. For the even-parity transport solution the solution vector is the moments of ψ^{+}.

$$F_\alpha(\boldsymbol{\phi}, \alpha) = \alpha - \frac{A\boldsymbol{\phi} \cdot \boldsymbol{\phi}}{\boldsymbol{\phi} \cdot \boldsymbol{\phi}} = 0 \tag{5-2}$$

Expanding the non-linear function in the first two terms of a Taylor series about the current solution ${}^{s}\boldsymbol{U}$, where $\boldsymbol{U}$ represents both alpha and the scalar flux of equations (5-1) and (5-2), derives the Newton iteration [8].

$$F({}^{s+1}\boldsymbol{U}) = F({}^{s}\boldsymbol{U}) + \frac{\partial F({}^{s}\boldsymbol{U})}{\partial {}^{s}\boldsymbol{U}}({}^{s+1}\boldsymbol{U} - {}^{s}\boldsymbol{U}) = 0 \tag{5-3}$$

Redefining the terms of equation (5-3) in the following manner,

- The Jacobian, $\mathbb{J} \equiv \frac{\partial F({}^{s}\boldsymbol{U})}{\partial {}^{s}\boldsymbol{U}}$
- $\delta {}^{s}\boldsymbol{U} \equiv ({}^{s+1}\boldsymbol{U} - {}^{s}\boldsymbol{U}) \longrightarrow {}^{s+1}\boldsymbol{U} = {}^{s}\boldsymbol{U} + \delta {}^{s}\boldsymbol{U}.$

Substituting the above definitions and derivation into equation (5-3) provides equation(5-4).

$$\mathbb{J}\delta {}^{s}\boldsymbol{U} = -F({}^{s}\boldsymbol{U}) \tag{5-4}$$

Equation (5-4) is a linear set of equations of the form, $A\boldsymbol{x} = \boldsymbol{b}$ (see Appendix J). Solving this equation for $\delta {}^{n}\boldsymbol{U}$ provides the update,

$${}^{s+1}\boldsymbol{U} = {}^{s}\boldsymbol{U} + \delta {}^{s}\boldsymbol{U} \tag{5-5}$$

for the next Newton iteration. For a system of equations, like those used to solve the discretized forms of the diffusion and even-parity transport equations, the function $F(\boldsymbol{U})$ is a set of functions [8].

$$F(\boldsymbol{U}) = \{F_1, F_2, \dots, F_i, \dots, F_n\} \tag{5-6}$$

U is the solution vector for the set of functions.

$$\boldsymbol{U} = \{u_1, u_2, \dots, u_i, \dots, u_n\} \tag{5-7}$$

The Jacobian is a matrix with elements of the form found in equation (5-8) where *i* and *j* are the row and column indexes, respectively.

$$\mathbb{J}_{i,j} = \frac{\partial F_i(\boldsymbol{U})}{\partial \boldsymbol{U}_j} \tag{5-8}$$

Each element of the Jacobian requires taking derivatives of the equation with respect to ***U***. This is the main difficulty in using Newton's Method. However, choosing a *Krylov* based linear solver can simplify this process. This process is detailed in a later section.

Expanding ***U*** back into the problem of interest provides the nonlinear set.

$$\begin{bmatrix} \mathbb{J}_{\phi,\phi} & \mathbb{J}_{\phi,\alpha} \\ \mathbb{J}_{\alpha,\phi} & \mathbb{J}_{\alpha,\alpha} \end{bmatrix} \begin{bmatrix} \delta\boldsymbol{\phi} \\ \delta\alpha \end{bmatrix} = - \begin{bmatrix} \boldsymbol{F_\phi} \\ F_{\boldsymbol{\alpha}} \end{bmatrix} \tag{5-9}$$

$$\mathbb{J}_{\phi,\phi} = \frac{\partial \boldsymbol{F_\phi}}{\partial \boldsymbol{\phi}}, \mathbb{J}_{\phi,\alpha} = \frac{\partial \boldsymbol{F_\phi}}{\partial \alpha}, \mathbb{J}_{\alpha,\phi} = \frac{\partial F_{\boldsymbol{\alpha}}}{\partial \boldsymbol{\phi}}, \mathbb{J}_{\alpha,\alpha} = \frac{\partial F_{\boldsymbol{\alpha}}}{\partial \alpha} \tag{5-10}$$

The dimensions of the Jacobians making up the block matrix in equation (5-9) are as follows [7]:

$$\mathbb{J}_{\phi,\phi} = \begin{bmatrix} \frac{\partial F_{\phi 1}}{\partial \phi_1} & \cdots & \frac{\partial F_{\phi 1}}{\partial \phi_n} \\ \vdots & \ddots & \vdots \\ \frac{\partial F_{\phi n}}{\partial \phi_1} & \cdots & \frac{\partial F_{\phi n}}{\partial \phi_n} \end{bmatrix} \tag{5-11}$$

$$\mathbb{J}_{\phi,\alpha} = \begin{bmatrix} \frac{\partial F_{\phi 1}}{\partial \alpha} \\ \vdots \\ \frac{\partial F_{\phi n}}{\partial \alpha} \end{bmatrix} \tag{5-12}$$

$$\mathbb{J}_{\alpha,\phi} = \begin{bmatrix} \frac{\partial F_{\alpha}}{\partial \phi_1} & \cdots & \frac{\partial F_{\alpha}}{\partial \phi_n} \end{bmatrix} \tag{5-13}$$

$$\mathbb{J}_{\alpha,\alpha} = \frac{\partial F_{\boldsymbol{\alpha}}}{\partial \alpha} = 1 \tag{5-14}$$

Block Gaussian Elimination

The dimensions of the elements of equation (5-9) are not consistent and the system is complicated by having two functions and a block matrix. This situation could complicate the algorithm required to solve the system. Additionally, the dimensions and evaluations

of the alpha associated function, and Jacobian are simple and convenient. These factors make desirable the simplification of the system through *block Gaussian elimination* [65].

Writing the system in equation (5-9) as a set of two equations begins the process.

$$\begin{aligned} \mathbb{J}_{\phi,\phi}\delta\boldsymbol{\phi} + \mathbb{J}_{\phi,\alpha}\delta\alpha &= -\boldsymbol{F_{\phi}} \\ \mathbb{J}_{\alpha,\phi}\delta\boldsymbol{\phi} + \mathbb{J}_{\alpha,\alpha}\delta\alpha &= -F_{\boldsymbol{\alpha}} \end{aligned} \tag{5-15}$$

Now a solution for $\delta\alpha$ in terms of $\delta\boldsymbol{\phi}$ is now available in equation (5-16) from the second equation of (5-15).

$$\delta\alpha = \mathbb{J}_{\alpha,\alpha}^{-1}\left(-F_{\boldsymbol{\alpha}} - \mathbb{J}_{\alpha,\phi}\delta\boldsymbol{\phi}\right) \tag{5-16}$$

Substituting into the first equation in (5-15) provides equation (5-17).

$$\left(\mathbb{J}_{\phi,\phi} - \mathbb{J}_{\phi,\alpha}\mathbb{J}_{\alpha,\alpha}^{-1}\mathbb{J}_{\alpha,\phi}\right)\delta\boldsymbol{\phi} = -\boldsymbol{F_{\phi}} + \mathbb{J}_{\phi,\alpha}\mathbb{J}_{\alpha,\alpha}^{-1}F_{\boldsymbol{\alpha}} \tag{5-17}$$

Equation (5-14) immediately simplifies equation (5-17) to equation (5-18).

$$\left(\mathbb{J}_{\phi,\phi} - \mathbb{J}_{\phi,\alpha}\mathbb{J}_{\alpha,\phi}\right)\delta\boldsymbol{\phi} = -\boldsymbol{F_{\phi}} + \mathbb{J}_{\phi,\alpha}F_{\boldsymbol{\alpha}} \tag{5-18}$$

Qualitatively, equation (5-18) now contains a residual function on the right hand side (rhs) that includes a correction based on the change in ϕ with respect to α. On the left hand side (lhs), the Jacobian is adjusted by a scalar resulting from the product of the change in ϕ with respect to α, and the change in α with respect to ϕ. This effect is captured in practice, by a technique called *nonlinear elimination* [7]. Redefining $\boldsymbol{F_{\phi}}$ so the α terms are a function of $\boldsymbol{\phi}$ starts the process.

$$\boldsymbol{F_{\phi}} = F_{\phi}(\boldsymbol{\phi}) = A\,\boldsymbol{\phi} - \alpha\,\boldsymbol{\phi} = 0 \tag{5-19}$$

and

$$\alpha = \frac{A\boldsymbol{\phi} \cdot \boldsymbol{\phi}}{\boldsymbol{\phi} \cdot \boldsymbol{\phi}} \tag{5-20}$$

In practice the algorithm never explicitly forms the the Jacobian matrix, but instead approximates it by evaluation of $\boldsymbol{F}_{\phi}$ in a finite difference scheme. Therefore, evaluation of the newly defined residual function $\boldsymbol{F}_{\phi}$ in the scheme will adequately approximate the action of $\left(\mathbb{J}_{\phi,\phi} - \mathbb{J}_{\phi,\alpha}\mathbb{J}_{\alpha,\phi}\right)$ in the reduced system. Now the linear system for solution is in the form of equation

$$\mathbb{J}\delta\boldsymbol{\phi} = -\boldsymbol{F}_{\boldsymbol{\phi}}. \tag{5-21}$$

Where $\boldsymbol{F}_{\phi}$ is given in equation (5-19), and $\mathbb{J} = \left(\mathbb{J}_{\phi,\phi} - \mathbb{J}_{\phi,\alpha}\mathbb{J}_{\alpha,\phi}\right)$.

Incremental implementation using the algorithms depicted in Figure 5.1, Figure 5.2, Figure 5.3[1] verified the application of this somewhat complex technique.

[1] See Figure 5.4 for the JFNK algorithm.

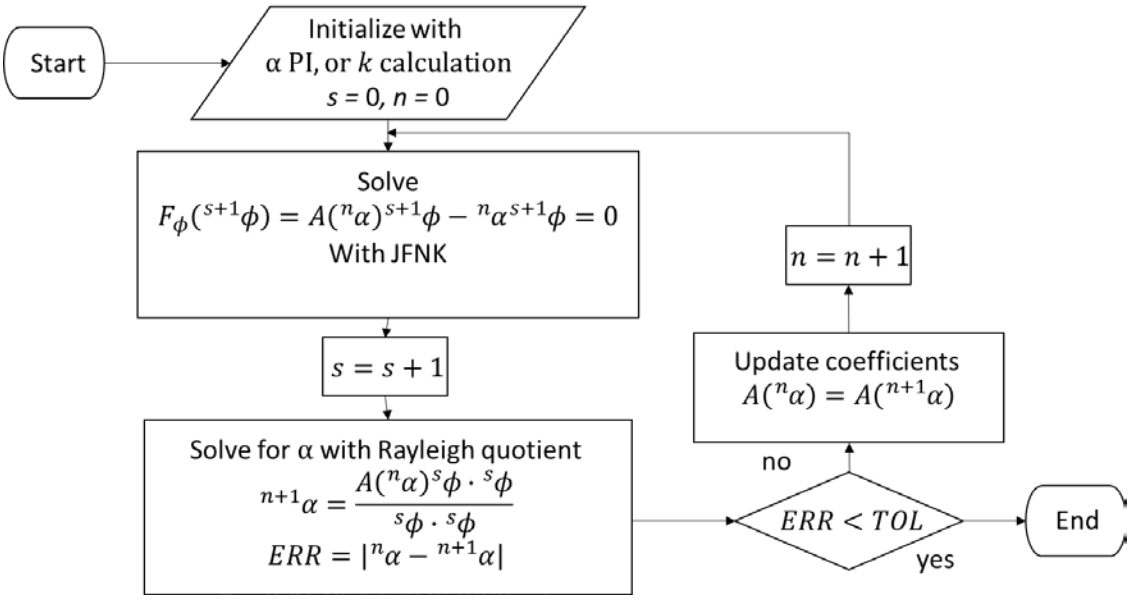

Figure 5.1 JFNK Flux and Fixed Point alpha Algorithm Flowchart

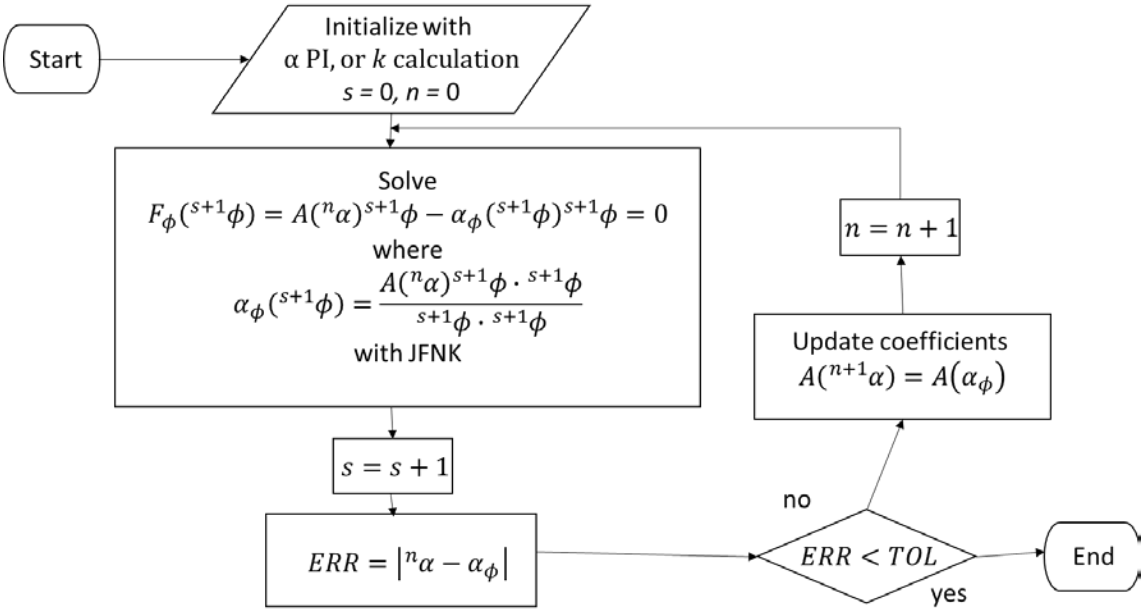

Figure 5.2 JFNK Flux & alpha With Fixed Point alpha in Coefficients Algorithm Flowchart

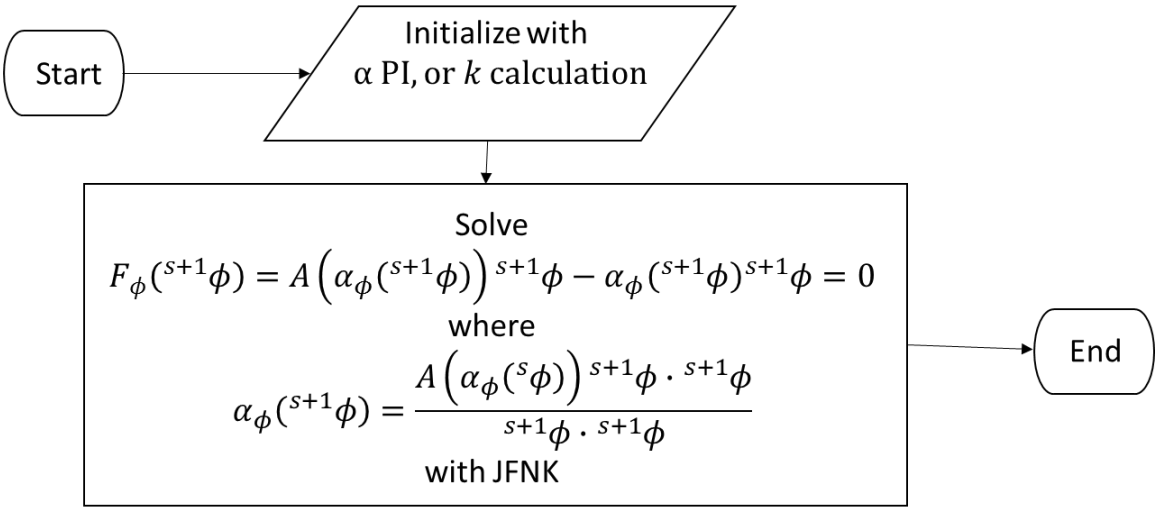

Figure 5.3 Full Nonlinear Elimination JFNK Flux & alpha Solution Algorithm Flowchart

Generalized Minimum Residual

The complexities associated with the Jacobian and the desire to avoid the explicit forming of a matrix for memory efficiency leads to the conclusion that a Krylov method is best suited to solve the linear system of equations (5-21). Krylov subspace methods are considered among the most important iterative techniques available for solving large linear systems [65]. The initial linear residual of equation (5-21) is,

$$\boldsymbol{r}_0 = -\boldsymbol{F}_{\boldsymbol{\phi}} - \mathbb{J}\delta\boldsymbol{\phi}_0. \tag{5-22}$$

The *Krylov subspace* is then [60, 8, 65],

$$\mathcal{K} = \mathcal{K}_k(\mathbb{J}, \boldsymbol{r}_0) = \text{span}(\boldsymbol{r}_0, \mathbb{J}\boldsymbol{r}_0, \mathbb{J}^2\boldsymbol{r}_0 \ldots \mathbb{J}^{k-1}\boldsymbol{r}_0). \tag{5-23}$$

In equation (5-23), *k* is the iteration index for the linear solver. Krylov methods seek a solution from the subspace,

$$\delta \boldsymbol{\phi}_k = \delta \boldsymbol{\phi}_0 + \mathcal{K} = \delta \boldsymbol{\phi}_0 + \sum_{i=0}^{k-1} \gamma_i \mathbb{J}^i \boldsymbol{r}_0. \tag{5-24}$$

The γ terms are constants resulting from the span and are chosen to minimize the residual [8]. In practice, calculating the Arnoldi vectors provides the solution [8]. The Arnoldi procedure produces an orthogonal projection onto the Krylov subspace and results in the ability to rewrite equation (5-24) in the following way [65].

$$\delta \boldsymbol{\phi}_k = \delta \boldsymbol{\phi}_0 + V_k \boldsymbol{y} \tag{5-25}$$

The matrix is V_k is an n by k matrix formed by column vectors $\mathbf{v_1}$ through $\mathbf{v}_k$. An intermediate step in the Arnoldi process involves determining the matrix-vector product $\mathbb{J}\mathbf{v}_j$. Forming the Jacobian is not required to adequately approximate this product. Instead, finite difference approximates the product by evaluating the residual function [7].

$$\mathbb{J}\mathbf{v}_j \approx \frac{\boldsymbol{F}_{\boldsymbol{\phi}}(\boldsymbol{\phi} + \epsilon \mathbf{v}_j) - \boldsymbol{F}_{\boldsymbol{\phi}}(\boldsymbol{\phi})}{\epsilon} \tag{5-26}$$

Where epsilon is a small value optimized for the algorithm. The Generalized Minimum Residual (GMRES) is a Krylov subspace method of solving linear systems of equations [65, 60, 8]. The *k*th iterate of a GMRES method seeks to minimize the residual by a least squares method.

$$\text{minimize}_{\delta \boldsymbol{\phi}_k \in \delta \boldsymbol{\phi}_0 + \mathcal{K}} \left\| -\boldsymbol{F}_{\boldsymbol{\phi}} - \mathbb{J}\delta \boldsymbol{\phi}_0 \right\|_2 \tag{5-27}$$

Again, in practice, GMRES does this by utilizing an Arnoldi procedure. Therefore, the computation does not form matrixes. Only matrix-vector products are required. Of the

various Krylov methods, GMRES is arguably the best and is the default linear solution method for both the ANL PETSc and SNL Trilinos scientific computational packages [40, 66]. Both are exceptional pieces of software for scientific calculations and incorporate the latest and best methods from applied math and computer science. Because of the quality of the software and the complications of the GMRES algorithm great effort was taken to incorporate PETSc[1] into JAKES, and retain the independence of remaining functions of the JAKES code. This was the most difficult technical task of the research, and one of the greatest contributions.

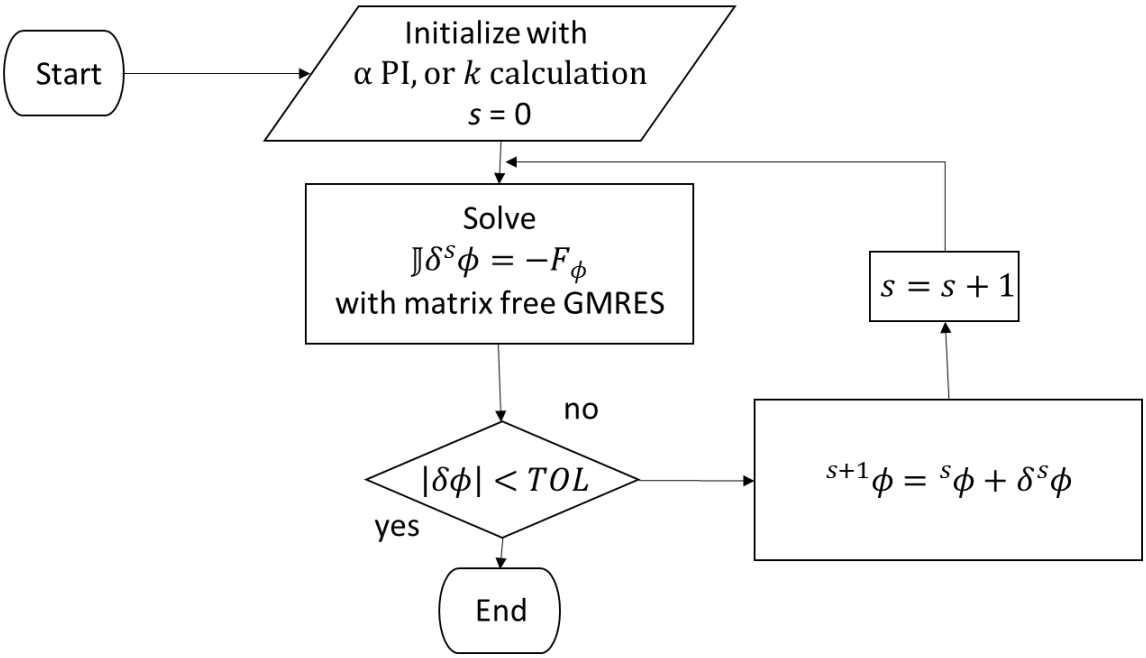

Figure 5.4 JFNK Algorithm Flowchart

[1] Both PETSc and Trilinos are written in C. PETSc was chosen for use in JAKES due to its superior FORTRAN interfaces.

Chapter 6

Results and Analyses

One-Dimensional Diffusion Case

The one-dimensional diffusion case provides a good model for *verification* of the solution techniques developed in Chapter 3 and Chapter 5. The one-dimensional case keeps the neutronics as simple as possible in order to study the computational performance, and mathematical accuracy of the solution methods. The one-dimensional calculations use one-group cross-sections [67]. The calculations only consider the isotopes of U235 and U238 in the modeled reactor. Comparisons to MCNP calculations and reference data of the Lady Godiva FBR provide a reasonable *validation* of the technique before considering two-dimensional neutron transport calculations in later sections.

Nuclear Data

This section provides the nuclear data used for the one-dimensional case based on the Lady Godiva FBR. Table 6.1 provides the average neutrons per fission, ν, the *delayed neutron fraction*, β, and the microscopic cross-sections for U235 and U238 [55, 68, 67, 69].

Table 6.1 One-D, One-Group, Microscopic Cross-section Data

	neutrons	*fraction*	*barns*		
	ν	β	$\tilde{\sigma}_f$	$\tilde{\sigma}_a$	$\tilde{\sigma}_{tr}$
U^{235}	2.60	0.0065	1.40	1.65	6.80
U^{238}	2.60	0.0157	0.095	0.255	6.90

Table 6.2 contains the additional data required to complete the calculations [67, 55, 24].

Table 6.2 One-D, Enrichment, Density and Neutron Energy Data

	Enrichment	ρ[grams/cm^3]	Average neutron Energy[MeV]
HEU	93	18.75	1.45
LEU	19.75%[1]	18.80	1.2

Numerical Performance Analysis

A spatial discretization of 30 cells serves as the verification test case. This spatial discretization is not adequate for desired accuracy, but is convenient to assess whether or not the algorithm is solving the problem correctly in a mathematical sense. The first test is to verify that the algorithm is correctly converging to the desired eigenvalue and eigenvector. In this case, mathematically, the eigen-pair that is associated with the largest algebraic eigenvalue of the matrix. For this small matrix, Mathematica was used to calculate all eigen-pairs [48]. All tested algorithms converged to the desired eigenvalue and eigenvector. Additionally, this test provided limited validation that the coefficients of the equations used in the algorithm adequately represented the physical problem by comparing the plots of the first five eigen-pairs of the numerical solution, Figure 6.1, and of the analytical solution found in Figure 3.2.

[1] 19.75 percent enrichment is used in all LEU cases. This enrichment level is below the threshold set by the NRC and is the chosen enrichment level by NNSA for production [79, 6, 5].

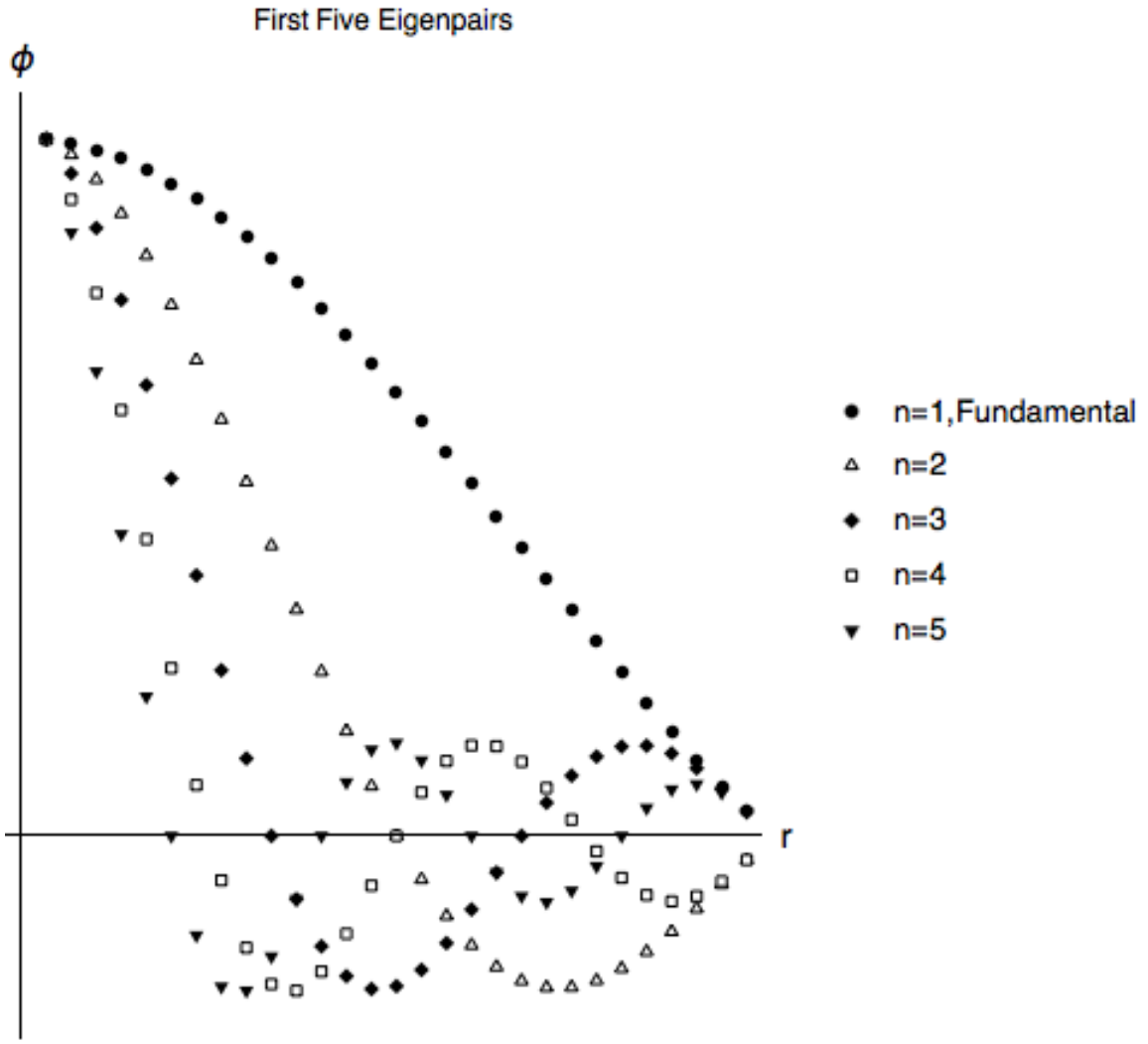

Figure 6.1 First Five Eigen-pairs of the Numerical Test Case

Though all algorithms did converge to the desired mathematical result for the test problem, not all algorithms did so with the same efficiency. Power Iteration, in particular, had significant difficulty. Table 6.3 contains iteration and timing data for the various algorithms presented in Chapter 3 and Chapter 5.

Table 6.3 Comparisons of Numerical Performance

	JAKES-JFNK[1]	JAKES-Hybrid[2]	JAKES-Fixed Point[3]	JAKES-PI-JFNK[4]	JAKES-PI[5]
Power Iterations	19	19	19	1452	~1000/ α update
α-updates	--	5	8	--	497
Newton Iterations/ α update	3	1 - 2	2 - 3	4	--
GMRES Iterations/ Newton Iteration	19	29	29 to 55	17 to 84	--
CPU-time [sec]	2.08E-2	6.53E-2	7.67E-2	4.026E-2	.305

The *dominance ratio* is the primary explanation for the difficult convergence of the alpha PI algorithm. A dominance ratio near unity is likely to cause a prohibitively slow convergence rate [7, 36, 37]. This ratio was the primary motivation for JFNK techniques

[1] This method uses the algorithm described in Figure 5.3 with a *k* calculation initialization.

[2] This method uses the algorithm described in Figure 5.2 with a *k* calculation initialization.

[3] This method uses the algorithm described in Figure 5.1 with a *k* calculation initialization.

[4] This method uses the algorithm described in Figure 5.3 with an alpha PI initialization.

[5] This method uses the algorithm described in Figure 3.6.

applied to *k* calculations in slow reactors [37, 7]. Equation (6-1) determines the dominance ratio.

$$\text{Dominance Ratio} = \frac{\alpha_2}{\alpha_1}, (|\alpha_1| > |\alpha_2| > \cdots > |\alpha_n|) \tag{6-1}$$

Table 6.4 lists all thirty eigenvalues from the numerical test case in the order specified by equation (6-1).

Table 6.4 Complete List of Eigenvalues for the Numerical Test Matrix

-9049.65	-8979.88	-8864.4	-8704.39	-8501.49
-8257.78	-7975.77	-7658.34	-7308.76	-6930.61
-6527.78	-6104.39	-5664.8	-5213.5	-4755.14
-4294.41	-3836.05	-3384.76	-2945.16	-2521.77
-2118.94	-1740.79	-1391.21	-1073.79	-791.775
-548.067	-345.166	-185.154	-69.6717	0.0949545

The data from Table 6.4 lists all thirty eigenvalues from the numerical test case in the order specified by equation (6 1). Table 6.4 determines the dominance ratio, in alpha, for this problem is 1.008. This condition will only worsen as the number of spatial cells and the number eigenvalues increase. This analytical solution predicts this condition. Equation (3-7) indicates eigenvalues of ever increasing negative magnitude as *n* approaches infinity. Fortunately, the dominance ratio for a *k* calculation of the same system is greater than two. This is apparent by the relatively low power iterations required to initialize the problem

using a *k* calculation. Power iteration for alpha calculations quickly becomes unusable for our problems of interest[1] and all calculations for *validation* use a *k-initialized* algorithm.

Additional analysis of the problem reveals other potential numerical issues with the alpha eigenvalue calculation. The potential issues are associated with instability, stiffness, and ill conditioning. However, the JFNK solution method seems to overcome these with ease for the present calculations. These issues are identified from the eigenvalues, $\alpha_i (i = 1, \dots, n)$. For stability, the condition of the following equation is desirable to reduce computational effort [63].

$$|\alpha_i| \leq 1 \ (i = 1, \dots, n) \tag{6-2}$$

Table 6.4 clearly indicates that this condition does not exist for alpha eigenvalue problems, and again will only worsen with a larger matrix.

Stiffness arises from the fact that the system has eigenvalues with large negative real parts. This causes corresponding components of the solution to vary rapidly when compared to other parts of the solution. A low stiffness ratio is desired to avoid the challenges and computational efforts required by stiff systems [63].

$$\text{Stiffness Ratio} = \frac{\text{Max}|\alpha_i|}{\text{Min}|\alpha_i|} \tag{6-3}$$

[1] Early calculations showed promise for using the alpha power iteration algorithm of Figure 3.6. However, the set up was for an unrealistically reactive system and still took hundreds of iterations.

The stiffness ratio calculated by equation (6-3) from Table 6.4 is 95,259.

The *condition number* of the matrix also provides insight to the relative security that a small residual vector is indicative of an accurate approximate solution vector [62]. The condition number of a matrix is related to the norms of the matrix and its inverse.

$$\text{Condtion Number } (A) = \|A\| \cdot \|A\|^{-1} \tag{6-4}$$

A matrix is ill conditioned if the condition number is significantly greater than one [62]. Using the infinity norm the condition number for the matrix associated with the alpha eigenvalue problem has a condition number of 190,085 [48]. Although all solution methods proved accurate for the 30 by 30 problem used for numerical analysis, the power iteration did fail to converge accurately for larger problems. This was not observed for the JFNK solution methods.

Table 6.5 Summary of Numerical Performance Metrics

	Dominance Ratio	Stability	Stiffness Ratio	Condition #
α-problem metrics value	0.99	True for only one. All others >>1	95,259	190,085
Desired metrics value	<<1	$\|\alpha_i\| \leq 1$ for all	low	~1

Validation of the One-Dimensional Case

The initial test case uses a basis for comparison with Lady Godiva and consists of a homogeneous sphere of HEU. The nuclear data for the JAKES calculations is provided in Table 6.1 and Table 6.2. MCNP calculations are listed for comparison even though the

MCNP calculation uses ENDF/B VI cross-section data. Published data from the Lady Godiva operation is also included for comparison. Two cases are calculated by JAKES and MCNP. The first is fueled with HEU and based on the Lady Godiva design. The second is 19.75% enriched LEU and designed to provide a reasonable balance between increased burst width and an increase in peak flux that is a result of using LEU fuel. Both cases only consider U235 and U238 as fuel constituents. Table 6.6 provides the results.

Table 6.6 One-Dimensional Test Case Results

	HEU			LEU	
	JAKES	MCNP[1]	Godiva[2]	JAKES	MCNP
Radius [cm]		8.741	8.692 – 8.741	21.562	21.562
Enrichment	93%	93.7%	93 – 94%	19.75%	19.75%
Mass [kg]	51.28	52.43	52 – 52.42	789.878	789.43
Volume [cm^3]	2735.188	2797.5	--	41990.953	41991.0
Cells	1000	--	--	1000	--
Analytical *k*	1.000279	--	--	1.0010736	--
Numerical *k*	1.000280	0.995	--	1.0010742	0.995
Analytical α [$\mu sec]^{-1}$	0.1032	--	--	7.455E-2	--
Numerical α [$\mu sec]^{-1}$	0.1035	--	--	7.458E-2	--
n-lifetime[3] [μ-sec]	2.706E-3	5.729E-3	--	1.440E-2	3.298E-2
FWHM [μ-sec]	34.034	--	35 – 50	47.246	
Max	1.0	--	--	2.76	
Max/ volume	1.0	--	--	0.180	
Max/ mass	1.0	--	--	0.179	
CPU-time [sec]	0.131	111.2	--	0.133	380

[1] For the HEU case, the data for the MCNP benchmark calculation is used [102].

[2] Data represents ranges found in multiple sources [56, 22, 55, 12, 102, 67].

[3] At least on expert questions the validity of the lifetimes calculated by MCNP for these types of problems [72].

Figure 6.2 shows fitted plots of the burst characteristics of HEU and LEU spherical reactors. JAKES calculations of alpha, *k*, and the prompt neutron lifetime provide the parameters needed by the Nordheim-Fuchs model to determine burst width and peak flux. The calculated values are from Table 6.6. The LEU design still has a pulse width comparable to the high end of Godiva, but also experiences a ~3 times increase in peak flux.

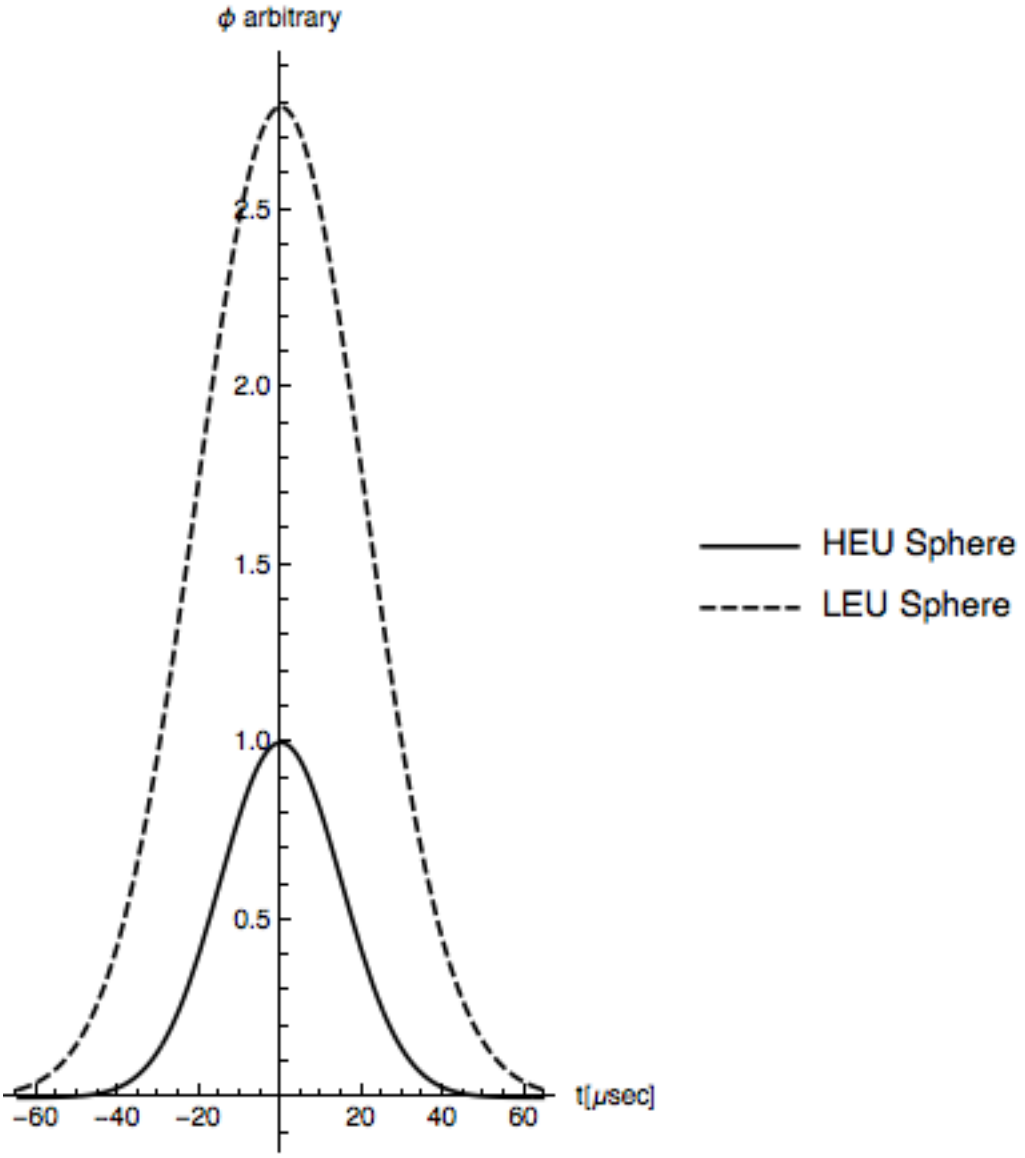

Figure 6.2 Calculated Burst Characteristics of a HEU and LEU Spherical FBR

Figure 6.3 shows a combined plot of the eigenvectors associated with the analytical alpha calculation, and the numerical *k*, and alpha calculations. Near perfect agreement is seen between all three. Again, this demonstrates the geometric and material dependence on the shape of flux. This is what allows the *k* calculation to initialize the alpha JFNK calculation so well.

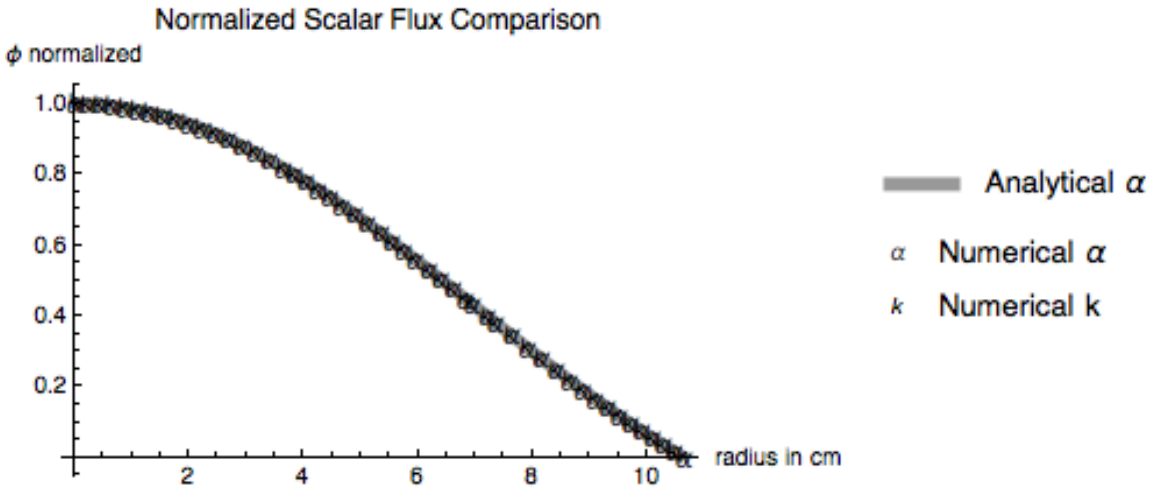

Figure 6.3 Analytical & Numerical Scalar Flux Comparison

Table 6.7 Historical FBR Reference Data

	Mass [kg]	Burst Yield [Fissions]	FWHM [μ-sec]
Lady Godiva	52-52.42	2E16	35-50
MollyG	97.142	5E15-1.1E17	31-50
Super Kukla	~4500	2-5E18	600-950

Two-Dimensional Transport Case

Table 6.8 provides the enrichment value for MollyG [15] and the HEU case. HEU density with 10% molybdenum if found in reference [70] . The density for LEU with 10% molybdenum is also in reference [70]. The density for LEU 1.5% molybdenum is from reference [71].

Table 6.8 Two-D, Material Enrichment and Density

	Enrichment		
	U235	Moly	ρ[grams/cm^3]
HEU	93.2%	10%	17.09
LEU	19.75%	1.5%	18.3
	19.75%	10%	17.14

Table 6.9 provides the data from EVENT calculations using the internal modified *k* eigen-solver. Dimensions of MollyG are from reference [15]. An associated program to EVENT called GEM, the *mesh-generating program* [45, 42], processes the cross section data using the Hansen-Roach 16 group data set.

Table 6.9 Two-Dimensional EVENT Test Case Results[1]

	HEU 10%Moly		LEU 10%Moly	LEU 1.5%Moly
	EVENT	MolyG	EVENT	EVENT
Enrichment	93.2%	93.2%	19.75%	19.75%
Radius	9.771	10.3	23.692	20.53
Height	18.31	19.3	44.398	38.474
Numerical *k*	1.000885	--	1.0032347	1.0029585
Numerical α [μsec]$^{-1}$	9.664E-2	--	7.434E-2	7.292E-2
n-lifetime [μ-sec]	9.110E-3	--	4.351E-2	3.854E-2
FWHM [μ-sec]	36.4803	35 – 50	47.400	49.665
Max	1.0	--	2.83	2.28
k calculations	21	--	33	16

The burst characteristics as determined by the Nordheim-Fuchs model and the data of Table 6.9 are depicted in Figure 6.4.

[1] It is not clear whether the search routine that generates the data in Table 6.9 includes the nonlinearity in the streaming term of the even-parity transport equation.

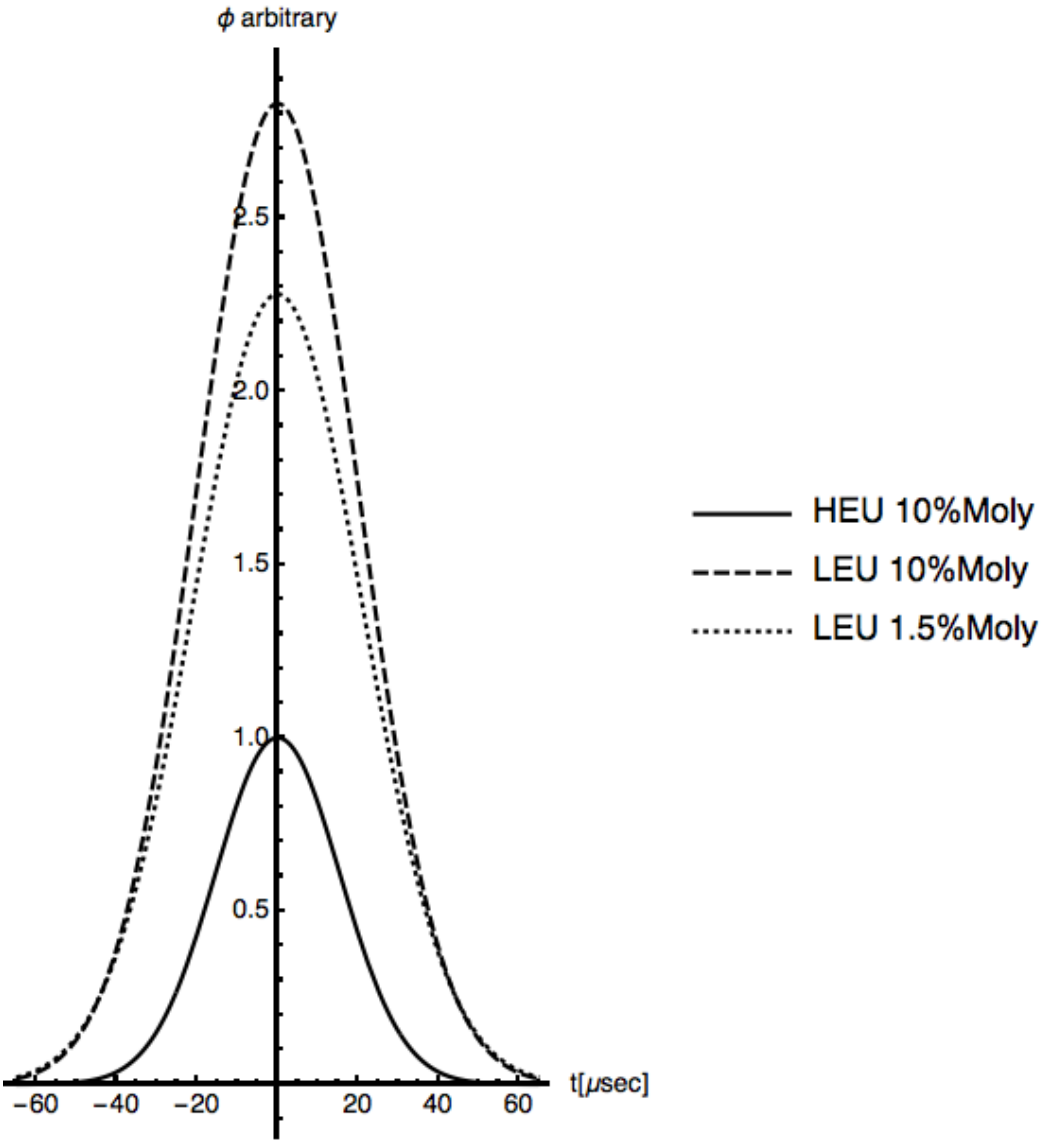

Figure 6.4 Calculated Burst Characteristics of HEU and LEU Cylindrical FBRs

Table 6.10 contains the data from the integrated JAKES-EVENT code. The values differ from Table 6.9 primarily due to a difficulty in EVENT that prevented reliable updates to the coefficients of the even-parity transport equation that required a lower order transport approximation. This difficulty also resulted in JAKES using the hybrid solution method outlined in Figure 5.2 to solve for the eigen-value in this case. This was done to monitor,

and minimize updates to the even-parity transport coefficients. As was the case in the one-dimensional calculations, the JFNK solution routines in JAKES were initialized by a *k* eigen-value calculation.

Table 6.10 Two-Dimensional JAKES-EVENT Test Case Results

	HEU 10%Moly			LEU 10%Moly	LEU 1.5%Moly
	JAKES-EVENT	MolyG	MCNP	EVENT	EVENT
Enrichment	93.2%	93.2%	93.2	19.75%	19.75%
Radius	10.540	10.3	10.3	24.57	21.076
Height	19.752	19.3	19.3	46.044	39.496
Numerical *k*	1.000882	--	1.09	1.0027996	1.0024298
Numerical α $[\mu sec]^{-1}$	8.4869E-2	--	--	5.937E-2	5.987E-2
n-lifetime [μ-sec]	1.0397E-2	--	8.9108E-3	4.716E-2	4.059E-2
FWHM [μ-sec]	41.5228	35 – 50	--	59.359	58.864
Max	1.0	--	--	2.220	1.943
k calculations (if JAKES not used)	38	--	--	64	64
alpha updates	1	--	--	1	1
Newton Iterations/alpha update	1	--	--	1	1
GMRES iterations/Newton Iteration	9	--	--	12	30

The burst characteristics as determined by the Nordheim-Fuchs model and the data of Table 6.10 are depicted in Figure 6.4.

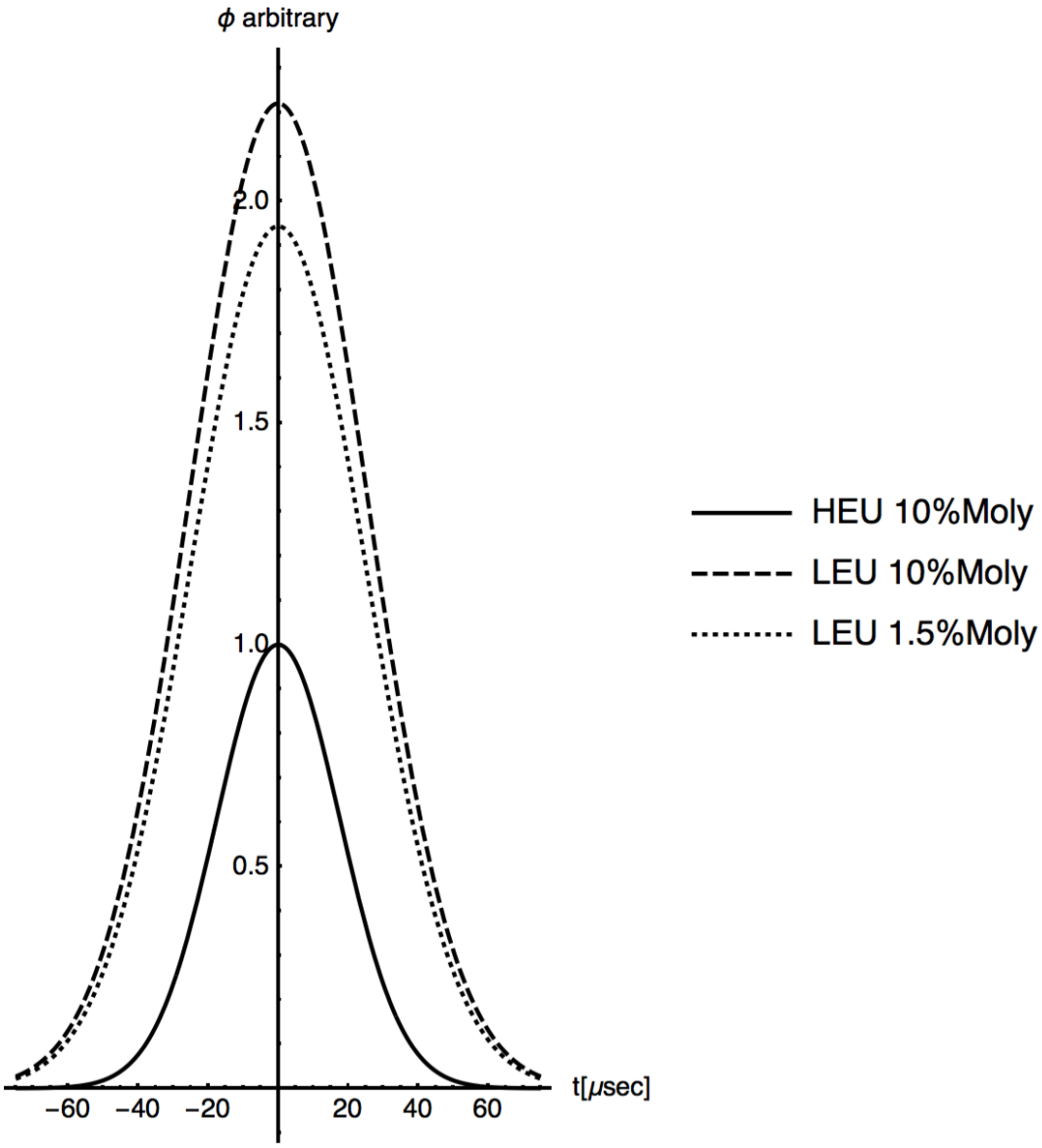

Figure 6.5 JAKES Calculated Burst Characteristics of HEU and LEU Cylindrical FBRs

Chapter 7

Conclusions

Conclusions from the Numerical Analyses of Performance

The time-eigenvalue problem presents itself as a classic eigenvalue problem in the analytical and linear algebra sense. However, numerically it is difficult to solve, and the dominance ratio of the problem makes solution by power iteration unpractical in almost every case. The eigenvectors of a system are scalable and the shape of the flux is dependent on the material and geometry of the system. The eigenvectors are not dependent in terms of shape on the time-dependent terms of the solution. In a fast reactor, *k* calculations are particularly efficient, and *k* is related to alpha by the neutron lifetime. Application of this analyses lead to using a *k* calculation to initialize Newton's method, and effectively eliminated all historical difficulties with calculation of the alpha eigenvalue.

The use of nonlinear elimination effectively combined all variables into a single residual for evaluation of the JFNK routine. This method's accuracy was identical to fixed-point iterative approaches, but had much better convergence efficiency. This approach effectively provided Newton convergence performance to the entire algorithm.

Conclusions from the Test Cases

The calculations indicated that use of LEU is capable of producing bursts on the microsecond scale of HEU fueled reactor at the cost of a longer rise time and increased peak flux. Initial calculations indicate the peak flux of the system is greater in an LEU

design, but the integrated flux over mass and volume is less. The increased density of the 1.5% moly LEU fuel as compared to the 10% moly LEU fuel alleviated the difference in burst width and peak flux from the 10% moly HEU reactor somewhat. However, coupled multi-physics calculations using this neutronic solution would be beneficial in providing resolution to the effects these differences will have on the reactors, and facilities. It is not clear from the calculations independently, what effect, if any, these differences will have on users of FBRs, and their experiments. Nevertheless, this new calculation method will provide options and predictions of LEU performance.

Continued Related Work & Improvements

The development of the new algorithm required a simplified approach in order to verify and validate the new techniques. Now that this work is complete, the algorithm is ready for more incremental improvements. This work developed the one-dimensional diffusion case primarily or verification purposes only. Now that results show good agreement with historical Lady Godiva data, the diffusion algorithm would benefit from the following improvements:

1. Update the spatial discretization in one-dimension from finite difference to finite volume to increase accuracy in curvilinear coordinates.
2. Incorporate the Bessel function based two-dimensional, cylindrical, analytical solution, and a corresponding two-dimensional finite volume numerical solution.

The spatial discretization upgrade to finite volume is significant even in the homogeneous material cases. In one-dimensional slab geometry, the finite difference approach is

equivalent to finite volume for a homogeneous system. This is not the case in spherical coordinates. The availability of a two-dimensional analytical and numerical case will provide added verification capability as well as serving pedagogical purposes, and is worthy of further development.

This work completed the difficult task of linking PETSc solution capability to a nuclear engineering code in an exceptionally transparent and modularized way. Now that this is complete, and available for verification purposes, the solution algorithm would benefit from continued research into the following:

1. Development of a JFNK solution scheme inherent to the using engineering code.
2. An efficient preconditioning scheme to aid the linear solver.

EVENT contains multiple Preconditioned Conjugant Gradient (PCG) solvers. PCG is a Krylov method and capable of incorporating the matrix-free methods used in this work. Not only will the development of an inherently integrated JFNK solver serve the purpose of academic development, but would also harden the code against unexpected incompatibilities from external developers with conflicting priorities. This work successfully completed all problems efficiently and completely matrix free. The *k* calculation initialization procedure is largely responsible for the efficiency obtained from the GMRES iterations. However, as problems become more general it is very likely that even the GMRES routine in PETSc will become prohibitively inefficient without the use of a preconditioner [8, 7]. It is also likely that the *k* calculation may not be as efficient in systems that are more complicated or operate on slow or intermediate neutron energies.

Modifying EVENT to solve the challenging time-eigenvalue problem proved difficult. These difficulties persisted even with direct coordination with the author of EVENT during the integration effort. Efficiency in using JAKES to solve the problem was demonstrated by the results. There is high confidence in the verification of mathematical accuracy in the solution method. However, the many efficiencies and pre-processing requirements incorporated into EVENT that make it such a quality tool for traditional transport, proved detrimental in integrating the complexities of the time-eigenvalue problem. This resulted in only a proof of concept of JAKES-EVENT integration, at best. To achieve full confidence in validation of this integration, a simpler even-parity transport code that is written with JAKES integration as a key performance parameter in development is recommended. This would provide a baseline for incremental changes to EVENT. This simpler routine could then support debugging, verification and validation of the new EVENT capability.

Of course, completing the spatial discretization to a three-dimensional Cartesian system is always a challenge and a worthy improvement. However, FBRs experience extreme transients in heat and shock as well as the neutronic state. The most beneficial improvement to this research is to work with other engineering disciplines and incorporate this robust asymptotic neutronic solution into existing, and new multi-physics modeling software.

Summary

This work has achieved success in developing a new algorithm for estimating the burst characteristics of FBRs of varying fuel compositions and levels of enrichment. The

nonlinear solution techniques using modern solution software and the JFNK method have successfully solved a very difficult problem in a direct, straightforward, accurate, and efficient manner. The solution method is efficient enough to replace other more elementary neutronic schemes typically used in multi-physics modeling of FBRs. The initialization using a *k* calculation allows complete avoidance of previous difficulties found in typical time-eigenvalue calculations used for initialization. This has allowed Newton's method efficiency to dominate the algorithm. There are many improvements, and applications to FBR modeling software that are now available because of this work. An asymptotic neutronic solution of the diffusion and even-parity transport equation with Newton's method efficiency is now available for use in FBR modeling.

Appendix A Acronyms and Abbreviations

ANL – Argonne National Laboratory

ARPACK – Arnoldi Package

BNL – Brookhaven National Laboratory

C.F.R. – Code of Federal Regulations

cm – centimeter

CPU – Central Processing Unit

Cyl – Cylinder

DSA – Diffusion Synthetic Acceleration

DSB – Defense Science Board

EDNA – Externally Driven Neutron Assembly

EVENT – EVEn-parity Neutron Transport

ERR – Error

FBR – Fast Burst Reactor

FORTRAN – FORmula TRANslation

FWHM – Full Width at Half Maximum

GEM – Mesh generating program

GMRES – Generalized Minimum Residual

GTRI -- Global Threat Reduction Initiative

HEU – Highly Enriched Uranium

HO – High Order

JAKES – JFNK Alpha and *k* Eigen-value Solver

JFNK – Jacobian-Free Newton-Krylov

kg – kilogram

LANL – Los Alamos National Laboratory

LASL – Los Alamos Scientific Laboratory

LDG – Linear Discontinuous Galerkin

LEU – Low Enriched Uranium

LLNL – Lawrence Livermore National Laboratory

LO – Low Order

LRL – Lawrence Radiation Laboratory

MCNP – Monte Carlo N-Particle

MeV – Mega electron-Volt

M^3 – Material Management & Minimization

MollyG – Molybdenum Godiva

NCA – Newton-based nonlinear Criticality Acceleration

NDA – Nonlinear Diffusion Acceleration

NK – Newton-Krylov

NRC – Nuclear Regulatory Commission

ORNL – Oak Ridge National Laboratory

P_N – Legendre or spherical harmonics transport approximation

PDE – Partial Differential Equation

PCG – Preconditioned Conjugate Gradient

PETSc – Portable, Extensible Toolkit for Scientific Computation

PI – Power Iteration

RERTR – Reduced Enrichment for Research and Test Reactors

rhs – right hand side

RSICC – Radiation Safety Information Computational Center

S_N – Discrete ordinates transport approximation

SC – Step Characteristics

sec – second

SI – Source Iteration

SNL – Sandia National Laboratory

Sph -- Sphere

SPR – Sandia Pulsed Reactor

Surf – Surface

SWLA – Simplified Wareing Larsen & Adams

TOL – Tolerance

USAEC – United States Atomic Energy Commission

Vol – Volume

WSMR – White Sands Missile Range

Appendix B Delayed Neutrons

The majority of neutrons resulting from a fission are in the form of *prompt neutrons*, and arrive on a time scale of within 10^{-14} seconds. The decay of certain nuclides produced from a fission, *fission products*, produce neutrons that that arrive in the system a relatively long time after the fission of the parent nuclide. These neutrons are *delayed neutrons*, and account for less than 1% of neutrons produced from a fission. *Precursors* are the nuclides that produce delayed neutrons [38]. Delayed neutrons arrive from very complex phenomena, but nuclear data sets traditionally simplify them into a six-group description of delayed neutron emission [67]. Table B.1 provides delayed neutron data for uranium. The shortest-lived precursors have half-lives of ~ 1/10 of a second. This is significantly longer than the operating time of the FBRs studied here. Therefore, it is prudent to adjust the value of the average neutrons per fission, ν, to exclude these neutrons. Equation (B-1) calculates the average number of prompt neutrons per fission.

$$\nu_{\text{prompt}} = \nu(1 - \beta) \tag{B-1}$$

- $\nu =$ the total average number of neutrons per fission
- $\beta =$ the delayed neutron fraction

Table B.1 Delayed Neutron Data for Uranium Fuel, Fast Spectrum

	ANL-5800		MCNP[1]
	U235	U238	93.7% HEU
β	0.0065 ± 0.0003	0.0157 ± 0.0012	0.00667 ± 0.0003
ν	2.6	2.6	2.598
$\nu_{delayed}$[2]	0.0165 ± 0.0005	0.0412 ± 0.0017	--
Half-life [sec]			
1	54.51 ± 0.94	52.38 ± 1.29	51.96582
2	21.84 ± 0.54	21.58 ± 0.39	21.18847
3	6.00 ± 0.17	5.00 ± 0.19	5.73659
4	2.23 ± 0.06	1.93 ± 0.07	2.28502
5	0.496 ± 0.029	0.49 ± 0.023	0.81341
6	0.179 ± 0.017	0.172 ± 0.009	0.24233
Relative Abundance			
1	0.038 ± 0.003	0.013 ± 0.001	0.041 ± 0.009
2	0.213 ± 0.005	0.137 ± 0.002	0.108 ± 0.012
3	0.188 ± 0.016	0.162 ± 0.020	0.114 ± 0.012
4	0.407 ± 0.007	0.388 ± 0.012	0.253 ± 0.019
5	0.128 ± 0.008	0.225 ± 0.013	0.109 ± 0.012
6	0.026 ± 0.003	0.075 ± 0.005	0.042 ± 0.008

[1] Calculated from the Godiva MCNP benchmark with point kinetic options [102].

[2] This quantity is the average number of delayed neutrons per fission and is very convenient for converting ν to only include prompt neutrons. However, it is not a popular tabulated quantity and using the delayed neutron fraction, β, is only slightly more difficult and is a much more universally useful and available quantity [67] .

The multiplication factor, *k*, is also adjusted similarly to exclude delayed neutron.

$$k = k_{eff}\left(1 - \beta_{\text{system}}\right) \tag{B-2}$$

It is important to realize when using equation (B-2) that the delayed neutron fraction must be for the entire system. Like the one presented in the MCNP column of Table B.1.

Delayed neutrons make control of steady state reactors possible by extending the effective neutron lifetime to ~0.1 sec [38]. However, for an FBR designed to produce a prompt critical pulse on a microsecond scale, they are of little interest.

Appendix C Characteristic Equation

The following is an equation for an eigenvalue problem,

$$A\boldsymbol{x} = \lambda\boldsymbol{x} \tag{C-3}$$

where A is a square matrix. An equivalent form of the problem is,

$$(\lambda I - A)\boldsymbol{x} = 0. \tag{C-4}$$

Equation (C-2) has non-zero solutions if and only if $(\lambda I - A)$ is singular (the determinate of $(\lambda I - A)$ equals zero). The equation,

$$\det(\lambda I - A) = |\lambda I - A| = 0 \tag{C-5}$$

is the *characteristic equation* of *A* [61].

As a simple example, consider the matrix,

$$A = \begin{bmatrix} a_{1,1} & a_{1,2} \\ a_{2,1} & a_{2,2} \end{bmatrix} \tag{C-6}$$

The characteristic equation of *A* is,

$$|\lambda I - A| = \left|\begin{bmatrix} \lambda & 0 \\ 0 & \lambda \end{bmatrix} - \begin{bmatrix} a_{1,1} & a_{1,2} \\ a_{2,1} & a_{2,2} \end{bmatrix}\right| = \begin{vmatrix} \lambda - a_{1,1} & -a_{1,2} \\ -a_{2,1} & \lambda - a_{2,2} \end{vmatrix}. \tag{C-7}$$

Completing the determinate operation results in a polynomial,

$$|\lambda I - A| = \lambda^2 - (a_{1,1} + a_{2,2})\lambda + (a_{1,1} * a_{2,2}) - (a_{2,1} * a_{1,2}) \tag{C-8}$$

the solutions of which are the eigenvalues of A.

Appendix D Diffusion Equation

The Time-Eigenvalue form of the Diffusion Equation

To arrive at the time-eigenvalue form of the diffusion equation, first begin with the time-dependent form of the transport equation, derived extensively elsewhere [58, 38],

$$\frac{1}{\mathrm{v}}\frac{\partial \phi}{\partial t} = \nu\,\sigma_f\,\phi - \sigma_a\,\phi + D\nabla^2\phi. \tag{D-1}$$

Recall the solution form derived in chapter 2,

$$\phi(r,t) = \phi(r)e^{\alpha t} \tag{D-2}$$

and substitute into equation (D-1),

$$\frac{1}{\mathrm{v}}\phi(r)\frac{\partial e^{\alpha t}}{\partial t} = \nu\,\sigma_f\,\phi(r)e^{\alpha t} - \sigma_a\,\phi(r)e^{\alpha t} + D\nabla^2\phi(r)e^{\alpha t}. \tag{D-3}$$

Analytically taking the time derivative on the left hand side of equation (D-3) provides,

$$\frac{1}{\mathrm{v}}\phi(r)\alpha e^{\alpha t} = \nu\,\sigma_f\,\phi(r)e^{\alpha t} - \sigma_a\,\phi(r)e^{\alpha t} + D\nabla^2\phi(r)e^{\alpha t}. \tag{D-4}$$

Dividing by $e^{\alpha t}$, rearranging algebraically and dropping the explicit space dependent notation, delivers the time-eigenvalue form of the diffusion equation,

$$D\nabla^2\phi - \sigma_a\,\phi + \nu\,\sigma_f\,\phi = \frac{\alpha}{\mathrm{v}}\phi. \tag{D-5}$$

The Diffusion Coefficient

The above derivation of the time-eigenvalue diffusion coefficient is correct. However, in order to use an appropriate value for "*D*" in calculations, the derivation of Fick's law must assume the time-dependent form of the solution to the neutron population derived in chapter 2. This is most efficiently done by noting that current is the first moment of the angular flux [56, 23].

$$\boldsymbol{J} = \int \hat{\boldsymbol{\Omega}}\, \psi \, d\Omega \tag{D-6}$$

In chapter 2 the time-dependent form of the angular flux is derived to be,

$$\psi\,(r,t) = \psi\,(r) e^{\alpha t}. \tag{D-7}$$

Substituting this form of the angular flux into equation (D-6) yields,

$$\boldsymbol{J}(r,t) = e^{\alpha t} \int \hat{\boldsymbol{\Omega}}\, \psi(r)\, d\Omega = e^{\alpha t} \boldsymbol{J}(r). \tag{D-8}$$

We can now make the usual simplifying assumptions to the P_1equations made elsewhere in the derivation of Fick's law, except for letting the $\frac{1}{\mathrm{v}}\frac{\partial \boldsymbol{J}}{\partial t}$ term equal zero [38],

$$\frac{1}{\mathrm{v}}\frac{\partial e^{\alpha t}}{\partial t}\boldsymbol{J}(r) + \frac{1}{3}\nabla\phi(r) e^{\alpha t} + \sigma_{tr}\boldsymbol{J}(r) e^{\alpha t} = 0. \tag{D-9}$$

Taking the analytical time derivative of $e^{\alpha t}$ and dividing by $e^{\alpha t}$gives,

$$\frac{\alpha}{\mathrm{v}}\boldsymbol{J} + \frac{1}{3}\nabla\phi + \sigma_{tr}\boldsymbol{J} = 0. \tag{D-10}$$

Solving for $\boldsymbol{J}$ provides the time-eigenvalue form of Fick's law [56].

$$\boldsymbol{J} = \frac{1}{3\left(\sigma_{tr} + \frac{\alpha}{\mathrm{v}}\right)}\nabla\phi \tag{D-11}$$

The Analytical Solution to the Time-Eigenvalue Diffusion Equation

Analytically solving equation (D-5) is useful in analyzing the problem and avoiding difficulties in numerical solutions. To begin it is best to rewrite the equation in a form suitable for determining the homogeneous solution to the differential equation.

$$\phi''(r) + \frac{2}{r}\phi'(r) + \left(\frac{\nu\,\sigma_f - \sigma_a - \frac{\alpha}{\mathrm{v}}}{D}\right)\phi = 0 \tag{D-12}$$

Excluding the imaginary components, the solution to equation (D-12) is,

$$\phi(r) = \frac{\mathrm{c}_1\cos(Br)}{r} + \frac{\mathrm{c}_2\sin(Br)}{r}. \tag{D-13}$$

Where,

$$B^2 = \left(\frac{\nu\,\sigma_f - \sigma_a - \frac{\alpha}{\mathrm{v}}}{D}\right) \tag{D-14}$$

A plot of sine and cosine is provided in Figure D.1 for reference.

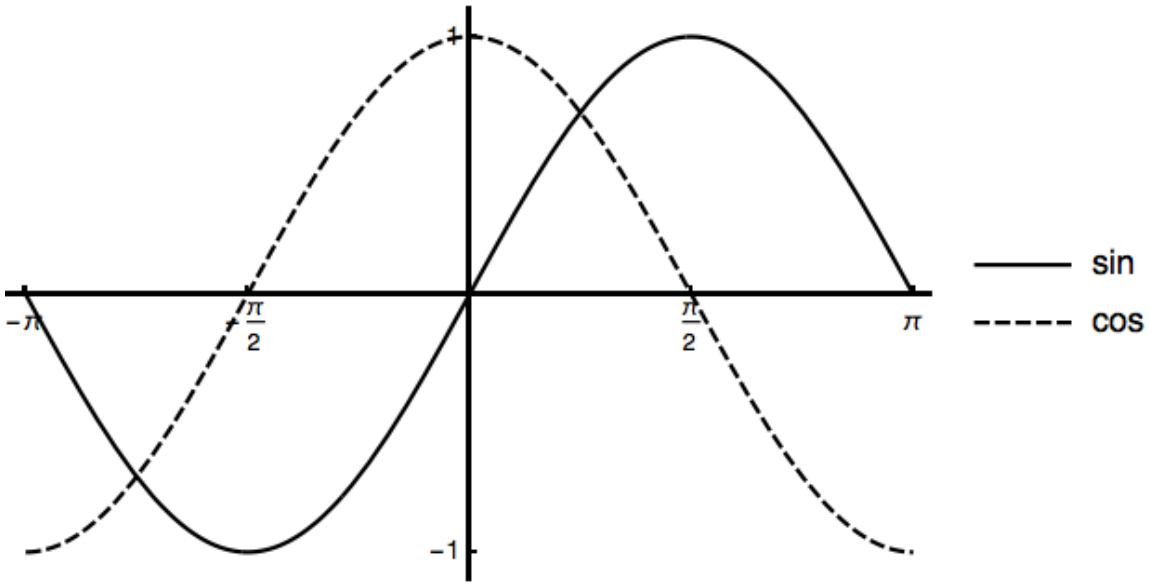

Figure D.1 Reference Plot of Sine and Cosine

As the first boundary condition, the flux must be finite and positive (or zero) at all points on the sphere.

$$\lim_{r\to 0} \frac{c_1 \cos(Br)}{r} = \infty \tag{D-15}$$

$$\lim_{r\to 0} \frac{c_2 \sin(Br)}{r} = B \tag{D-16}$$

Equation (D-15) and the first boundary condition require that $c_1 = 0$. The second boundary condition requires the flux be zero at the extrapolated boundary. The extrapolated boundary is the geometric radius of the sphere plus two times the diffusion coefficient [38]. For reasons outlined in Chapter 3, the diffusion coefficient derived in the previous section is not used in this work to calculate the extrapolated boundary. Instead, the diffusion coefficient associated with a *k* calculation is used. Further motivation for this

approximation is made at the end of this section. Equation (D-17) defines the extrapolated boundary.

$$\tilde{R} = R + 2\,\frac{1}{3\sigma_{tr}} = R + 2\,D_k \tag{D-17}$$

So,

$$\frac{c_2\,\sin(B\tilde{R})}{\tilde{R}} = 0 \longrightarrow B = \frac{n\,\pi}{\tilde{R}}. \tag{D-18}$$

Where $n = 1, 2, 3, \ldots$ The solution for $c_2 = 1$, and $n = 1$ is plotted in Figure D.2.

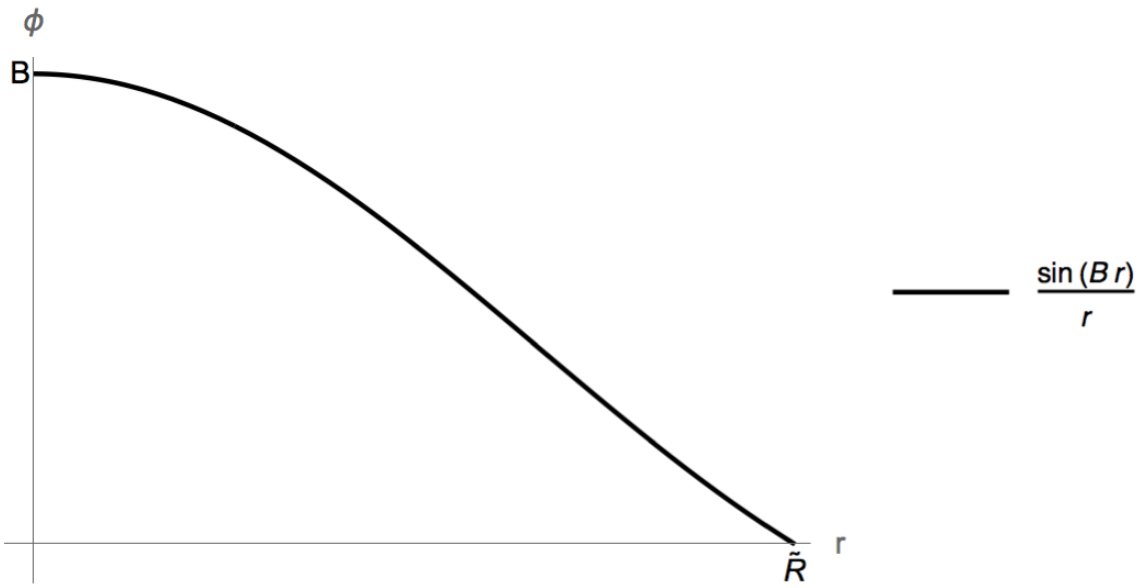

Figure D.2 Spatial Solution of the Flux

Substituting the result of equation (D-18) into equation (D-14) provides

$$\left(\frac{n\,\pi}{\tilde{R}}\right)^2 = \left(\frac{\nu\,\sigma_f - \sigma_a - \frac{\alpha}{v}}{D}\right) \tag{D-19}$$

Solving equation (D-19) for alpha yields equation (D-20), which is equivalent to equation (3-8).

$$\alpha_n = \mathrm{v}\, D \left[\frac{\left(\nu\, \sigma_f - \sigma_a\right)}{D} - \left(\frac{n\, \pi}{\tilde{R}}\right)^2 \right] \tag{D-20}$$

For the remainder of this section only the fundamental mode is considered.

$$\alpha = \mathrm{v}\, D \left[\frac{\left(\nu\, \sigma_f - \sigma_a\right)}{D} - \left(\frac{\pi}{\tilde{R}}\right)^2 \right] \tag{D-21}$$

The analytical solution to equation (D-21) results in two roots of a quadratic equation.

$$\alpha_- = \mathrm{v} \left[\frac{\left(\nu\, \sigma_f - \sigma_a - \sigma_{tr}\right)}{3} - \frac{\sqrt{3\, \tilde{R}^2 \left(\nu\, \sigma_f - \sigma_a + \sigma_{tr}\right)^2 - 4\pi^2}}{2\sqrt{3}\, \tilde{R}} \right], \tag{D-22}$$

and

$$\alpha_+ = \mathrm{v} \left[\frac{\left(\nu\, \sigma_f - \sigma_a - \sigma_{tr}\right)}{3} + \frac{\sqrt{3\, \tilde{R}^2 \left(\nu\, \sigma_f - \sigma_a + \sigma_{tr}\right)^2 - 4\pi^2}}{2\sqrt{3}\, \tilde{R}} \right]. \tag{D-23}$$

Substituting the value of the extrapolated radius required for criticality will provide the correct root for the problem of interest. The criticality condition is found by equation (D-24) [38].

$$\tilde{R} = \left(\frac{\pi^2}{\left(\nu\, \sigma_f - \sigma_a\right) 3\, \sigma_{tr}} \right)^{1/2} \tag{D-24}$$

For a critical system alpha must equal zero. Substituting equation (D-24) into equations (D-22), and (D-23) determines the following results [48]:

1. α_-, equation (D-22), will only equal zero when $\nu\,\sigma_f > \sigma_a + \sigma_{tr}$. This is a very unlikely condition that would require a significant number of prompt neutrons per fission, ν.

2. α_+, equation (D-23), will equal zero when $\nu\,\sigma_f \leq \sigma_a + \sigma_{tr}$. This condition is much more probable and matches all cases studied in this work.

Using the nuclear data of HEU one-dimensional case found in Chapter 6, Table 6.1, and Table 6.2 provides the following values for α_-, and α_+:

1. $\alpha_- = -398.133$. Clearly, this value is incorrect in a physical sense as predicted by the analyses above.

2. $\alpha_+ = 0.1032$. This matches the analytical value of alpha computed by JAKES using a fixed-point iteration and a Newton's method on equation (D-21).

Forming a residual function, equation (D-25), from equation (D-21) provides insight into determining the right answer through numerical methods is accomplished.

$$F(\alpha) = \alpha - \mathrm{v}\,D\left[\frac{\left(\nu\,\sigma_f - \sigma_a\right)}{D} - \left(\frac{\pi}{\tilde{R}}\right)^2\right] \tag{D-25}$$

Equation (D-25) is plotted in Figure D.3 using the same nuclear data referenced in the preceding paragraph.

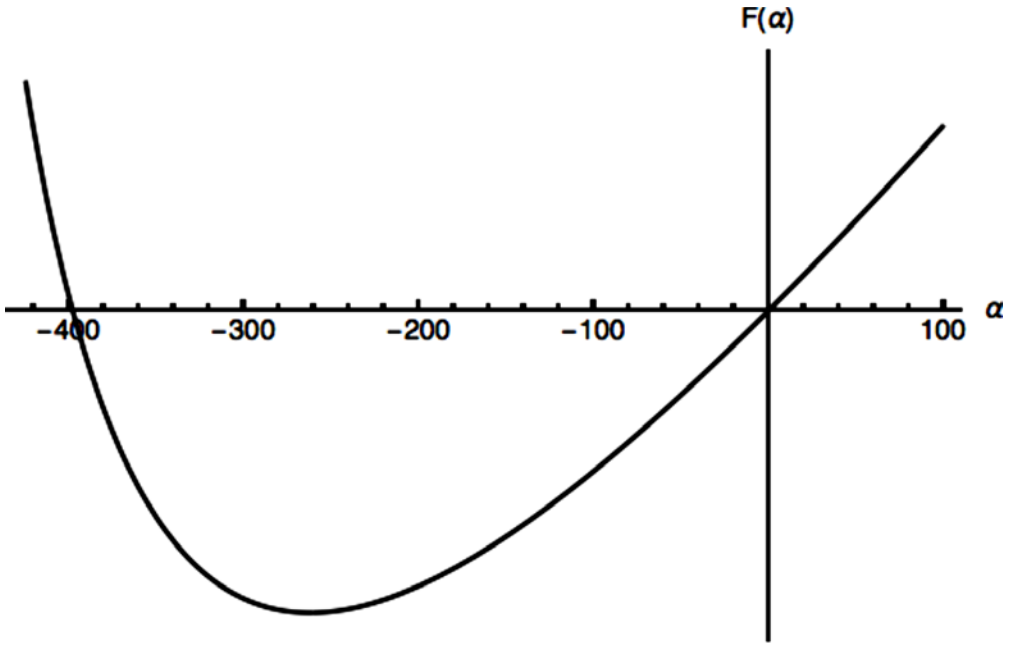

Figure D.3 Residual Function Plot of the Analytical Alpha Solution Using D_k

The curve of Figure D.3 is the key to converging to the correct root. Starting the search near the correct result with an educated initial guess based on knowledge of the system is the key. If a guess for the solution that is to the left of the valley presented in Figure D.3, it is very likely that the computation will converge to the wrong root.

Another potential difficulty in obtaining convergence is the case where the dimensions of the sphere are such that the value under the radicals in the numerators of equations (D-22), and (D-23) are negative. This is possible for relatively small values of $\tilde{R}$. These cases are not of interest to this research since the geometries and materials required for the critical assemblies studied do not approach these small values of $\tilde{R}$. However, if this situation occurred additional analyses would be required to form the real solution.

If the extrapolated boundary was not approximated by the D_k diffusion coefficient, and the coefficient that contains alpha was used, the solution would be in the form of a quartic that at best would reduce to a cubic [72]. The solution to the cubic contains one real root and two with imaginary components [48]. Additionally, the difficulty in the numerical method developed in this research for the diffusion case would require a nonlinear iteration to determine the extrapolated boundary. However, for the analytical case, tests converged to the expected value of alpha when an appropriate initial guess was provided to the routine. Figure D.4 provides a plot of the residual function, equation (D-26), for this case using the same nuclear data as above.

$$F(\alpha) = \alpha - \mathrm{v}\, D \left[\frac{\left(\nu\, \sigma_f - \sigma_a\right)}{D} - \left(\frac{\pi}{R + 2D}\right)^2 \right] \tag{D-26}$$

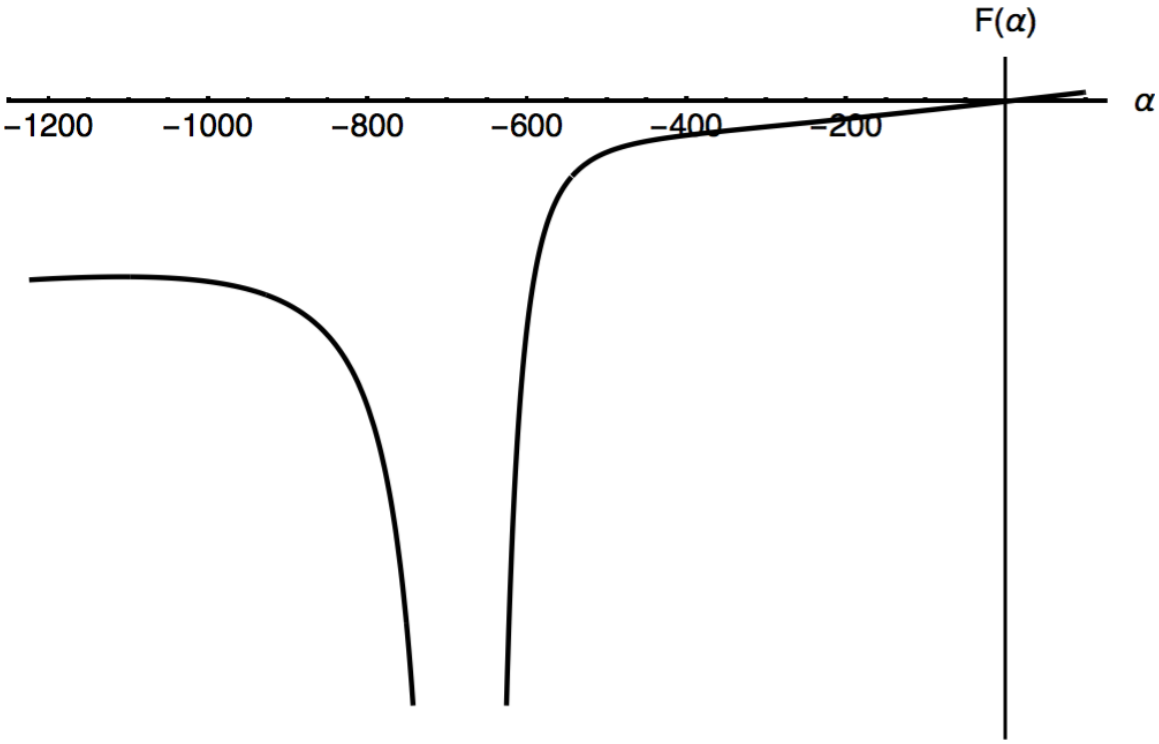

Figure D.4 Residual Function Plot of the Analytical Alpha Solution

Appendix E Even Parity Transport Equation

The Time-Eigenvalue Even-Parity Transport Equation

To derive the time-eigenvalue form of the even-parity transport equation it is beneficial to begin with the first order form, derived extensively elsewhere [56, 23].

$$\begin{aligned}&\left[\frac{1}{\mathrm{v}}\frac{\partial}{\partial t}+\hat{\boldsymbol{\Omega}}\cdot\nabla+\sigma(r,E,t)\right]\psi\left(r,\hat{\boldsymbol{\Omega}},E,t\right)\\&=q_{ex}\left(r,\hat{\boldsymbol{\Omega}},E,t\right)\\&+\int dE'\int d\Omega'\,\sigma_s\left(r,\hat{\boldsymbol{\Omega}}'\cdot\hat{\boldsymbol{\Omega}},E'\rightarrow E,t\right)\psi\left(r,\hat{\boldsymbol{\Omega}},E,t\right)\\&+\int dE'\,\nu(E)\sigma_f(r,E,t)\int d\Omega'\,\psi\left(\vec{r},\hat{\boldsymbol{\Omega}},E,t\right)\end{aligned}\tag{E-1}$$

The external source does not affect the reactivity of the system and is set to zero for this derivation. In addition, to simplify notation the equation is within one energy group, and the cross sections are constant.

$$\left[\frac{1}{\mathrm{v}}\frac{\partial}{\partial t}+\hat{\boldsymbol{\Omega}}\cdot\nabla+\sigma\right]\psi\left(r,\hat{\boldsymbol{\Omega}},t\right)=\sigma_s\int d\Omega'\,\psi\left(r,\hat{\boldsymbol{\Omega}},t\right)+\nu\sigma_f\int d\Omega'\,\psi\left(r,\hat{\boldsymbol{\Omega}},t\right)\tag{E-2}$$

Using the stated form of the angular flux solution derived in chapter 2,

$$\psi\left(r,\hat{\boldsymbol{\Omega}},t\right)=\psi\left(r,\hat{\boldsymbol{\Omega}},0\right)e^{\alpha t}\tag{E-3}$$

Omitting the initial condition at $t = 0$, for now, equation (E-3) is substituted into (E-2).

$$\begin{aligned}&\frac{1}{\mathrm{v}}\psi\left(r,\hat{\boldsymbol{\Omega}}\right)\frac{\partial e^{\alpha t}}{\partial t}+\hat{\boldsymbol{\Omega}}\cdot\nabla\,\psi\left(r,\hat{\boldsymbol{\Omega}}\right)e^{\alpha t}+\sigma\,\psi\left(r,\hat{\boldsymbol{\Omega}}\right)e^{\alpha t}\\&\quad=\sigma_s e^{\alpha t}\int d\Omega'\,\psi\left(r,\hat{\boldsymbol{\Omega}}\right)+\nu\sigma_f e^{\alpha t}\int d\Omega'\,\psi\left(r,\hat{\boldsymbol{\Omega}}\right).\end{aligned}\tag{E-4}$$

Analytically solving the time derivative yields,

$$\frac{1}{\mathrm{v}}\psi(r,\hat{\mathbf{\Omega}})\alpha\, e^{\alpha\, t} + \hat{\mathbf{\Omega}}\cdot\nabla\,\psi(r,\hat{\mathbf{\Omega}})e^{\alpha\, t} + \sigma\,\psi(r,\hat{\mathbf{\Omega}})\, e^{\alpha\, t} = \sigma_s e^{\alpha\, t}\int d\Omega'\,\psi(r,\hat{\mathbf{\Omega}}) + \nu\sigma_f e^{\alpha\, t}\int d\Omega'\,\psi(r,\hat{\mathbf{\Omega}})\,. \tag{E-5}$$

Dividing both sides by $e^{\alpha\, t}$ provides the first order time-eigenvalue transport equation.

$$\left[\frac{\alpha}{\mathrm{v}} + \hat{\mathbf{\Omega}}\cdot\nabla\, + \sigma\right]\,\psi(r,\hat{\mathbf{\Omega}})\, = \sigma_s\int d\Omega'\,\psi(r,\hat{\mathbf{\Omega}}) + \nu\sigma_f\int d\Omega'\,\psi(r,\hat{\mathbf{\Omega}}) \tag{E-6}$$

To derive the even-parity form begin by replacing $\hat{\mathbf{\Omega}}$ with $-\hat{\mathbf{\Omega}}$.

$$\left[\frac{\alpha}{\mathrm{v}} + (-\hat{\mathbf{\Omega}}\cdot\nabla)\, + \sigma\right]\,\psi(r,-\hat{\mathbf{\Omega}}) = \sigma_s\int d\Omega'\,\psi(r,-\hat{\mathbf{\Omega}}) + \nu\sigma_f\int d\Omega'\,\psi(r,-\hat{\mathbf{\Omega}}) \tag{E-7}$$

Now let,

$$\psi^{+}(r,\hat{\mathbf{\Omega}})\, =\, \psi(r,\hat{\mathbf{\Omega}}) +\, \psi(r,-\hat{\mathbf{\Omega}}) \tag{E-8}$$

which is an even function in $\hat{\mathbf{\Omega}}$, and let,

$$\psi^{-}(r,\hat{\mathbf{\Omega}})\, =\, \psi(r,\hat{\mathbf{\Omega}}) -\, \psi(r,-\hat{\mathbf{\Omega}}) \tag{E-9}$$

which is an odd function in $\hat{\mathbf{\Omega}}$. Now the angular flux becomes,

$$\psi(r,\hat{\mathbf{\Omega}})\, =\, \psi^{+}(r,\hat{\mathbf{\Omega}}) +\, \psi^{-}(r,\hat{\mathbf{\Omega}}), \tag{E-10}$$

and

$$\psi(r,-\hat{\boldsymbol{\Omega}}) = \psi^{+}(r,\hat{\boldsymbol{\Omega}}) - \psi^{-}(r,\hat{\boldsymbol{\Omega}}). \tag{E-11}$$

The scalar flux is now,

$$\phi(r) = \int \psi(r,\hat{\boldsymbol{\Omega}})\, d\Omega = \int \psi^{+}(r,\hat{\boldsymbol{\Omega}})\, d\Omega + \int \psi^{-}(r,\hat{\boldsymbol{\Omega}})\, d\Omega. \tag{E-12}$$

Since,

$$d\Omega = \sin\theta\, d\theta\, d\omega = d\mu\, d\omega \rightarrow \int d\Omega = \int_{0}^{2\pi} d\omega \int_{-1}^{1} d\mu = 4\pi \tag{E-13}$$

the scalar flux is now

$$\phi(r) = \int_{-1}^{1}\int_{0}^{2\pi} \psi^{+}(r,\hat{\boldsymbol{\Omega}})\, d\omega\, d\mu + \int_{-1}^{1}\int_{0}^{2\pi} \psi^{-}(r,\hat{\boldsymbol{\Omega}}) d\omega\, d\mu. \tag{E-14}$$

Equation (E-13) illustrates an even function $\psi^{+}(r,\hat{\boldsymbol{\Omega}})$, and an odd function $\psi^{-}(r,\hat{\boldsymbol{\Omega}})$ integrated evenly over their axis of symmetry. So, the scalar flux becomes,

$$\phi(r) = 2\int_{0}^{1}\int_{0}^{2\pi} \psi^{+}(r,\hat{\boldsymbol{\Omega}})\, d\omega\, d\mu. \tag{E-15}$$

This is the same value as when integrating $\psi(r,-\hat{\boldsymbol{\Omega}})$ over $\hat{\boldsymbol{\Omega}}$ using equation (E-11). So, the dependence of $\psi(r,\hat{\boldsymbol{\Omega}})$ and $\psi(r,-\hat{\boldsymbol{\Omega}})$ on the right hand sides of equations (E-6) and (E-7) is only in terms of the scalar flux $\phi(r)$. So now let,

$$\begin{aligned} Q &= \sigma_s \int d\Omega'\, \psi(r,\hat{\boldsymbol{\Omega}}) + \nu\sigma_f \int d\Omega'\, \psi(r,\hat{\boldsymbol{\Omega}}) \\ &= \sigma_s \int d\Omega'\, \psi(r,-\hat{\boldsymbol{\Omega}}) + \nu\sigma_f \int d\Omega'\, \psi(r,-\hat{\boldsymbol{\Omega}}) \\ &= \sigma_s\phi(r) + \nu\sigma_f\phi(r). \end{aligned} \tag{E-16}$$

Since functional dependencies are clearly established, they are dropped for the remainder of the derivation to simplify notation. Now making the substitution of equation (E-16) into the right hand side of equations (E-6) and (E-7) and substituting equations (E-10) and E-11) into equations (E-6) and (E-7) respectively provides,

$$\left[\frac{\alpha}{\mathrm{v}} + \hat{\boldsymbol{\Omega}}\cdot\nabla + \sigma\right](\psi^+ + \psi^-) = Q \tag{E-17}$$

and

$$\left[\frac{\alpha}{\mathrm{v}} - \hat{\boldsymbol{\Omega}}\cdot\nabla + \sigma\right](\psi^+ - \psi^-) = Q. \tag{E-18}$$

The sum of equations (E-17) and (E-18) is,

$$\frac{\alpha}{\mathrm{v}}\psi^+ + \hat{\boldsymbol{\Omega}}\cdot\nabla\psi^- + \sigma\psi^+ = Q\,. \tag{E-19}$$

The difference of equations (E-17) and (E-18) is,

$$\frac{\alpha}{\mathrm{v}}\psi^{-} + \widehat{\mathbf{\Omega}} \cdot \nabla \psi^{+} + \sigma\psi^{-} = 0\,. \tag{E-20}$$

Solving equation (E-20) for ψ^{-}yields,

$$\psi^{-} = -\frac{1}{\sigma + \frac{\alpha}{\mathrm{v}}}\widehat{\mathbf{\Omega}} \cdot \nabla \psi^{+}. \tag{E-21}$$

Substituting equation (E-21) into equation (E-19) provides the second order, even-parity time-eigenvalue transport equation.

$$\widehat{\mathbf{\Omega}} \cdot \nabla \frac{1}{\sigma + \frac{\alpha}{\mathrm{v}}}\widehat{\mathbf{\Omega}} \cdot \nabla \psi^{+} - \sigma\psi^{+} + Q = \frac{\alpha}{\mathrm{v}}\psi^{+}\,. \tag{E-22}$$

Appendix F Finite Difference Approximation

For the one-dimensional case, this work uses a finite difference spatial discretization scheme for the numerical solution of the diffusion equation in spherical coordinates. Spherical coordinates are chosen to provide practicality in reactor design. A one-dimensional spherical calculation models a homogenous spherical reactor reasonably well.

To arrive at the spatially discretized equation, begin with a *Taylor series* expansion of the scalar flux. Equation (F-1) is a Taylor series for a function *f*(*x*) about *x* = *a* [59].

$$f(x) = f(a) + (x-a)\frac{df(x)}{dx} + \frac{1}{2!}(x-a)^2\frac{d^2f(x)}{dx^2} + \cdots + \frac{1}{n!}(x-a)^n\frac{d^nf(x)}{dx^n} + \cdots \quad \text{(F-1)}$$

In this case, the objective is to discretize the sphere spatially in order to arrive at an approximation for the *Laplacian* in one-dimensional spherical coordinates.

$$\nabla^2 = \frac{d^2\phi}{dr^2} + \frac{2}{r}\frac{d\phi}{dr}. \quad \text{(F-2)}$$

First, to simplify notation, $\phi(r_i) \equiv \phi_i$, $\phi(r_{i+1}) \equiv \phi_{i+1}$, and $\phi(r_{i-1}) \equiv \phi_{i-1}$.If the radius of the sphere is discretized in the manner depicted in Figure 3.4 the flux is expanded in a Taylor series about r_i in the following manner [38].

$$\phi_{i+1} = \phi_i + (r_{i+1} - r_i)\frac{d\phi_i}{dr} + \frac{1}{2!}(r_{i+1} - r_i)^2 \frac{d^2\phi_i}{dr^2} \quad \text{(F-3)}$$

$$\phi_{i-1} = \phi_i + (r_{i-1} - r_i)\frac{d\phi_i}{dr} + \frac{1}{2!}(r_{i-1} - r_i)^2 \frac{d^2\phi_i}{dr^2} \quad \text{(F-4)}$$

Only the first three terms are needed since the objective is to determine an approximation for equation (F-2). Using the discretization depicted in Figure 3.4 allows simplification of equations (F-3) and (F-4).

$$\phi_{i+1} = \phi_i + \Delta\frac{d\phi_i}{dr} + \frac{1}{2}\Delta^2 \frac{d^2\phi_i}{dr^2} \quad \text{(F-5)}$$

$$\phi_{i-1} = \phi_i - \Delta\frac{d\phi_i}{dr} + \frac{1}{2}\Delta^2 \frac{d^2\phi_i}{dr^2} \quad \text{(F-6)}$$

Adding and subtracting equations (F-5) and (F-6) results in following equations.

$$\phi_{i+1} + \phi_{i-1} = 2\phi_i + \Delta^2 \frac{d^2\phi_i}{dr^2} \quad \text{(F-7)}$$

$$\phi_{i+1} - \phi_{i-1} = 2\Delta\frac{d\phi_i}{dr} \quad \text{(F-8)}$$

Solving equation (F-7) for $\frac{d^2\phi_i}{dr^2}$ results in equation (F-9) [38].

$$\frac{d^2\phi_i}{dr^2} = \frac{\phi_{i+1} - 2\phi_i + \phi_{i-1}}{\Delta^2} \quad \text{(F-9)}$$

Solving equation (F-8) for $\frac{d\phi_i}{dr}$ results in equation (F-10).

$$\frac{d\phi_i}{dr} = \frac{\phi_{i+1} - \phi_{i-1}}{2\Delta} \tag{F-10}$$

Recognizing that the radius is discrete and calculated by,

$$r = \Delta i \tag{F-11}$$

and substituting equations (F-9), (F-10) and (F-11) into (F-2) gives a numerical approximation for the *Laplacian*.

$$\nabla^2 = \frac{\phi_{i+1} - 2\phi_i + \phi_{i-1}}{\Delta^2} + \frac{2(\phi_{i+1} - \phi_{i-1})}{2i\Delta^2} \tag{F-12}$$

Replacing the two in the numerator of the second term with a variable, c, generalizes equation (F-12) for multiple one-dimensional geometries.

$$\nabla^2 = \frac{\phi_{i+1} - 2\phi_i + \phi_{i-1}}{\Delta^2} + \frac{c(\phi_{i+1} - \phi_{i-1})}{2i\Delta^2} \tag{F-13}$$

By letting $= 2, 1 \text{ or } 0$, equation (F-13) will approximate the *Laplacian* for one-dimensional spherical, cylindrical and slab geometries, respectively [38].

Appendix G Glossary

A

Adjoint – An operator, **O**, and a function, *f*, has an adjoint operator, $\mathbf{O}^{\dagger}$, and an adjoint function, $f^{\dagger}$, if the relationship, $\langle f^{\dagger}, \mathbf{O}f \rangle = \langle f, \mathbf{O}^{\dagger} f^{\dagger} \rangle$ is satisfied. A *Hermitian* or *self-adjoint* operator satisfies $\mathbf{O} = \mathbf{O}^{\dagger}$ [23, 56].

Albedo – When used in the context of neutron transport, the albedo is the probability that neutron incident on a surface will return through that same surface [73].

Algabraic equation – Equaitons that follow the rules of algebra [74]. Polynomial equations. Algabraic equations are non-linear when they contain variables with powers not eaqual to one [64].

Algebraically – According to the laws of algebra.

Angular flux – The total of path lengths traveled by all particles in direction, $\hat{\mathbf{\Omega}}$, per unit volume per unit time [23]. Angular flux is derived from the angular particle density, *N* [#/(steradian-volume)] and the velocity of the particles, v [length/time]. So that,

$\psi = \mathrm{v}\, N \rightarrow \left[\frac{\text{length}}{\text{time}}\right]\left[\frac{\#}{\text{steradian}\cdot\text{volume}}\right] \rightarrow \left[\frac{\#}{\text{steradian}\cdot\text{area}}\right]$ [56].

Asymptote – A straight line where the perpendicular distance from it to a function value becomes less than an any postitive value assigned to it as the function recedes indefinately from the origin [75].

Asymptotic – Approaching a value or curve arbitrarily close [74].

B

barn – A common unit of microscopic neutron cross sections. $\text{barn} = 10^{-24}\text{cm}^2$ [38]. Scientist at Purdue University named the unit in 1942 after noting that the cross section of 10^{-24} cm^2 was as big as a barn in terms of nuclear processes [76].

C

cgs units – "A system of units based upon the centimeter, gram, and second. The cgs system has been supplanted by the International System (SI)." [77]

Condition Number – The product of a matrix norm and the norm of its inverse.

$$K(A) = \|A\| \cdot \|A^{-1}\|$$

Ther condition number infers the relative safety that a small residual vector of a solution process implies a correspondingly accurate approximation. If $K(A)$ is close to 1 then the matrix is considered well-conditioned, and is ill-conditioned if significantly greater than 1 [62].

Cross section – 1. *Macroscopic cross section* – the probability of collision per unit path length. Has units of inverse length. 2. *Microscopic cross section* – the effective cross-sectional area seen by a particle. Has units of area [23].

Current – 1. Net current ***J***, is the net number of particles crossing per unit area of surface per unit time. For comparison with scalar flux, ϕ , ***J***, is the first moment of angular flux ψ, $\boldsymbol{J} = \int (\mathbf{n} \cdot \hat{\boldsymbol{\Omega}}) \hat{\boldsymbol{\Omega}} \, \psi \, d\Omega$. 2. Directional current is the number of particles crossing a surface in a given direction [23, 56].

D

Diffusion Length – The neutron diffusion length is essentially the distance that a neutron will diffuse from a source before being absorbed. The length is calculated by, $L = \sqrt{D/\sigma_a}$ [38].

Dollar Reactivity – Reactivity in dollars is equal to the reactivity divided by the delayed neutron fraction, $\frac{\rho}{\beta}$. The prompt critical condition where, $\rho = \beta$, defines one dollar of reactivity [52].

Dominance Ratio – "ρ", the ratio of the second greatest eigenvalue and the dominate eigenvalue, $\rho = \lambda_2/\lambda_1$ (without units). Where, $\{\lambda_i\}_{i=1}^{N}$ is a set of eigenvalues ordered as, $|\lambda_1| > |\lambda_2| > \ldots > |\lambda_N|$ [7].

Dominate Eigenvalue – The eigenvalue that is largest in absolute value [61].

G

Generation – A neutron of one generation absorbed in fissionable material that causes a fission gives birth to the next generation of neutrons [57].

Glory Hole – Cavity located in the interior of a reactor used to hold experiments [11].

I

Inner Product – If *f* and *g* are both functions of the same variables, the inner product of these functions is, $\langle f, g \rangle \equiv \int f(x)g(x)dx$. Evaluate the integral over the entire range of all independent variables [56, 23].

Isotopes – "Nuclides having the same atomic number, but different mass numbers." [73]

J

Jacobian – The matrix formed by the partial derivatives of a system of functions [74].

$$\mathbb{J}_{i,j} = \frac{\partial F_i(\boldsymbol{U})}{\partial \boldsymbol{U}_j} \longrightarrow \mathbb{J} = \begin{bmatrix} \frac{\partial F_1(\boldsymbol{U})}{\partial \boldsymbol{U}_1} & \cdots & \frac{\partial F_1(\boldsymbol{U})}{\partial \boldsymbol{U}_n} \\ \vdots & \ddots & \vdots \\ \frac{\partial F_n(\boldsymbol{U})}{\partial \boldsymbol{U}_j} & \cdots & \frac{\partial F_n(\boldsymbol{U})}{\partial \boldsymbol{U}_n} \end{bmatrix}$$

K

Kernel – Is a function, $K(x,x')$ of several variables, including the variables of integration in an integral of the form, $\int dx' K(x,x') f(x')$ [38].

Kinetics – Nuclear reactor kinetics is the topic of predicting the time behavior of the neutron population as a result of changes in reactor multipication [38].

Kronecker delta – Is the discrete form of the delta function, $\delta_{mn} \equiv \begin{cases} 1, & m = n \\ 0, & m \neq n \end{cases}$ [74, 78].

The Kronecker is used in the description of Legendre polynomial orthogonality relationship [23].

L

Low Enriched Uranium – "Fuel in which the weight percent of U-235 in the uranium is less than 20%" [79].

M

MKS units – "The system of units based on measuring lengths in meters, mass in kilograms, and time in seconds" [74].

N

Neutronics – The study of the processes related to the neutron economy (production and losses) in a system [38].

Nuclide – "A species of atom characterized by its mass number, atomic number, and nuclear energy state provided the mean life in that state is long enough to be observable" [73].

O

Orthogonal – 1. Perpendicular. 2. Two vectors with a dot product equal to zero 3. Polynomials are orthogonal if defined over a range [*a*, *b*] and adhere to the relationship,

$\int_a^b w(x)p_m(x)p_n(x) = \delta_{mn}c_n$. Where $w(x)$ is a weighting function and c_n is a constant. If c_n is equal to one, then the polynomials are also *orthonormal* [74].

Optical thickness, distance or path – Is "the geometrical distance between points, multiplied by the inverse of the mean free path averaged over the line segment between them" [80]. The mean free path is $1/\sigma$ [56]. The term optically thick commonly means a medium with a high total or specific cross-section [43].

P

Picard linearization – Iterative scheme to solve the nonlinear problem, $Ax = x$, by the fixed point iteration of the form ${}^{s+1}\boldsymbol{x} = A\ {}^{s}\boldsymbol{x}$ [60].

Poison – Material that removes neutrons from a system [52].

Preconditioning – Operation that "replaces a given system with one having the same solutions but with better convergence characteristics." [62]

R

Reactor Period – "The amount of time required for the flux to change by a factor of *e* [52].

Richardson Iteration – Iterative scheme to solve the linear equation, $Ax = b$, by a fixed point iteration of the form ${}^{s+1}\boldsymbol{x} = (I - A)\,{}^{s}\boldsymbol{x} + b$ [60].

S

Scalar flux – (or total flux) The total of path lengths traveled by all particles in any direction per unit volume per unit time. Scalar flux is derived from the particle density, *n* [#/volume] and the velocity of the particles, v [length/time]. So that, $\phi = \mathrm{v}\,n \rightarrow \left[\frac{\text{length}}{\text{time}}\right]\left[\frac{\#}{\text{volume}}\right] \rightarrow \left[\frac{\#}{\text{area}}\right]$. For comparison with current **J**, ϕ is the zero moment of angular flux ψ, $\phi = \int \left(\mathbf{n} \cdot \widehat{\boldsymbol{\Omega}}\right) \psi \, d\Omega$ [56] [23].

Symmetric Matrix – A matrix that is equal to its transpose [61].

Singularity – "Points at which functions are not analytic." [78]

Span – The span of a set of vectors is the sum of the each vector multiplied by any real scalar [74].

$$\underline{\text{Span}(\mathbf{v}1, \mathbf{v}2) \equiv \{r\mathbf{v}1 + s\mathbf{v}2 : r, s \in \mathbb{R}\}}$$

T

Telegrapher equation – An equation governing the propagation of electromagnetic waves in conducting media [81, 78]. The equation itself is a hyperbolic differential equation that is similar to the diffusion equation, but that includes a second order time derivative [82].

$$\tau \frac{\partial^2}{\partial t^2}\rho + \frac{\partial}{\partial t}\rho = D\nabla^2$$

The term comes up occasionally when discussing neutron diffusion theory presumably since telegraphist predated nuclear scientists.

Transcendental equation – An equation that contains transcendental functions. Examples of transcendental functions include exponentials, logarithmic, trigonometric, and hyperbolic [83]. Transcendental equations are non-linear [64].

Transport sweep – A single source iteration in the numerical solution to the discrete ordinates transport equation [43].

Trilinos – A collection scientific computational software packages produced and maintained by Sandia National Laboratories. A Greek term meaning "a string of pearls". Developers chose the name to convey that each package in the Trilinos collection is a "pearl" of useful software [84].

Verification – The determination that the system is built right or the problem is solved correctly [85].

Validation – The determination that the right system was built or that the correct problem is solved [85].

Appendix H PDE Classification & Characteristics

Classification of Partial Differential Equations

The classification for the problems addressed in this work from Ordinary Differential Equation (ODE) is of the eigen-problem class [63]. However, from a broader perspective the neutron transport equation is described as crossing many classifications of a Partial Differential Equation (PDE) [86]. A PDE is classified as elliptical, parabolic or hyperbolic [63]. In optically thick, high scattering material, the transport equation behavior limits to parabolic, or elliptic. In void streaming regions, the limiting behavior is parabolic [86]. The diffusion equation and even-parity transport equations are considered parabolic or elliptic depending on spatial dimensions and time-dependence. This classification is most often initially determined by a characterizing polynomial of the form found in equation (H-1) [63].

$$A\frac{\partial^2 u}{\partial x^2} + B\frac{\partial^2 u}{\partial x \partial y} + C\frac{\partial^2 u}{\partial y^2} + D\frac{\partial u}{\partial x} + E\frac{\partial u}{\partial y} + Fu = G \qquad \text{(H-1)}$$

The classification is determined by the value of the discriminant, $B^2 - 4AC$ [63].

Table H.1 PDE Classification

$B^2 - 4AC$	Classification
Negative	Elliptic
Zero	Parabolic
Positive	Hyperbolic

The plots resulting from the polynomial and the various cases of its discriminant are plotted in Figure H.1.

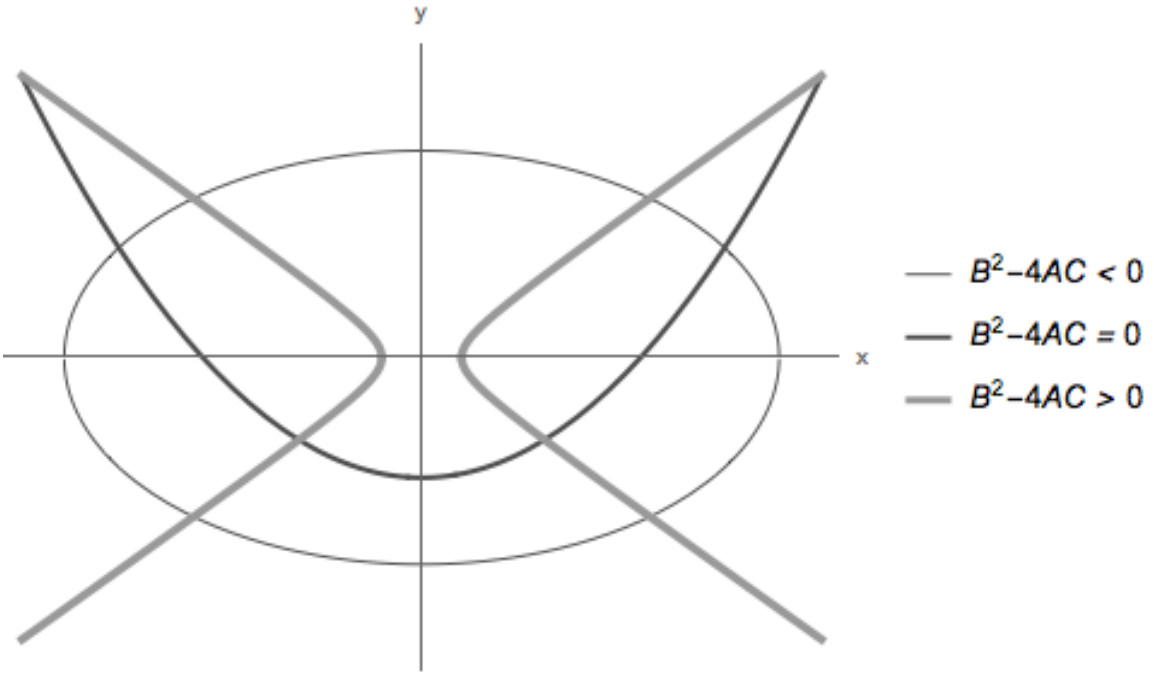

Figure H.1 Plots of the descriptive polynomial of PDE classifications

"The analogy is to the classification of the PDEs is obvious. There is no other significance to the terminology." [63] In fact, the terminology is misleading in at least one case. "A single first order PDE is always hyperbolic." [63] However, the resulting discriminant of the classifying polynomial implies it is parabolic. Possibly an "open" parabola where the *fulcrum* equals the *vertex*, see Figure H.2.

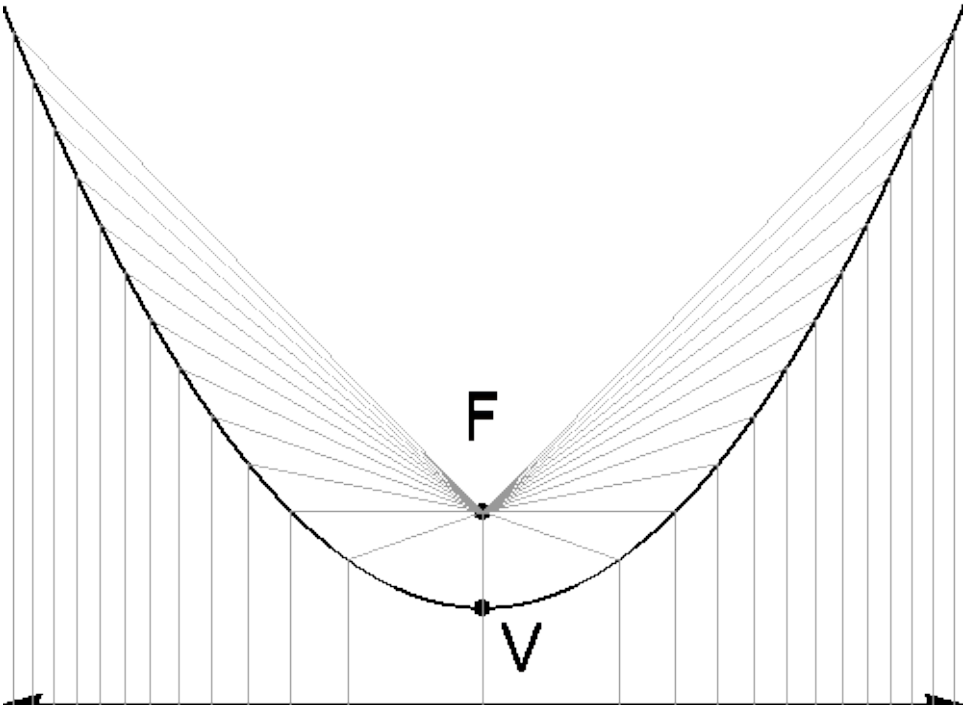

Figure H.2 Parabola: A geometric representation.

The real classification comes from a much more complicated analysis of the characteristics of the solution domain. Reference [63] provide details on this analysis.

Appendix I Symbols and Notation

Symbols

α – *alpha* – Time eigenvalue associated with the asymptotic neutronic solution.

$\forall$ – For all.

$|\ \ |$ – Absolute value or magnitude.

$\cong$ – Approximately equal to.

$\bar{\ }$ – Average or mean value

* – *asterisk* – Multiplication

β – *beta* – Delayed neutron fraction.

c – 1. Scattering ratio, σ_s/σ_t. 2. Generic constant.

D – The diffusion coefficient

δ_{mn} – Kronecker delta.

$\equiv$ – defined as.

e – The natural number. Exponential.

E – Energy.

$\mathfrak{E}$ – Eddington factor, also called the quasi-diffusion tensor.

$\in$ – Element of.

g – Energy group index.

h – height.

$\langle \_, \_ \rangle$ – Inner product.

i – 1. Imaginary number. 2. Spatial discretization index.

I – 1. The identity matrix. 2. The max number in a set indexed by i.

j – Spatial discretization index.

$\boldsymbol{J}$ – Current.

$\mathbb{J}$ – The Jacobian

k – 1. Neutron multiplication factor, typically prompt only. 2. Spatial discretization index.

k_{eff} -- Neutron multiplication factor, typically including delayed neutrons.

l – Neutron lifetime.

L – Neutron diffusion length.

ℓ – 1. Angular discretization index (P_N). 3. Legendre polynomial index.

ln – Natural logarithm.

Λ – Neutron generation or importance lifetime.

m – Associated Legendre polynomial index.

μ – *mu* – 1. The cosine of the polar angle. 2. Micro.

n – 1. Particle density. 2. Angular discretization index (S_N) 3. Generic counter.

$\|\ \ \|$ -- Norm.

$\hat{\mathbf{\Omega}}$ – *omega "hat"* – Directional unit vector.

† – *obelisk* – Adjoint.

$\perp$ -- Perpendicular or orthogonal to.

ϕ – *phi* – Scalar flux.

ϕ_l – *phi "sub el"* – Legendre moments.

' – *prime* – 1. A different value, often used in notional definite integrals. 2. Derivative.

φ – The azimuthal angle.

ψ – *psi* – Angular flux.

r – Radius, usually variable.

R – Radius, usually geometric as in the total radius of a FBR

$\tilde{R}$ – The extrapolated boundary used in diffusion calculations

$\mathbb{R}$ – The set of real numbers

ρ – *rho* – 1. Reactivity. 2. Density.

s – Iteration index.

σ – *sigma* – Macroscopic cross-section.

$\tilde{\sigma}$ – *sigma tilde* – Microscopic cross-section.

$\sum$ – Summation.

Θ – Energy coefficient of feedback reactivity

θ – *theta* – The polar angle.

T – Temperature.

$\mathcal{T}$ – Time, used when use of "*t*" is confusing due to a time-step index.

t – 1. Time. 2. Discrete time index.

τ – *tau* – The Full Width at Half Maximum

$\rightarrow$ – 1. Vector. 2. Indicator of the value that a variable tends to in a limit. 3. Yields.

Notation

$\psi^{+}(r_i, \hat{\Omega}_n, E_g, \mathcal{T}_t)$ reads as, the even-parity angular flux at spatial cell *i*, for a discrete direction *n* in energy group *g* at time step *t*. The chosen angular approximation will determine the specific form of the $\hat{\Omega}$ term as appropriate direction cosines or sums of Legendre polynomials and coefficients. The Figure C.1 shows an abbreviated representation of the discretized flux as well as well as an example representation of Legendre moments if a P_N approximation is used.

$$\left({}^{\text{iteration, energy, time}}_{\text{space}} \psi^{\text{angular parity}}_{\text{angle}} \right)^{\text{exponent}}$$

(a)

$$\left({}^{s,g,t}_{i} \psi^{+}_{n} \right)^{2}$$

(b)

$$^{s,g,t}_{i} \phi_{\ell}$$

(c)

Figure I.1 Discrete Notation for the Transport Equation:

(a) The standard locations for indices and exponents of the unknown. In cases where it obvious the angle index does not apply then the spatial index may occupy the right lower subscript. (b) The even-parity angular flux for solution iteration *s*, energy group *g*, at time step *t*, in cell *i*, for discrete angle n, squared. (c) The ℓ^{th} Legendre moment, for solution iteration *s*, energy group *g*, at time step *t*, in cell *i*.

Appendix J Nordheim-Fuchs

In the transient operation of a FBR, the neutron population rises and falls in an exponential way [87]. The instantaneous alpha describes this dynamic behavior [55].

$$n(t) = n(0)\, e^{\int_0^t \alpha(t')dt'} \tag{J-1}$$

The primary contribution of this research is the JFNK solution method of alpha for ultimate use in time-dependent codes that approximate equation (J-1). However, in the interim the Nordheim-Fuchs model proves a valuable tool to assist in validation of the solution methods, and to provide immediate utility of calculated values.

The Nordheim-Fuchs model is meaningful in cases of power excursions that are self-limiting and short-lived. Additionally, the insertion of reactivity must be large enough, and the time of the excursion short enough that delayed neutron contributions are negligible [22]. These conditions assume that the neutron population, or power, satisfies equation (J-2).

$$\frac{dn}{dt} = \frac{\rho - \beta}{\Lambda} n = \frac{k-1}{l} n \tag{J-2}$$

Equation (J-2) is identical to equation (2-20) except here the complications of *reactivity*, *delayed neutron fraction*, β (see Appendix B), and the *generation lifetime*, are introduced to align with traditional representation of the model found elsewhere [22, 1].

$$reactivity \equiv \rho = \frac{k_{eff} - 1}{k_{eff}} \tag{J-3}$$

$$generation\ lifetime\ \equiv \Lambda = \frac{l}{k_{eff}} \tag{J-4}$$

The initial conditions are of a reactor that is either subcritical or critical at a low power level [22]. The Nordheim-Fuchs model does not account for changes in the reactivity in the way represented in equation (J-1). Instead, the model describes the system in terms of initial peak reactivity, ρ_0, and feedback coefficients [1, 22].

$$\rho = \rho_0 - b\,T \tag{J-5}$$

Where, *b*, is the negative of the temperature coefficient of reactivity [87, 22], and, *T*, is the temperature increase above the initial value [22]. Due to the short time scale of the excursion, the change in temperature with respect to time uses an adiabatic model [22].

$$\frac{\mathrm{d}T}{\mathrm{d}t} = K\,n \tag{J-6}$$

Where, *K*, is the reciprocal of heat capacity [22]. Taking the derivative with respect to time of equation (J-5) provides equation (J-7).

$$\frac{\mathrm{d}\rho}{\mathrm{d}t} = 0 - b\frac{\mathrm{d}T}{\mathrm{d}t} \tag{J-7}$$

Substituting equation (J-6) into equation (J-7) gives equation (J-8).

$$\frac{\mathrm{d}\rho}{\mathrm{d}t} = -b\,K\,n = -\Theta\,n \tag{J-8}$$

Where, *b K*, is the *energy coefficient of feedback reactivity*, Θ. So, now the system is described in terms of the first order differential equations of (J-2) and (J-8). From these equations the derived peak power is [1, 22],

$$\hat{n} = \frac{(\rho_0 - \beta)^2}{2\,\Theta\,\Lambda}. \tag{J-9}$$

Which simplifies to equation (2-22) in terms of scalar flux, and the values calculated by JAKES. The *full width at half maximum* (FWHM) is also derived from these equations and is found to be [22, 1],

$$FWHM \equiv \tau = \frac{4\cosh^{-1}\sqrt{2}}{\alpha_0} \cong \frac{3.524}{\alpha_0}. \tag{J-10}$$

Equations (J-9) and (J-10) are solved using values predictively calculated by the new algorithms developed in this research to model the burst characteristics of historic, and postulated FBRs.

Appendix K Leakage Minimization

Based on diffusion theory the leakage of a system is,

$$L = DB^2. \tag{K-1}$$

Where D is the diffusion coefficient and B is *geometric buckling* [38]. For a two-dimensional cylinder, *r-z*, the leakage is,

$$L = D\left(\left(\frac{\upsilon_0}{R}\right)^2 + \left(\frac{\pi}{H}\right)^2\right). \tag{K-2}$$

Where, υ_0 is the first (smallest) zero of the *Bessel function* J_0 and equals 2.405 [38].

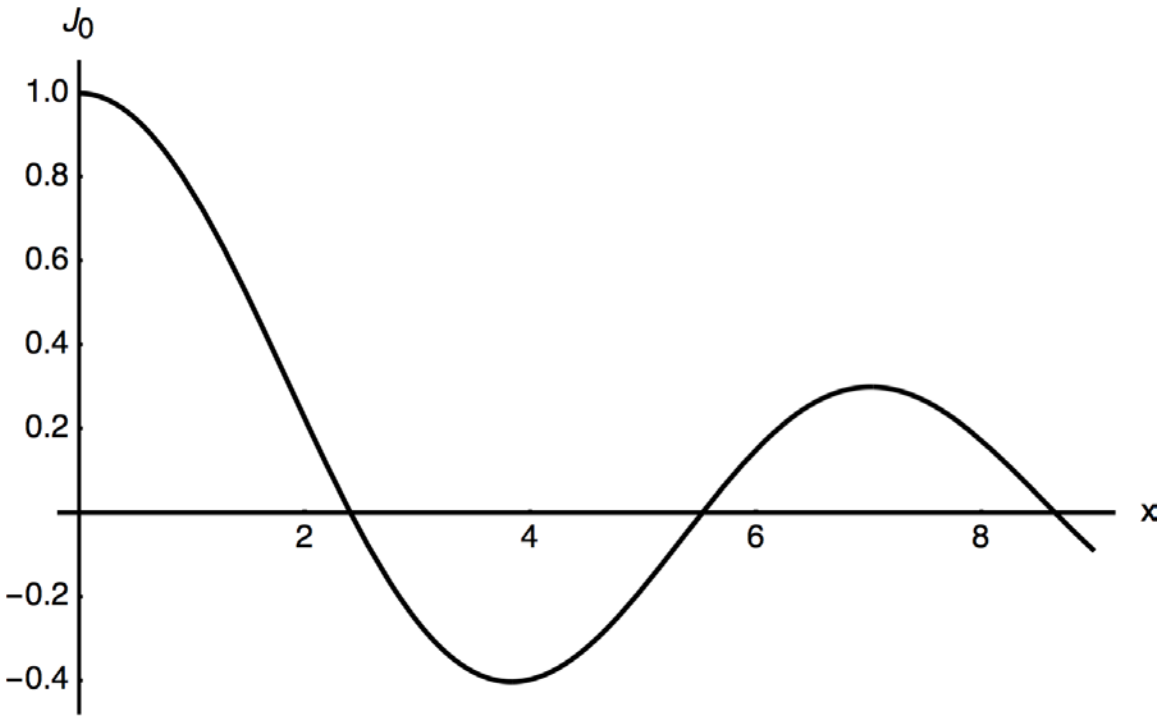

Figure K.1 Bessel Function, J_0

Defining *H* as a multiple of *R*, equation (K-2) becomes,

$$L = D\left(\left(\frac{v_0}{R}\right)^2 + \left(\frac{\pi}{cR}\right)^2\right). \tag{K-3}$$

The volume of a cylinder is,

$$V = \pi R^2 H = \pi R^3 c. \tag{K-4}$$

Solving for *R* in terms of volume yields,

$$L = D\left(\left(\frac{v_0}{\left(\frac{V}{\pi c}\right)^{1/3}}\right)^2 + \left(\frac{\pi}{c\left(\frac{V}{\pi c}\right)^{1/3}}\right)^2\right). \tag{K-5}$$

Now taking the derivative with respect to *c* and setting to zero will minimize the value of *c* [72].

$$0 = \frac{\partial}{\partial c}\left[D\left(\left(\frac{v_0}{\left(\frac{V}{\pi c}\right)^{1/3}}\right)^2 + \left(\frac{\pi}{c\left(\frac{V}{\pi c}\right)^{1/3}}\right)^2\right)\right] \rightarrow \tag{K-6}$$

$$0 = \frac{2}{3}{v_0}^2 c^{-1/3} - \frac{4}{3}\pi^2 c^{-7/3} \tag{K-7}$$

Solve for *c*.

$$c^2 = 2\frac{\pi^2}{{v_0}^2} \rightarrow \tag{K-8}$$

$$c = \sqrt{2}\frac{\pi}{v_0} = 1.847 \qquad \text{(K-9)}$$

Therefore, to minimize leakage based on diffusion theory the optimum height of a cylindrical reactor is 1.847 times the radius [72].

Appendix L Linearity

Linear Equations

Intuitively, linear implies a straight line. All equations of the form

$$Ax + By + C = 0 \tag{L-1}$$

are equations of a straight line provided that *A* and *B* are not both zero [51].

Equation (L-1) is an equation of a straight line in the *x*-*y* plane and is sometimes referred to as linear equation in two variables. In three-dimensional Cartesian coordinates the equation

$$Ax + By + Cz + D = 0. \tag{L-2}$$

is an equation of a two dimensional plane and is referred to as a linear equation in three variables [88]. Beyond three variables the visualization of a linear geometry fails, but linear equations are generalized as

$$a_1x_1 + a_2x_2 + a_3x_3 + ... + a_nx_n = b, \text{ or } \sum_{j=1}^{n} a_jx_j = b. \tag{L-3}$$

Equation (L-3) is an equation of *n* variables in the first degree and thus is a linear equation. In this instance, "first degree" means the all exponents of the variables are one, and is the unifying principle that defines a linear equation [89]. Additionally, none of the variables are multiplied by each other. This condition would cause the equation to be non-linear as well [29].

Systems of Linear and Nonlinear Equations

Most often, interest is in solving for *n* unknowns in a system of *m* linear equations. Therefore, the notation of equation (L-3) is expanded to represent this type of system as

$$a_{i,1}x_1 + a_{i,2}x_2 + a_{i,3}x_3 + \ldots + a_{i,n-1}x_{n-1} + a_{i,n}x_n = b_i \text{ or } \sum_{j=1}^{n} a_{i,j}x_j = b_i \text{ where } (1 \le i \le m). \quad \text{(L-4)}$$

These systems are *consistent* if at least one solution exists and *inconsistent* if no solution exists [89].

If $n < m$, then the system is *over determined* and no solution exists. If $n = m$ then a unique solution will exists provided the matrix of the coefficients, *a*, is *nonsingular* (the determinant of the matrix of coefficients is not equal to zero). If $n > m$ then the system *underdetermined* and multiple solutions exist [74].

This work typically writes linear equations like those in equation (L-4) in matrix form,

$$\boldsymbol{Ax} = \boldsymbol{b} \quad \text{(L-5)}$$

where, A is the matrix of the coefficients, and $\boldsymbol{x}$ and $\boldsymbol{b}$ are column vectors containing the variables and solutions of equation (L-4) [60].

Many nonlinear equations such as the ones found in this work are formulated as fixed-point problems [60],

$$A\boldsymbol{x} = \boldsymbol{x}. \tag{L-6}$$

Fixed-point iteration is often the method used to solve equations of this type.

$$A({}^{s}\boldsymbol{x}) = {}^{s+1}\boldsymbol{x} \tag{L-7}$$

This iteration technique is also called *nonlinear Richardson iteration, Picard iteration,* or, *the method of successive substitution* [60].

The system depicted by equation (L-6) is nonlinear because other than the case where $A = I$, equation (L-6) is only true for certain $\boldsymbol{x}$ vectors. This concept is difficult to place in a matrix equation form since there is no sensible "vector inverse" to apply. A vector is in fact a non-square matrix and thus has no inverse [61]. However, if we consider the action of A on $\boldsymbol{x}$ as similar to an operation on a single variable we can show that,

$$O(x) = x \tag{L-8}$$

is only true for cases where,

$$O(x)x^{-1} = 1 \tag{L-9}$$

and since equation (L-9) is not of first degree, it is not a linear equation. Additionally, in eigenvalue problems,

$$A\boldsymbol{x} = \lambda\boldsymbol{x} \qquad \text{(L-10)}$$

the solution is a multiple of two variables, the eigenvalue, λ, and $\boldsymbol{x}$ and thus are non-linear in this manner also [29].

Transcendental and *algebraic* are the two types of non-linear equations [64]. In the algebraic case these are equations that contain powers of the independent variable other than one. Transcendental equations are those that are not algebraic, and are always non-linear. These include, but are not limited to Exponentials, logarithms, trigonometrics and hyperbolics [83]. Strictly speaking, a transcendental equation must contain a transcendental function, such as those listed previously, but transcendental is often applied generally to equations that are particularly difficult to deal with [64].

Linear Systems

The term linear as it applies to functions and systems (not equations and systems of equations) is slightly different and often causes confusion when discussing physical problems and numerical techniques. The following definitions and discussion should clarify the use of the term linear in this context.

Definition: "A system is any structure of inter-connected components created to complete some desired function. It has distinct inputs and outputs and it produces an output signal in response to an input signal. The functional relationship between the input and the output is given by a set of mathematical equations and this set is called a *model of the system*" [90].

Definition: A system is linear if and only if it possesses both homogeneity and superposition properties [90].

Setting $C = 0$ and solving for y gives the slope-intercept form of equation (L-1), $y = -\frac{A}{B}x$. Letting $-\frac{A}{B} = m$ gives a more familiar form of an algebraic equation of a straight line with the y-intercept at zero and slope of *m*,

$$y = mx. \tag{L-10}$$

Given that the straight line of equation (L-10) is not parallel to the x-axis (*y* is not held constant), the line may be thought of as a function of *x* [51]. That is, *x* is an input to a system and *f(x)* is an output.

$$f(x) = mx \tag{L-11}$$

The property of homogeneity requires that an input "*x*" resulting in an output *f* (*x*) when multiplied by any real number *k* results in,

$$f(kx) = kf(x). \tag{L-12}$$

Multiplying the input "*x*" and the output *f* (*x*) by *k* demonstrates homogeneity of equation (L-11).

$$f(kx) = mkx = kf(x) \tag{L-13}$$

The superposition property requires that the addition of two inputs "x" and "*t*" results in the sum of the outputs of each input individually,

$$f(x+t) = f(x) + f(t). \tag{L-14}$$

Applying (L-14) to (L-11) shows the superposition of A-2.

$$f(x+t) = m(x+t) = mx + mt = f(x) + f(t) \tag{L-15}$$

Figure L.1 graphically depicts the homogeneity and superposition properties of equation (L-11).

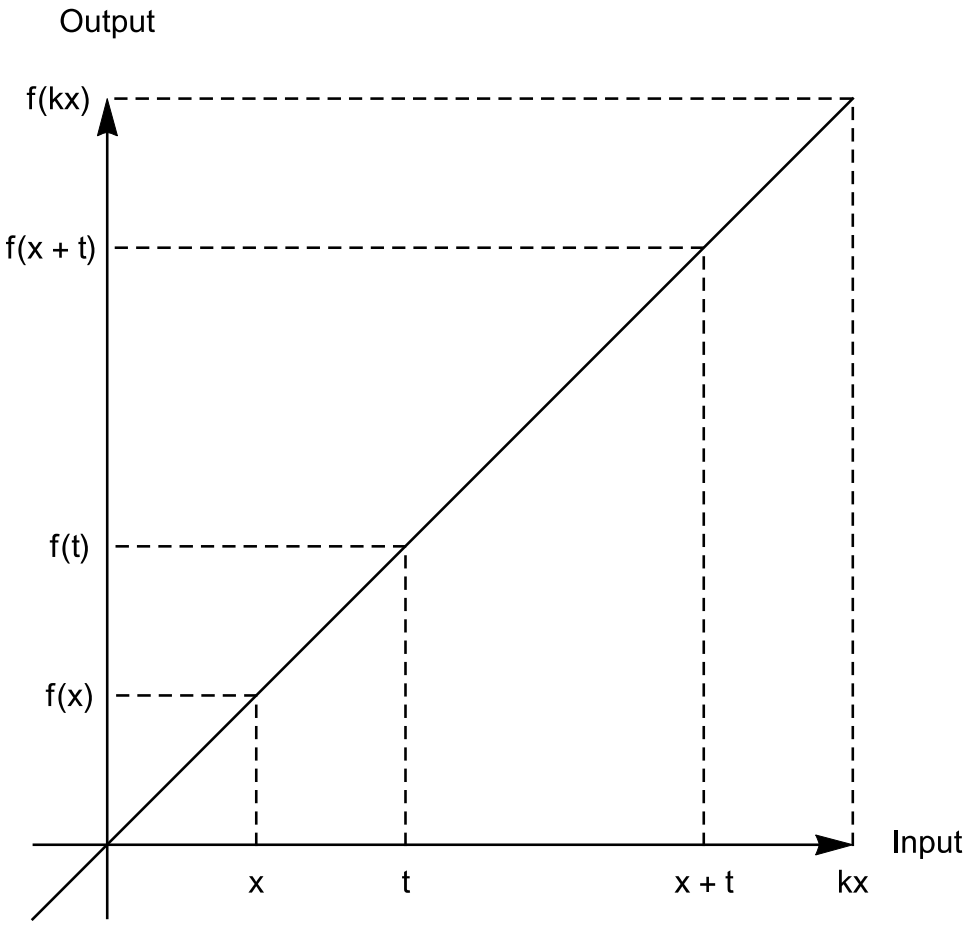

Figure L.1 Homogeneity and Superposition Properties of Linear Systems

Now consider equation (L-11) if *C* was not set to zero in the derivation,

$$f(x) = mx + C. \tag{L-16}$$

Checking equation (L-16) with the superposition property of linear systems gives,

$$f(x+t) = m(x+t)+C = mx+mt+C \neq f(x)+f(t)$$
$$= mx+C+mt+C = mx+mt+2C \qquad \text{(L-17)}$$

and it is shown that the property of superposition fails in this case. Checking the homogeneity property gives a similar result,

$$f(kx) = mkx+C \neq kf(x) = kmx+kC\,. \qquad \text{(L-18)}$$

The somewhat counterintuitive result that the function in (L-16) does not meet the criteria of a linear system is best explained by noting that an input, *x*, of zero does not result in an output, *f(x)*, of zero (see figure L.2). These systems are called *initially relaxed*, and as long as the constant, *C*, is treated as an initial condition the techniques of linear analysis apply to systems described by the function of (L-16) [90]. In fact, math references differ in describing the function in (L-16) as linear or non-linear function [51, 59].

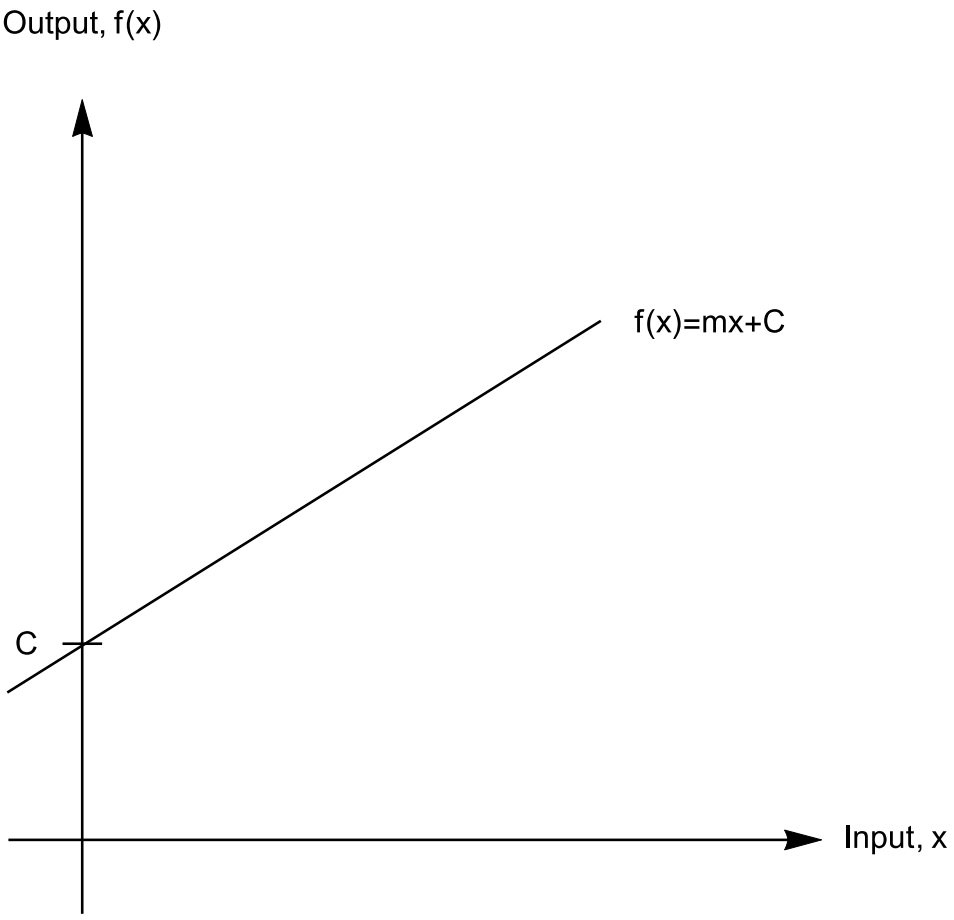

Figure L.2 Example of an Initially Relaxed System

An operator is a rule or instruction to apply to a function. Similar to the requirements for linear systems, if an operator, *O*, meets the following criteria,

$$O(f+g)=O(f)+O(g) \text{ and } O(kf)=kO(f), \tag{L-19}$$

then *O*, is a linear operator. In this case *k* is a number. *f* and *g* are functions, but could also be numbers or vectors [59]. Differentiation is an example of a linear operator [83].

References

[1] E. P. Shabalin, Fast Pulsed and Burst Reactors, Moscow: Pergamon Press, 1979.

[2] T. F. Wimett, "Fast Burst Reactors in the U.S.A.," Los Alamos Scientific Laboratory, Los Alamos, 1965.

[3] Defense Science Board, "Report of the Defense Science Board Task Force on Nuclear Weapon Effects Test, Evaluation, and Simulation," Department of Defense, San Bernardino, 2005.

[4] National Nuclear Security Administration, "Prevent, Counter, and Respons: A Strategic Plan to Reduce Global Nuclear Threats (FY 2016-FY2020," Department of Energy, Washington, DC, 2015.

[5] J. D. Sease, R. T. Primm, III and J. H. Miller, "Conceptual Process for the Manufacture of Low-Enrichment Uranium/Molybdenum Fuel for the High Flux Isotope Reactor," Oak Ridge National Laboratory, Oak Ridge, 2007.

[6] D. M. Wachs, C. R. Clark and R. J. Dunavant, "Conceptual Process for the Manufacture of Low-Enriched Uranium-Molybdenum Fuel," Idaho National Laboratory, Idaho Falls, 2008.

[7] H. Park, D. H. Knoll and C. K. Newman, "Nonlinear Acceleration of Transport Criticality Problems," *Nuclear Science and Engineering*, vol. 172, pp. 52-65, September 2012.

[8] D. A. Knoll and D. E. Keyes, "Jacobian-free Newton-Krylov Methods: a Survey of Approaches and Applications," *Journal of Computational Physics*, no. 193, pp. 357-397, 2004.

[9] H. Park, D. A. Knoll, D. R. Gaston and R. C. Martineau, "Tightly Coupled Multiphysics Algorithms for Pebble Bed Reactors," *Nuclear Science and Engineering*, no. 166, pp. 118-133, 2010.

[10] R. E. Malenfant, "Experiments with the Dragon Machine," Los Alamos National Laboratory, Los Alamos, 2005.

[11] USAEC Division of Technical Information, Fast Burst Reactors, Oak Ridge, TN: U.S. Atomic Energy Commision, 1969.

[12] R. E. Peterson, "Lady Godiva: An Unreflected Uranium-235 Critical Assembly," Los Alamos Scientific Laboratory, Los Alamos, 1953.

[13] P. J. Bendt, H. J. Karr and F. R. Scott, "Alpha Measurements on the Godiva Critical Assembly Using a Betatron," Los Alamos Scientific Laboratory, Los Alamos, 1953.

[14] G. E. I. McKenzie, "Modern Alpha Rossi Measurements," University of Illinois at Urbana-Champaign, Urbana, 2014.

[15] R. L. Long, "Operating Characteristics of the WSMR Fast Burst Reacor," in *Neutron Dynamics and Control*, Oak Ridge, TN: Oak Ridge National Laboratory, 1966, pp. 386-397.

[16] T. F. Luera and D. L. Welch, "Methodology Investigation: Characteristics of the White Sands Missile Range Fast Burst Reactor," Army Missile Test and Evaluation, White Sands Missile Range, 1970.

[17] F. Kloverstrom, "Operating Characteristics of the Super Kukla Prompt Burst Reactor," Lawrence Radiation Laboratory, Livermore, 1969.

[18] W. S. Gilbert, F. A. Kloverstrom and F. J. Rienecker, "Safety Analysis Report for the Super Kukla Prompt Reactor," Lawerence Radiation Laboratory, Livermore, 1964.

[19] T. R. Schmidt, B. F. Estes and J. A. Reuscher, "Recent Operational History of the New Sandia Pulsed Reactor III," Sandia National Laboratories, Albuquerque, 1977.

[20] T. C. Green, "Simulation of Reactor Pulses in Fast Burst and Externally Driven Nuclear Assemblies," University of Texas, Austin, 2008.

[21] S. C. Wilson, "Development and Implementation of a Finite Element Solution of the Coupled Neutron Transport and Thermoelastic Equations Governing the Behavior of Small Nuclear Assemblies," The University of Texas, Austin, 2006.

[22] D. L. Hetrick, Dynamics of Nuclear Reactors, Chicago, IL: The University of Chicago Press, 1971.

[23] E. E. Lewis and W. F. Miller, Computational Methods of Neutron Transport, La Grange Park, Illinois: American Nuclear Society, Inc., 1993.

[24] T. Goorely and e. al, "Initial MCNP6 Release Overview," *Nuclear Technology,* pp. 298-315, December 2012.

[25] B. R. Betzler, "Calculating Alpha-Eigenvalue Spectra with Monte Carlo," Los Alamos National Laboratory, Los Alamos, 2013.

[26] K. D. Parsons, "Alpha-Like Calculations with MCNP," Los Alamos National Laboratory, Los Alamos, 1997.

[27] R. S. Modak and A. Gupta, "A Scheme for the Evaluation of Dominant Time-Eigenvalues of a Nuclear Reactor," *Annals of Nuclear Energy,* no. 34, pp. 213-221, 2007.

[28] K. P. Singh, R. S. Modak, S. B. Degweker and K. Singh, "Iterative Method for Obtaining the Prompt and Delayed Alpha-Modes of the Diffusion Equation," *Annals of Nuclear Energy,* vol. 38, pp. 1996-2004, 2011.

[29] E. D. Fichtl and J. S. Warsa, "Computing the Alpha-Eigenvalue Using Nonlinear Solvers," in *American Nuclear Society Annual Meeting*, Washington DC, 2013.

[30] K. P. Singh, R. S. Modak, S. B. Degweker and K. Singh, "Iterative Schemes for Obtaining Dominant Alpha-Modes of the Neutron Diffusion Equation," *Annals of Nuclear Energy,* vol. 36, pp. 1086-1092, 2009.

[31] D. Lathouwers, "Iteritive Compution of Time-Eigenvalues of the Neutron Transport Equation," *Annals of Nuclear Energy,* vol. 30, pp. 1793-1806, 2003.

[32] D. Lathouwers, "Computing Time-Eigenvalues Using the Even-Parity Transport Form," *Annals of Nuclear Energy,* no. 33, pp. 941-943, 2006.

[33] J. E. Morel, J. M. McGhee and W. F. Walters, "3-D Research Transport Codes at Los Alamos," Los Alamos National Laboratory, Los Alamos, 1995.

[34] Radiation Safety Information Computational Center, "Software Catalog," Oak Ridge National Laboratory, [Online]. Available: https://rsicc.ornl.gov/CustomerService.aspx. [Accessed November 2016].

[35] D. F. Gill and Y. Y. Azmy, "Newton's Method for Solving k-Eigenvalue Problems in Neutron Diffusion Theory," *Nculear Science and Engineering,* no. 167, pp. 141-153, 2011.

[36] J. Willert, H. Park and D. A. Knoll, "A Comparison of Acceleration Methods for Solving the Neutron Transport k-Eigenvalue Problem," *Journal of Computational Physics*, no. 274, pp. 681-694, 2014.

[37] D. A. Knoll, H. Park and C. Newman, "Acceleration of k-Eigenvalue/Criticality Calcualations Using the Jacobian-Free Newton-Krylov Method," *Nuclear Science and Engineering*, no. 167, pp. 133-140, 2011.

[38] J. J. Duderstadt and L. J. Hamilton, Nuclear Reactor Analysis, New York: John Wiley & Sons, 1976.

[39] S. Balay, W. D. Gropp, L. C. McInnes and B. F. Smith, "Efficient Management of Parallelism in Object Oriented Numerical Software Libraries," in *Modern Software Tools in Scientific Computing*, A. Bruaset, E. Arge and H. P. Langtangen, Eds., Boston, Burkhauser, 1997, pp. 163-202.

[40] S. Balay, A. Shrirang, M. F. Adams, J. Brown, P. Brune, K. Buschelman, L. Dalcin, V. Eijkhout, W. D. Gropp, D. Kaushik, M. G. Knepley and L. C. McKines, "PETSc User Manual," Argonne National Laboratory, Chicago, 2016.

[41] S. Balay, A. Shrirang, M. F. Adams, J. Brown, P. Brune, K. Buschelman, L. Dalcin, V. Eijkhout, W. D. Gropp, D. Kaushik, M. G. Knepley and L. C. McKines, "PETSc Web Page," 2016. [Online]. Available: http://www.mcs.anl.gov/petsc.

[42] C. R. E. de Oliveira, "Finite Element Techniques for Multigroup Neutron Transport Calculations with Anisotropic Scattering," University of London, London, 1987.

[43] M. L. Adams and E. W. Larsen, "Fast Iterative Methods for Discrete-Ordinates Particle Transport Calculations," *Progress in Nuclear Energy*, vol. 40, no. 1, pp. 3-159, 2002.

[44] W. J. Martin, "Nonlinear Acceleration Methods for Eeven-Parity Neutron Transport," Albuquerque, 2010.

[45] C. R. E. de Oliveira, "Solving Radiation Transport Problems with the GEM/EVENT Codes," Albuquerque, 2011.

[46] W. L. Myers, T. J. Grove, D. K. Hayes, R. H. Kimpland and W. R. Stratton, "One and Two-Dimensional Excursion Modeling of GODIVA-IV and CALIBAN Using MRKJ Code," LANL, Los Alamos, 2011.

[47] S. K. Klein and R. H. Kimpland, "Concept for LEU Burst Reactor," Los Alamos National Laboratory, Los Alamos, 2016.

[48] Wolfram Research Inc., *Mathematica,* Version 11.0 ed., Champaign, IL: Wolfram Research Inc., 2016.

[49] T. F. Wimett, "Time Behavior of Godiva Through Prompt Critical," Los Alamos Scientific Laboratory, Los Alamos, 1956.

[50] J. T. Mihalczo, "Superprompt-Critical Behavior of an Unmoderated, Unreflected Uranium-Molybdenum Alloy Reactor," *Nuclear Science and Engineering*, no. 2, pp. 291-298, 1963.

[51] M. H. Protter and P. E. Protter, Calculus With Analytical Geometry, 4th Edition ed., Boston, Massachusetts: Jones and Bartlett Pubishers, 1988.

[52] R. A. Knief, Nuclear Engineering: Theory and Technology of Commercial Nuclear Power, Washington, DC: Hemisphere Publishing Corporation, 1992.

[53] A. L. Hanson and D. J. Diamond, "Prompt Neutron Lifetime for the NBSR Reactor," Brookhaven National Laboratory, Upton, 2012.

[54] J. D. Orndoff, "Prompt Neutron Periods of Metal Critical Assemblies," *Nuclear Science and Engineering,* no. 2, pp. 450-460, 1957.

[55] G. R. Keepin, Physics of Nuclear Kinetics, Reading, MA: Addison-Wesley Publishing Company, Inc., 1965.

[56] G. I. Bell and S. Glasstone, Nuclear Reactor Theory, New York: Van Nostrand Reinhold Company, 1970.

[57] E. E. Lewis, Fundamentals of Nuclear Reactor Physics, Burlington, MA: Elsevier Inc., 2008.

[58] J. R. Lamarsh, Nuclear Reactor Theory, Reading, MA: Addison-Wesley Publishing Company, Inc., 1966.

[59] M. L. Boas, Mathematical Methods in The Physical Sciences, 2nd Edition ed., New York, New York: John Wiley & Sons, 1983.

[60] C. T. Kelley, Iterative Methods for Linear and Nonlinear Equations, Philadelphia: Society for Industrial and Applied Mathematics, 1995.

[61] R. Larson, B. H. Edwards and D. C. Falvo, Elementary Linear Algebra, New York: Houghton Mifflin Company, 2004.

[62] R. L. Burden and J. D. Faires, Numerical Analysis, 8th Edition ed., Belmont, California: Thomson - Brooks/Cole, 2005.

[63] J. D. Hoffman, Numerical Methods for Engineers and Scientists, Second ed., New York: McGraw-Hill, Inc., 2001.

[64] F. S. Acton, Real Computing Made Real, Princeton: Princeton University Press, 1996.

[65] Y. Saad, "Iterative Methods for Sparse Linear Systems, Second Edition," Society for Industrial and Applied Mathematics, 2003.

[66] M. A. Heroux, "Azrec00 User Guide," Sandia National Laboratories, Albuquerque, 2007.

[67] Argonne National Laboratory, Reactor Physics Constants, Second Edition ed., Chicago: United States Atomic Energy Commission, 1963.

[68] International Atomic Energy Agency, "Physics of Fast and Intermediate Reactors," in *The Seminar on the Physics of Fast and Intermediate Reactors*, Vienna, 1962.

[69] Cross Sections Evaluation Working Group, "ENDF-6 Formats Manual," Brookhaven National Laboratory, Upton, 2009.

[70] D. E. Burkes, G. S. Mickum and D. M. Wachs, "Thermophysical Properties of U-10Mo Alloy," Idaho National Laboratory, Idaho Falls, 2010.

[71] J. T. Creasy, "Thermal Properties of Uranium-Molybdenum Alloys: Phase Decomposition Effects of Heat Treatments," Texas A&M University, College Station, 2011.

[72] P. McDaniel, Interviewee, *Leakage Minimization and MCNP Calculated Lifetimes.* [Interview]. 2 October 2017.

[73] ANS-9, The American Nuclear Society Standards Subcommittee on Nuclear Terminology and Units, Glossary of Terms in Nuclear Science and Technology, La Grange Park, Illinois: American Nuclear Society, 1986.

[74] E. Weisstein, "Wolfram Research," 11 February 2014. [Online]. Available: http://scienceworld.wolfram.com.

[75] P. H. Selby, Geometry & Trigonometry for Calculus, J. Wilson and I. Brownstone, Eds., New York: John Wiley & Sons, 1975.

[76] M. G. Hollaway and C. P. Baker, "LAMS-523, Note on the Origin of the Term "barn"," Los Alamos National Laboratory, Los Alamos, 1944.

[77] Chemical Rubber Company (CRC), CRC Handbook of Chemistry and Physics, 84th ed., D. R. Lide, Ed., Boca Raton, FL: Chemical Rubber Publishing Company, 2003.

[78] P. M. Morse and H. Feshbach, Methods of Theoretical Physics, New York, NY: McGraw-Hill Book Company, Inc., 1953.

[79] NRC Regulations, *10 C.F.R. § 50.2*, 2017.

[80] B. Davidson and J. B. Sykes, Neutron Transport Theory, London: Oxford University Press, 1958.

[81] D. H. Staelin, A. W. Morgenthaler and J. A. Kong, Electromagnetic Waves, Upper Saddle River, New Jersey: Prentice Hall, 1998.

[82] V. e. a. Méndez, Reaction-Transport Systems, Verlag Berlin Heidelberg: Springer, 2010.

[83] D. A. McQuarrie, Mathematical Methods for Scientist and Engineers, Sausalito, CA: University Science Books, 2003.

[84] M. Heroux, R. Bartlett, V. Howle, R. Hoekstra, J. Hu, T. Kolda, R. Lehoucq, K. Long, R. Pawloski, E. Phipps, A. Salinger, H. Thornquist, R. Tuminaro, J. Willenbring and A. Williams, "Trilinos Overview," Sandia National Laboratories, Albuquerque, 2003.

[85] International Council on Systems Engineering (INCOSE), Systems Engineering Handbook, Fourth Edition ed., D. D. Walden, G. J. Roedler, K. J. Forsberg, R. D. Hamelin and T. M. Shortell, Eds., Hoboken: John Wiley & Sons, 2015.

[86] D. Kaushik, M. Smith, A. Wollaber, A. Siegel and W. S. Yang, "Enabling High Fidelity Neutron Transport Simulations on Petascale Architectures," Argonne National Laboratory, Argonne, 2010.

[87] J. C. Vigil, "Solution of the Nonlinear Reactor Kinetics Equations by Continuous Analytical Continuation," Los Alamos Scientific Laboratory, Los Alamos, 1966.

[88] C. Stover, "Linear Equation," 2014. [Online]. Available: http://mathworld.wolfram.com/LinearEquation.html. [Accessed 27 August 2014].

[89] E. W. Cheney and R. D. Kincaid, Linear Algebra: Theory and Applications, Jones & Bartlett Learning, 2009.

[90] A. N. Tripathi, Linear Systems Analysis, Second ed., New Dehli: New Age International (P) Ltd., 1998.

[91] R. K. Miller, Introduction to Differential Equations, 2nd Edition ed., Englewood Cliffs, New Jersey: Prentice Hall, 1991.

[92] H. A. Smith Jr., "The Measurement of Uranium Enrichment," in *Passive Non-Destructive Assay of Nuclear Materials*, Washington, DC: U.S. Government Printing Office, 1991, pp. 195-219.

[93] G. E. Hansen and C. Maier, "Material Replacement Experiments: Theory and Measurements for the Lady Godiva Assembly," Los Alamos Scientific Laboratory, Los Alamos, 1953.

[94] R. L. Long, R. A. Boor, M. C. William and G. E. Elder, "The White Sands Missile Range Pulsed Reactor Facility," Army Missile Test and Evaluation Directorate, White Sands, 1963.

[95] T. P. McLaughlin, S. P. Monahan, N. L. Pruvost, V. V. Frolov, B. G. Ryazanov and V. I. Sviridov, "A Review of Criticality Accidents," Los Alamos National Laboratory, Los Alamos, 2000.

[96] General Electric Company - TEMPO, "TREE Simulation Facilities," Defense Nuclear Agency, Santa Barbara, 1979.

[97] T. M. Flanders and M. H. Sparks, "Monte Carlo Calculation of the Neutron Environment Produced by the White Sands Missile Range Fast Burst Reactor," *Nuclear Science and Engineering*, no. 103, pp. 265-275, 1989.

[98] W. E. Kinney and J. T. Mihalczo, "Oak Ridge National Laboratory Fast Burst Reactor: Critical Experiments and Calculations," Oak Ridge National Laboratory, Oak Ridge, 1961.

[99] A. J. Suo-Anttila, "Dynamic Reactor Modeling," Sandia National Laboratory, Albuquerque, 2011.

[100] R. R. Paternoster, P. Jaegers, R. Kimpland and J. McGhee, "Coupled Hydro-Neutronic Calculations for Fast Burst Reactor Accidents," Los Alamos National Laboratory, Los Alamos, 1994.

[101] S. J. Chapman, Fortran 90/95 for Scientists and Engineers, 1st Edition ed., Boston, Massachusetts: WCB McGraw Hill, 1998.

[102] D. J. Whalen, D. A. Cardon, J. L. Uhle and J. S. Hendricks, "MCNP: Neutron Benchmark Problems," LANL, Los Alamos, 1992.